Università degli Studi di Ferrara

DOCTORAL COURSE IN

"Advanced Therapies and Experimental Pharmacology"

CYCLE XXXVI

COORDINATOR Prof. Varani Katia

Age-Related Macular Degeneration: a new prospect in cell therapy

Scientific/Disciplinary Sector (SDS) MED/30

Candidate

Dott. Daniele Elena

Supervisor

Prof. Parmeggiani Francesco

Co-supervisor

Dr. Ponzin Diego

Year 2020/2023

CONTENTS

LIST OF FIGURES

LIST OF TABLES

LIST OF ABBREVIATIONS

A-SMA	Alpha-smooth muscle actin
ABL	Anterior banded layer
AFM	Atomic force microscopy
AMD	Age-related macular degeneration
AIFA	Italian Medicines Agency
ANOVA	Analysis of Variance
ARVO	Association for Research in Vision and Ophthalmology
ATMPs	Advanced therapy medicinal products
BCVA	Best corrected visual acuity
Best1	Bestrophin 1
bFGF	Basic fibroblast growth factor
Blebb.	Blebbistatin
BM	Bruch's membrane
BMP	Bone morphogenetic protein
BrdU	Bromodeoxyuridine
BSA	Bovine serum albumin
Ca^{2+}	Calcium
Calcein-AM	Calcein-acetoxymethyl ester
CC	Choriocapillaris
cDNA	Complementary deoxyribonucleic acid
ChC-BL	Choriocapillaris basal lamina
CIV	Type IV collagen

Cl^-	Chlorine
CMV	Cytomegalovirus
CNN	Convolutional Neural Networks
CNV	Choroidal neovascularization
CPCB-RPE1	California Project to Cure Blindness-Retinal Pigment Epithelium 1
CRALBP	Cellular retinaldehyde-binding protein
Ct	Cycle threshold
DAPI	4´, 6´ diamidino-2-phenylidole
ddH_2O	Double distilled water
dDM	Decellularized Descemet's membrane
dhAM	De-epithelialized human amniotic membrane
Dkk-1	Dickkopf-1
DM	Descemet's membrane
DMEK	Descemet's membrane endothelial keratoplasty
DMEM	Dulbecco's Modified Eagle Medium
DMSO	Dimethyl sulfoxide
E8	Essential 8™ Flex Medium
EBs	Embryoid bodies
ECM	Extracellular matrix
EDTA	Ethylenediaminetetraacetic acid
EL	Elastin layer
ELISA	Enzyme-linked immunosorbent assay
EMA	European Medicines Agency
EMT	Epithelial-to-mesenchymal transition
ERG	Electroretinogram

EU	European Commission
FA	Fluorescein angiography
FACS	Fluorescence-activated cell sorting
FBS	Fetal bovine serum
FDA	Food and Drug Administration
FGF	Fibroblast growth factor
FITC	Fluorescein isothiocyanate
GA	Geographic atrophy
GAPDH	Glyceraldehyde 3-phosphate dehydrogenase
GMP	Good Manufacturing Practices
H&E	Hematoxylin and eosin
hAM	Human amniotic membrane
haRPE	Human adult RPE
hBM	Human Bruch’s membrane
hESC	Human embryonic stem cell
hfRPE	Human fetal RPE
HH	Hedgehog
HIV	Human immunodeficiency virus
hPSC	Human pluripotent stem cell
HTLV-I/II	Human T-lymphotropic virus type 1
ICG	Indocyanine green angiography
ICL	Inner collagenous layer
ID	Identifier
IGF	Insulin-like growth factor
IgG	Immunoglobulin G

IgM	Immunoglobulin M
IL	Interleuchine
ihAM	Intact human amniotic membrane
IPE	Iris pigment epithelium
iPSC	Induced pluripotent stem cell
K^+	Potassium
KO-DMEM	KnockOut™ Dulbecco's Modified Eagle's Medium
KO-SR	KnockOut™ Serum Replacement
LAMα5	Laminin α5
LN-521	Laminin-521
MA	Marketing Authorisation
MACS	Magnetic activated cell sorting
MEM	Minimum Essential Media
MERTK	c-mer proto-oncogene tyrosine-protein kinase
mfERG	Multifocal electroretinograms
MHC	Major histocompatibility complex
MITF	Microphthalmia-associated transcription factor
mRNA	Messanger ribonucleic acid
NA	Not applicable
NANOG	Nanog homeobox
NaK	Na^+K^+-ATPase
Na^+K^+-ATPase	Sodium–potassium pump
NCT	National clinical trial
NEI	National Eye Institute
NEIM	Neuroectoderm induction medium

NIH	National Institute of Health
OCL	Outer collagenous layer
OCT	Optical coherence tomography
OCT-3/4	Octamer-binding transcription factor 3/4
OCT-A	Optical coherence tomography angiography
OTX2	Orthodenticle Homeobox 2
PBS	Phosphate buffer saline
PCL	Polycaprolactone
PEDF	Pigment epithelium-derived factor
PET	Polyethylene terephthalate
PFA	Paraformaldehyde
PGE2	Prostaglandin E2
PLGA	Poly(lactic-co-glycolic acid)
PLA, PLLA	Poly(lactic acid)
PLCL	Poly(L-lactide-co-ecaprolactone)
PLDLA	Poly-L-co-D,L-lactic acid
PMEL	Premelanosome protein
PMMA	Poly(methyl methacrylate)
PNBL	Posterior non-banded layer
POS	Photoreceptor outer segment
PVR	Proliferative vitreoretinopathy
QMS	Quality management system
Q-Q	Quantile-quantile
RCS	Royal College of Surgeons
REShAPE	Retinal Epithelium Shape And Pigment Evaluator

RNU	Rowett nude
ROI	Region of interest
ROS	Reactive oxygen species
RP	Retinitis pigmentosa
RPE	Retinal pigment epithelium
RPE65	Retinoid isomerohydrolase
RPE-BL	RPE basal lamina
RPECM	RPE commitment medium
RPEGM	RPE growth medium
RPEIM	RPE induction medium
RPEMM	RPE maturation medium
RT	Room temperature
RT-PCR	Real-time polymerase chain reaction
s.d.	Standard deviation
SD	Sprague Dawley
SDS	Sodium dodecyl sulfate
SEM	Scanning electron microscope
SOX17	SRY-Box Transcription Factor 17
SSEA-4	Stage-specific embryonic antigen-4
TEM	Transmission electron microscope
TER	Transepithelial electrical resistance
TGF-β	Transforming growth factor-β
TYRP1	Tyrosinase-related protein 1
UV-C	Ultraviolet-C
VEGF	Vascular endothelial grow factor

WHO	World Health Organization
ZO1	Zona occludens protein 1

PREFACE

Among the wide range of retinal degeneration disorders, age-related macular degeneration (AMD) is the most common cause of blindness between the elderly in the Western world. The events occurring during the progression of the disease lead to retinal pigment epithelium (RPE) disruption and failure. Previous clinical studies suggest that RPE-cell replacement therapy may preserve vision and restore retinal function in AMD patients. New developments in the field of stem cells enabled the differentiation of RPE cells from pluripotent stem cells, thus ensuring a limitless source of RPE cells. Upon several approaches for delivering these cells in the back of the eye, scaffold-based methods are being tested in ongoing clinical trials. In this regard, borrowed materials from donor tissues can be used as cell supports in subretinal transplantation.

We first focused on the human amniotic membrane (hAM), owing to its relevant anti-inflammatory and anti-angiogenic properties. An alternative to hAM can be found within the eye: the Descemet's membrane (DM) is an ultimate example of high collagen-rich basement membrane.

This study aims to investigate human embryonic stem cell-derived RPE (hESC-RPE) cells survival and behaviour on de-epithelialized hAM and decellularized DM, which may be of clinical relevance in cell transplantation for AMD.

Considering the lack of literature data on DM transplantation in the subretinal space, we sought to assess the *in vivo* integration of this membrane using a rat animal model.

Lastly, a comparative study was conducted between human pluripotent-derived RPE cell cultures on different selected scaffolds including the DM, the synthetic poly(lactic-co-glycolic acid) (PLGA) scaffold taken as a "gold standard" of RPE cell transplantation and aged explants of Bruch's membrane. This part of the project intended to highlight morphological and functional features arising on RPE cell cultures when cultured on different substrates.

We generated RPE cells from a hESC line (named H09) subjected to spontaneous differentiation in feeder free conditions. In a second part of the study, we used a direct differentiation protocol to speed up and increase the rate of cell differentiation.

To allow the exposure of the hAM's basement membrane, we found that thermolysin provided better retention of tissue integrity compared to other de-epithelialization approaches. H09-RPE cells seeded over de-epithelialized hAM formed patches of pigmented cells interspersed throughout the membrane, but failed to organize into a regular monolayer of cells.

Samples of DM were retrieved from donor corneas and treated with thermolysin to allow proper decellularization. H09-RPE cells were then seeded onto the endothelial-side surface of the acellular DM. Thermolysin treatment ensured a reliable method to standardize the preparation of decellularized DM. On the new matrix, H09-RPE cells succeeded in forming an intact monolayer of cells with mature tight junctions and representative RPE morphology.

AMDCD-RPE and H09-RPE cells showed different phenotypes when cultured on the selected investigated scaffolds, thus supporting the hypothesis that the microenvironment where the cells reside can affect the characteristics of the cells, including cell morphology, polarity and function.

When transplanted in the subretinal space of rats, the DM and the PLGA scaffolds were both well tolerated and no sign of rejection was observed up to two months after surgery. Unlike the PLGA scaffold, the DM was generally unable to flatten in the subretinal space, leading to an abnormal rearrangement of the retinal structure.

Despite some studies reported promising results of the hAM as RPE cells carrier, the handling of this tissue remains a significant challenge and we found that the biological variability of the hAM could affect the successful culturing of the H09-derived RPE cells. On the other hand, we initially showed that acellular DM was capable of sustaining H09-RPE cells growth, thus confirming to be potentially a valid alternative to the Bruch's membrane.

The i*n vivo* study demonstrated that the natural folding of the DM prevents optimal cell culture to be established and proper positioning of the cell patch when implanted. Nonetheless, no sign of rejection was observed after the follow-up period, confirming the safety of the graft.

Overall, our findings discourage the use of the DM as a tissue engineering tool for retinal transplantation. Nonetheless, we acknowledged the presence of intrinsic attributes on the DM surface that could support *in vitro* pluripotent-derived RPE cell culture, thus suggesting the use of this membrane as a suitable template for future scaffolds for ocular tissue engineering.

1. INTRODUCTION

1.1 STRUCTURE OF THE RETINA

The retina is a thin, multilayered, transparent sheet of tissue that is derived from the neuroectoderm. Just like the film of a camera, the retina receives and modulates visual stimuli from the external world and transmits them to the brain through the optic nerve. The region of the brain that receives signals from the retina is the visual cortex. The retina is located in the back of the eye, between the choroid and the vitreous chamber of the eye, and it extends from the optic nerve, in the posterior pole, to the *ora serrata*, the anterior region of the eye that is connected to the iris. Many different cell types compose the retina in a highly organized structure (Figure 1). This arrangement has traditionally been described by the layers visible from transversal retina sections and the descriptive names given to these layers are still in use today (Hoon et al., 2014). A total of ten layers have been described (Hoon et al., 2014):

1. Retinal pigment epithelium (RPE) – As previously described, it is a monolayer of pigmented cells that form a part of the blood/retina barrier. In humans, there are 4 to 6 million RPE cells per eye and each cell interacts on average with 30 to 40 photoreceptors (Panda-Jonas et al., 1995; Young, 1971).
2. Photoreceptor cell layer – This layer contains the outer and inner segments of rods and cones, plus Müller cell projections.
3. External limiting membrane – It is not a real membrane, but it is composed by the *zonula adherens* junctions between photoreceptor cells and between photoreceptors and Müller cells. This junctional layer forms a metabolic barrier, restricting the passage of large molecules.
4. Outer nuclear layer – This plane is constituted by rod and cone cell bodies. Cones are short and their cell bodies lie close to the external limiting membrane. Rod cell bodies, instead, form several rows on top of cone cell bodies.
5. Outer plexiform layer – This area contains the synapses between photoreceptors and cells from the inner nuclear layer.

6. Inner nuclear layer – It comprises the cell bodies of horizontal cells, bipolar cells, amacrine cells, interplexiform neurons and Müller cells.
7. Inner plexiform layer – This layer is formed by synapses between the axons of bipolar cells and the dendrites of ganglion cells, amacrine processes and bipolar axons, amacrine processes and ganglion cell bodies and dendrites, amacrine cells, and amacrine cells and interplexiform neurons.
8. Ganglion cell layer – It is a single sheet of ganglion cell nuclei, except for the parafoveal region where it becomes 8-10 nuclei thick. Also, ganglion cells are separated by Müller cell processes.
9. Nerve fiber layer – It contains ganglion cell axons. These processes run parallel to the retinal surface toward the optic disk in the posterior pole, from which they exit the eye as optic nerve.
10. Internal limiting membrane – It is the innermost boundary of the retina and it is composed by the endings of Müller cell processes. The inner side of this membrane is in contact with the vitreous.

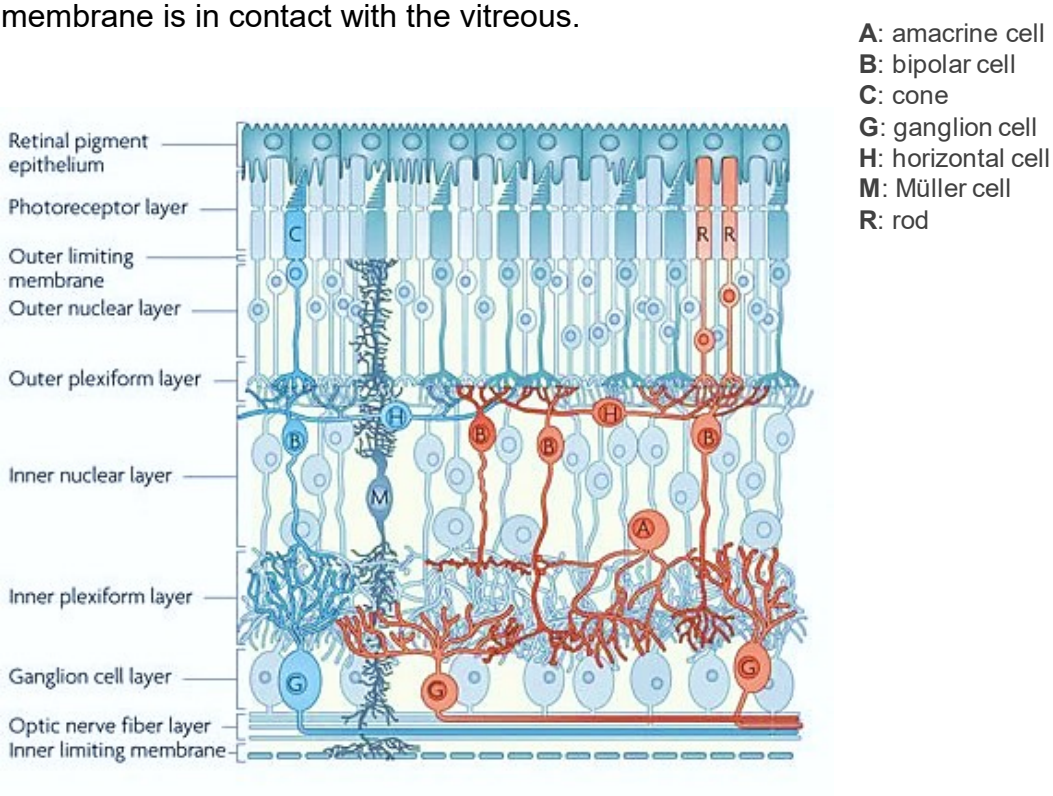

***Figure 1**: Transversal retina section combined with diagram of relative cell types (Swaroop et al., 2010). The ten layers of the retina (neuroretina and retinal pigment epithelium) are identified along the left and the different cell types in the box on the right.*

1.2 AGE-RELATED MACULAR DEGENERATION

Age-related macular degeneration (AMD) is a vision-threatening disabling disease that has drastically risen among the elderly population. As the leading cause of irreversible blindness worldwide, the global prevalence of the disease is expected to reach 288 million by 2040 (Wong et al., 2014). Despite the exact etiology still unclear, AMD occurs as a complex, multifactorial disease affecting the macular region of the retina (Flores et al., 2021). Several risks factors have been linked to the disease, mostly genes related to the complement pathway of the immune response or related to lipid metabolism. Environmental and behavioural factors that increase the likelihood of developing AMD include obesity and cigarettes smoking (Lim et al., 2012). Above these, aging remains the predominant risk factor in AMD.

AMD can be categorized by morphologic features based on the presence or absence of atrophic lesions referred to as geographic atrophy (GA) (“Dry AMD”) or the presence or the entity of choroidal neovascular membranes proliferation (“Wet AMD”) (Thomas et al., 2021) (Figure 2). Affecting only about 20% of patients with AMD, the latter is responsible for approximately 90% of severe central vision loss caused by AMD (Flaxel et al., 2020). It presents newly created blood vessels from the choroid that leak into the retina, resulting in bleeds underneath the retina and secondary scarring, which in turn disrupt and damage the layer of photoreceptors, leading to severe visual impairment (Vyawahare and Shinde, n.d.). Costly and labour intense treatments are now available for this AMD condition. These therapies block the activity of the vascular endothelial growth factor (VEGF), a pro-angiogenic factor involved in angiogenesis and vascular permeability increase. Despite prominent visual benefits, not all patients respond to anti-VEGF therapy and functional benefits of the intravitreal treatment with VEGF inhibitors tend to wane in the long term (Chakravarthy and Peto, 2020).

The majority of AMD patients suffer from dry AMD, identified by fatty protein deposits, known as drusen, which form between the RPE and the Bruch’s membrane (BM). The size and the number of drusen contribute to the risk of disease progression. The macular region of the retina is most vulnerable to the build-up of drusen. Over time, these small yellowish deposits can accumulate due to insufficient antioxidant defences and dysregulation of the extracellular matrix (ECM), leading to a chronic inflammation of the subretinal space with concurrent

transition to advanced stage of the disease in which GA in the macula is the predominant outcome (Flores et al., 2021; Gehrs et al., 2016). This form of AMD has no proven successful treatment, unlike wet AMD. Hence, an enlarging population of patients suffering from dry AMD require effective therapeutic options. Patients carrying AMD often report rapid worsening of vision in one or both eyes. In the early or intermediate stages of the disease, patients can be asymptomatic if the fovea is not yet involved. Proper diagnosis of AMD relies on imaging modalities such as optical coherence tomography (OCT), a widely used noninvasive tool that enables the visualization of the retinal layers and underlying choroid in cross section (Stahl, 2020). OCT uses light to provide a detailed display of retinal and choroidal structures, allowing the identification of specific retinal layers affected by AMD. OCT images can help to distinguish wet and dry AMD, as well as identifying disease stage and choroidal neovascularization (CNV) activity (Gess et al., 2011). Nowadays, optical coherence tomography angiography (OCT-A) has supplanted OCT imaging, owing to its higher resolution, faster imaging and ability to better visualize the choroid vascular network. OCT-A has replaced in many cases fluorescein angiography (FA) or indocyanine green angiography (ICG), the standard methods for assessing CNV in AMD. As invasive procedures, the techniques involve the injection of the dyes into the vein of a patient. The images of the chorioretinal circulation are taken over the course of several minutes that may detect the presence of leakage from CNV lesions (Thomas et al., 2021).

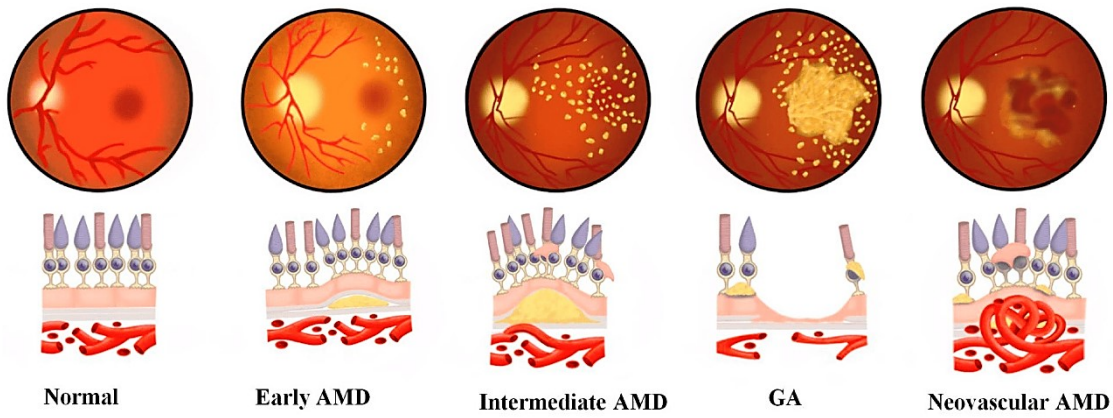

***Figure 2**: Clinical classification of age-related macular degeneration (Yahalomi et al., 2023). AMD, age-related macular degeneration; GA, geographic atrophy.*

1.3 RETINAL PIGMENT EPITHELIUM

The RPE is a polarized monolayer of pigmented, cobblestone-like cells located in the back of the eye. This epithelium maintains close interaction with the overlying photoreceptor cells and the underlying choroid (Ramsden et al., 2013). Along with a thin layer of extracellular matrix called Bruch's membrane and the endothelial cells of the choriocapillaris, the RPE form the homeostatic unit of the eye, referred as the outer blood retina barrier. The strategic interaction with the photoreceptor layer is essential for vision as the RPE is responsible for many critical functions (Sparrow et al., 2010; Strauss, 2005) (Figure 3).

- **Phagocytosis:** Photoreceptors are constantly exposed to light that damages proteins and lipids and leads to formation of photo-oxidative radicals. On a daily basis, the concentration of light-induced toxic substances increases inside photoreceptors (Beatty et al., 2000). Hence, the photoreceptor outer segment (POS) must undergo a constant renewal process (Bok, 1993; Bok and Hall, 1971). During this process, the tip of POS is phagocytosed by RPE and new portions of POS are built at the basis of the outer segment. Overall, POS maintain a constant length. In the RPE, shed POS are digested and important molecules, such as retinal, are recycled to photoreceptors after being transformed through reaction of the visual cycle (Bibb and Young, 1974; Bok, 1993).
- **Visual Cycle:** Light transduction is initiated by absorption of light by Rhodopsin, a molecule that is composed of a G-couple receptor protein, Opsin, and the chromophore 11-cis-retinal (Hargrave, 2001). Absorption of light changes the conformation of 11-cis-retinal to all-trans-retinal. The conformational change of retinal is the first step of the phototransduction cascade (Okada et al., 2001). After retinal photoconversion, Rhodopsin becomes inactive and releases the all-trans-retinal to bind a new molecule of 11-cis-retinal and begins a new phototransduction cycle. In order to have 11-cis-retinal available at all times, the all-trans-retinal is transported to the RPE where it gets re-isomerized and, subsequently, made available again for photoreceptor's use. The key reactions of the 11-cis-retinal regeneration are: reduction of all-trans-retinal to all-trans-retinol by the all retinol dehydrogenase (Haeseleer et al., 1998; Rattner et al., 2000), the esterification of all-trans-retinol to all-trans-retinyl ester, the conversion of

all-trans-retinyl ester to 11-cis-retinol by a isomer hydrolase (Deigner et al., 1989), and the oxidation of 11-cis-retinol to 11-cis-retinal by 11-cis-retinol dehydrogenase (Driessen et al., 1995). Re-isomerized 11-cis-retinal is transferred from the RPE to the photoreceptors.

- **Epithelial Transport:** The RPE transports nutrients and ions between photoreceptors and choriocapillaris to nourish the photoreceptors and to maintain homeostasis in the subretinal space. The RPE forms a semi-permeable barrier between the subretinal space and the choriocapillaris through the high expression of tight junctions (Ban and Rizzolo, 2000; Kniesel and Wolburg, 1993). A large amount of water is generated in the retina by the elevated metabolic rate of photoreceptors and neurons. Accumulation of water in the subretinal space is called edema and causes retinal detachment leading to its degeneration (Marmor, 1979). Water in the subretinal space is removed by the RPE and this constant process contributes to adhesion between RPE and retina (Frambach et al., 1989). Epithelial transport of Cl- and K+ drive transport of water (Adorante and Miller, 1990; Bialek et al., 1995; Bialek and Miller, 1994; Edelman et al., 1994). RPE is also responsible for the elimination of photoreceptors metabolic end products (Hamann et al., 2000; Kenyon et al., 1994), mostly lactic acid from POS (Hsu and Molday, 1994). In the opposite direction, RPE transports glucose and other nutrients from blood to photoreceptors. To transport glucose, RPE express a high amount of glucose transporters, the most abundant are GLUT1 and GLUT3 (Ban and Rizzolo, 2000; Bergersen et al., 1999; Sugasawa et al., 1994). In addition to recycling all-trans-retinol from photoreceptor, RPE transports vitamin A (all-trans-retinol) from the bloodstream as an additional supply, after conversion into 11-cis-retinal (Pfeffer et al., 1986).
- **Polarized Secretion:** The RPE is known to secrete a large number of growth factors (Tanihara et al., 1997) and factors that are important for maintaining the structural integrity of retina and choriocapillaris. For this purpose, the RPE secretes, in a polarized fashion, fibroblast growth factors (FGF-1, FGF-2 and FGF-5) (Bost et al., 1992; Caruelle et al., 1989; Connolly et al., 1992), transforming growth factor-β (TGF-β) (Khaliq et al., 1995; Kvanta, 1994), insulin-like growth factor-I (Martin et al., 1992; Slomiany and Rosenzweig, 2004), ciliary neurotrophic factor (Cao et al.,

1997; Walsh et al., 2001), platelet-derived growth factor (Campochiaro et al., 1994, 1989), VEGF (Adamis et al., 1993; Kuroki et al., 1996; Lopez et al., 1996), lens epithelium-derived growth factor (Ahuja et al., 2001), members of the interleukin family (Ishida et al., 2003; Streilein et al., 2002; Wenkel and Streilein, 2000), and pigment epithelium-derived factor (PEDF) (Dawson et al., 1999; King and Suzuma, 2000). In a healthy eye, RPE tightly regulates the polarized cytokines secretion. For instance, PEDF and VEGF are predominantly secreted on opposite sides of RPE: PEDF is secreted predominantly on the apical side of the RPE where it acts on photoreceptors and neurons, whereas VEGF is secreted predominantly on the basal side where it maintains choriocapillaris health (Becerra et al., 2004; Blaauwgeers et al., 1999).

- **Ion Buffering:** The subretinal space is subject to rapid changes in ion concentrations due to photoreceptor activity. The RPE not only stabilizes the ionic homeostasis in the subretinal space by transepithelial transport of ions, but it also mediates fast occurring changes in ion concentrations. RPE shares this role with Müller glia cells (Newman and Reichenbach, 1996). Stimulation of photoreceptors by light reduces the K+ efflux and its concentration in the subretinal space drops from 5 to 2 mM (Dornonville de la Cour, 1993; Steinberg et al., 1983). To compensate for this, the RPE apical membrane hyperpolarizes and the membrane conductance of K+ increases so that the ion can be transported back to the subretinal space (Hughes and Takahira, 1996; la Cour, 1985). The decrease in subretinal K+ concentration changes also Cl- transport (Bialek et al., 1995; Edelman et al., 1994). There's a decrease of Cl- influx from the RPE apical membrane that is compensated by an increase of Cl- influx from the basolateral membrane (Bialek et al., 1995; Bialek and Miller, 1994). These compensatory mechanisms can be monitored with an electroretinogram (ERG) as c-wave (Griff, 1990).
- **Light Absorption:** The RPE forms a dark pigmented wall in the back of the eye which absorbs scattered light improving visual acuity. In addition, the elevated oxygen supply and the high metabolic rate of the retina make this tissue prone to develop reactive oxygen species (ROS). The pigmentation of RPE plays a role in reducing ROS formation by absorbing the light

energy that is focused on the retina. The absorbed energy will not trigger ROS generation (Boulton and Dayhaw-Barker, 2001).

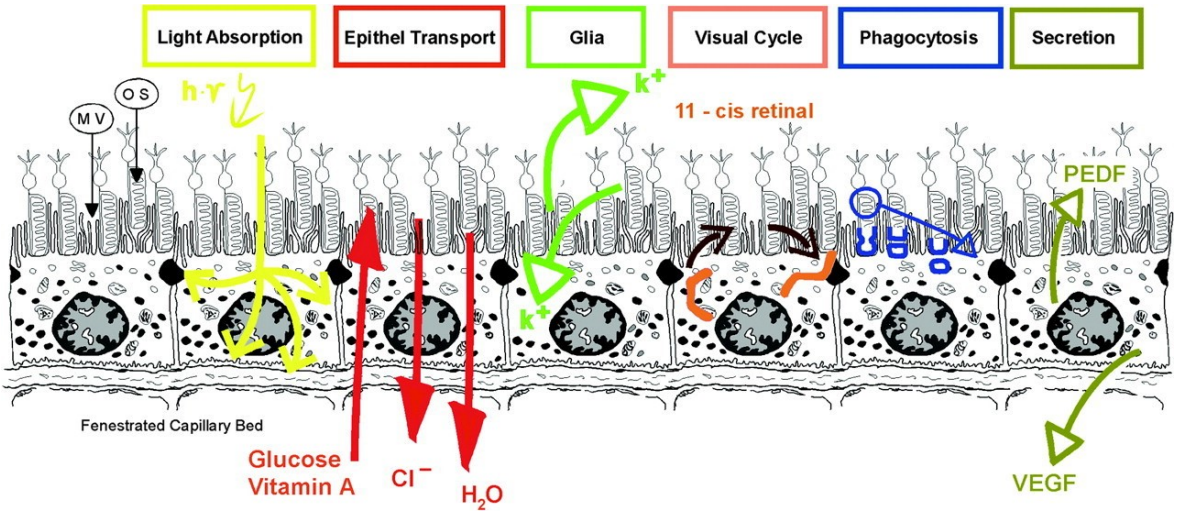

***Figure 3**: Schematic presentation of RPE functions (Strauss, 2005). Epithel, epithelium; MV, microvilli; PEDF, pigment epithelium-derived growth factor; OS, outer segment; VEGF, vascular epithelium growth factor.*

1.3.1 Function and role of the RPE in AMD

Age-related degenerative changes in the RPE, resulting in the disruption and failure of the RPE, trigger the development of AMD and the progression toward advance stages of the disease. Even though several pathogenic hypotheses have been proposed, the mechanism of RPE cell death in AMD remains controversial.

The retina is one of the highest oxygen-consuming tissues in the human body and this intense metabolic activity occurs mainly at the macula level. As a model of AMD pathogenesis, it is thought that with aging the RPE cells are no able anymore to sustain the highly demand of metabolic waste products breakdown and removal required from the macula. The continuum release of toxic free radicals during normal retina physiology increases the production of ROS which leads to oxidative stress with related damage to the RPE (Ramsden et al., 2016).

During aging, a derivative of the RPE phagocytosis known as bis-retinoid N-retinylidene-N-retinylethanolamine, can accumulate at the base of the RPE, contributing to drusen formation and RPE detachment from the overlying photoreceptor cell layer. This process combines oxidative stress with retinal

inflammation, causing secondary photoreceptors cell death in the late stages of the disease (Carr et al., 2013; Zeiss, 2010).
The accumulation of drusen between the RPE and the BM causes a thickening of this membrane, which becomes fragmented and calcified. These changes in BM composition lower the permeability to nutrients and macromolecules, further contributing to RPE dysfunction and loss of photoreceptors (Zeiss, 2010).

1.4 RPE REPLACEMENT AND REPAIR

GA lesions are characterized by a transition zone where unlike the central portion of the lesion, the photoreceptor cells are still preserved, albeit the RPE cells have already atrophied. In this area, a cell therapy approach based on RPE transplantation for replacing the damaged RPE cells could stop the disease from progressing further. This strategy would help reduce the prevalence of blindness in the general population and greatly improve patients' quality of life (Shah and Williams, 2016).

1.4.1 Proof-of-principle studies

Potential therapeutics have been tested for efficacy in proof-of-principles studies by many research groups using animal model of RPE dysfunction. Among commonly used models for testing AMD cellular therapies is the Royal College of Surgeons (RCS) rat. This retinal degenerative secondary to RPE failure animal model is a current accepted model for efficacy studies involving stem-cell derived RPE transplantation. These rats carry a mutation in the MERTK gene, which encodes an RPE cell surface protein essential for the phagocytosis of POS discs. This mutation leads to photoreceptor cell death and subsequent blindness within months after birth due to defective phagocytosis by the RPE (D'Cruz et al., 2000). First studies performed on these rats with donor RPE cells from different sources such as animal, fetal, neonatal or adult showed to delay the onset and prevent or reverse the degeneration of RPE in the RCS rat (Alvarez Palomo et al., 2015; Carr et al., 2009; Coffey et al., 2002; Lavail et al., 1992; Vugler et al., 2008). These experiments established the paradigm that RPE transplantation of healthy RPE

cells could prevent the degeneration if not completely reverse it and photoreceptor cells rescue is possible.

Early RPE transplants using xeno-grafts in animal model paved the way for the development of RPE allografts in animal and human eyes. Multiple human trials were initiated back in the 90's to test RPE sheet allografts derived from fetal and post-mortem adult human eyes (Algvere et al., 1997, 1994; Del Priore et al., 2001; Peyman et al., 1991; Tezel et al., 2007; Weisz et al., 1999). Due to allograft immune rejection without immunosuppression in patients carrying CNV, the focus on RPE transplantation shifted on autologous RPE grafts. Attempts were made using non-diseased autologous RPE cells harvested from the periphery and immediately transplanted under the macular region as a suspension of cells. These pioneering transplantations showed only temporary vision improvement, possibly related to cytokine secretion from the transplanted RPE cells. Long-term visual benefits were limited mainly for the lack of adhesion of the RPE cells over the native BM, thereby their inability to form a functional monolayer of polarized cells (Binder et al., 2004, 2002). Considering these issues, several groups attempted the so-called macular translocation, where an autologous RPE-choroidal complex is taken from the periphery and repositioned over a healthy area of RPE (Bindewald et al., 2004; Joussen et al., 2007, 2006; Ma et al., 2009; MacLaren et al., 2007, 2007; Stanga et al., 2001; Treumer et al., 2007). All these studies provided proof of principle for the RPE cell replacement therapy, by providing data on the advantages of this therapeutic option in AMD patients.

However, although these treatments can maintain visual function in some patients, these approaches proved limited success in the long-term and carried severe postoperative complications (MacLaren et al., 2007; Treumer et al., 2007; Whiting et al., 2015). Furthermore, the transplantation of post-mortem RPE cells had various results, possibly due to change in RPE physiology and function after harvest (Blenkinsop et al., 2015; Buchholz et al., 2009).

1.4.2 Cell sources

The transplantation of cadaver or fetal RPE as well as translocation of RPE surgeries are options for AMD treatment. However, none of these approaches can meet the large number of patients in need and provide an unlimited source of RPE cells required for a viable cellular therapeutic. Hence, the lack of abundantly

available RPE cells has led the research focus to shift toward alternative sources of cells for retinal transplantation.

In the last years, the emergence of human pluripotent stem cells (hPSCs) with the potential to generate every cell type of the human retina *in vitro* has sped up the development of treatments for retinal degenerative diseases. The use of stem cell to replace damaged RPE holds great promise. Besides being produced in limitless amounts, pluripotent stem-cell derived RPE has been shown to be capable of recapitulating the same functions *in vivo* as the native healthy human RPE (Carr et al., 2013; Coffey et al., 2000; Kokkinaki et al., 2011; Vugler et al., 2008).

Human embryonic stem cells (hESCs) are an attractive cell source for replacing RPE. If maintained under appropriate culture conditions, these cells have the capacity for indefinite self-renewal and have the differential potency of forming all three germ layers (). hESCs are harvested from the inner cell mass of blastocyst stage embryos and later cultured on various types of feeder cells or under feeder-free conditions on a suitable ECM substitute. The addition of knockout serum replacement to the culture, together with additional basic fibroblast growth factor, ensures the preservation of hESCs pluripotency ().

Ethical concerns on the use of hESCs led to the generation of adult somatic cells (such as fibroblasts) that have been reprogrammed back to pluripotency, namely induced pluripotent stem cells (iPSCs). First studies in 2006 made by Takahashi and Yamanaka used four transcription factors, Oct4, Sox2, c-Myc and Klf4 which were inserted into adult mouse fibroblasts through retroviral transfection (Takahashi and Yamanaka, 2006). Even if the mechanism is not completely understood, these transcription factors reprogram the somatic cells to their pluripotent stage and yielded hESC-like cells with compact morphology and maintenance of viability in culture for prolonged periods. As well as hESCs, under specific culture conditions they are able to differentiate into the three germ layers. Due to issues related with the use of oncogene in cell therapy for the derivation of these cells, the oncogenes c-Myc and Klf4 have been lately replaced with Nanog and Lin-28 (Yamanaka, 2020). The use of small molecules instead of the two oncogenes also showed proper induction of pluripotency from human fibroblasts (Hou et al., 2013). A second issue on the use of iPSCs was related to the use of viral transfection for the delivery of the pluripotency genes, owing the integration of the viral genome into the recipient genome (Augustyniak et al., 2014). However,

the employ of non-integrating adenovirus or episomal vectors has proven to be a successful alternative to iPSCs induction (Shao and Wu, 2010).

hESCs and iPSCs have unique features that make them irreplaceable. Besides their origin, they can cause a different immunity response in the recipient eye. As a natural counterpart of the RPE cells, hPSC-RPE cells exhibit immunological properties with some immunosuppressive effects. *In vitro* experiments showed that hESCs do not stimulate peripheral blood monocyte cell proliferation. These observations, together with the fail to express major histocompatibility complex (MHC) type II suggest that hESCs may have a lower potential of activating the immune system (Drukker et al., 2002). Nevertheless, mononuclear cell infiltration was observed around hESC-RPE xenografts in rabbit eyes (Petrus-Reurer et al., 2020). As to iPSCs, *in vitro* they could suppress T-cell activation which in turns inhibits activated T cell functions (Fujii et al., 2019). When injected as cell suspension *in vivo*, these cells have shown to elicit an innate T cell-mediated immune response marked with subretinal infiltration of macrophage and leukocyte in not immunosuppressed Yucatan mini-pigs. All these results emphasize the need for adequate immunosuppression. Major advantage of iPSCs in respect to hESCs is the autologous nature of an iPSC transplant. iPSC-derived RPE holds great promise for overcoming immune rejection, since RPE for transplantation could be created from the patient's own cells which theoretically should escape host immune system (Blenkinsop et al., 2015; Buchholz et al., 2009; Kokkinaki et al., 2011).

A major characteristic of iPSCs is the presence of unique features and potential of differentiation. iPSCs might inherit patients' genetic vulnerability or bear epigenetic memory of initial differentiation and long-term exposure to environmental insults (Kim et al., 2010), although these mechanisms of inheritance have not been unravelled yet. Genetic predispositions toward AMD contained within a patient's own cells should not be of concern since reintroduction of cells with genetic defect will probably take years to reveal pathology (Buchholz et al., 2009). In research, RPE cells derived from patient iPSCs can be used to resolve the molecular pathology of inherited mutations that contribute toward RPE diseases, an essential step in understanding AMD progression and identifying alternative novel and viable therapeutics for these patient groups (Schwartz et al., 2015).

The feasibility of using this stem cell technology for deriving RPE cells suitable for cell therapy and disease modelling has directed all the efforts to the development of robust differentiation protocols (Ben M'Barek and Monville, 2019).

1.4.3 Generation of RPE from pluripotent stem cells

The lack of model systems to reproduce the precise sequence and timing of cellular and molecular events that occur during human embryogenesis, organogenesis and tissue differentiation is a limit in the study of human development. The advent of human stem cell technology allows to follow all the stages of lineage-specific cell differentiation (Keller, 2005; Pera and Trounson, 2004). One of the first attempts of in-vitro differentiation of RPE was published in 2002 starting from embryonic stem cells co-cultured with feeder cells (Kawasaki et al., 2002). The authors were able to demonstrate that they could obtain RPE-like cells expressing Pax6 but with a yield of only 8%. Two years later, another publication showed that it is possible to differentiate RPE from hESCs without the help of feeder cells if cultured without the presence of FGF signal (Klimanskaya et al., 2004). In 2009, a group differentiated RPE from iPSC and transplanted it into a rat model that mimics retinal degeneration (Carr et al., 2009). The transplanted cells did not survive more than 13-15 weeks, even if they were able to show some visual improvement. Several groups reported an easy method to differentiate RPE by simply changing media without adding any growth factor (Buchholz et al., 2009; da Cruz et al., 2018; Kashani et al., 2018; Lane et al., 2014). Indeed, hESCs as well as iPSCs can be differentiated into RPE (Figure 4) by withdrawal of basic fibroblast growth factor (bFGF) from the tissue culture media, a process known as spontaneous differentiation. This method relies on the ability of stem cells to spontaneously generate all three germ layers (Carr et al., 2009; Vaajasaari et al., 2011; Vugler et al., 2008). Pigmented foci can be identified between weeks 3 and 5 after bFGF withdrawal. These foci can then be manually isolated to purify the RPE from the differentiated cultures. The isolated RPE cells can then be cultured as a monolayer and used for downstream assays in research facilities or for clinical use. The disadvantage of this spontaneous differentiation process is that the efficiency is low and it usually takes a lot of time.

The studies cited above set the stone for *in vitro* RPE differentiation from stem cells, but they had some limitations such as: (1) long protocols for differentiation; (2) low final yield of RPE cells from the stem cell culture, likely due to the fact that the ES or iPS cell culture is heterogeneous to begin with; (3) lack of purity of the differentiated cells. The purity of the differentiation becomes very important if the final goal is to transplant RPE into patients affected by retinal degeneration; and (4) the success of differentiation of hESCs and iPSCs into a specific lineage can vary with the choice of stem cell line (Feng et al., 2010). This difference might be even more evident in iPSC lines, since they might retain some epigenetic marks from the cell type they have been derived from (Kim et al., 2010). Cell line specific effects might have, therefore, influenced the variability of protocols for RPE differentiation.

The best way to achieve specific lineage differentiation is to supply defined media with known components and concentrations to culture stem cells at the right time windows. Stem cell differentiation using defined media improves efficiency, shortens time to obtain desired cells and reduces cell line-to-cell line variability. Several studies have tried this approach for RPE differentiation. The first step for production of RPE is the induction of the anterior neuroepithelium, precursor to the eye field. The role of insulin-like growth factor (IGF) in directing differentiation toward the anterior neuroepithelium has been first described in Xenopus, where ectopic expression of IGF mRNAs led to the induction of ectopic eyes and head-like structures containing brain tissue (Pera et al., 2001). The second step is the generation of eye field cells from the anterior neuroepithelium. Wnt and bone morphogenetic protein (BMP) pathways have been shown to be important for this phase, where Dickkopf-1 (Dkk-1) and Noggin expression, Wnt/β-catenin and BMP inhibitors respectively, were upregulated during eye field specification (Meyer et al., 2009). The third step is the appearance of RPE from the eye field. As mentioned in the “Developmental origin of RPE” section above, BMP, ACTIVIN, WNT and Hedgehog (HH) pathways appear to be important in determining RPE fate. Another important factor is the removal of FGFs from culture media for conversion of hES or iPS cells into RPE (Bharti et al., 2011). As mentioned above, FGFs secreted by the surface ectoderm induce neuroretinal differentiation while inhibiting RPE fate (Hyer et al., 1998; Nguyen and Arnheiter, 2000; Pittack et al., 1997). The fact that the simple inhibition of FGF signaling is sufficient to induce RPE differentiation (Hodgkinson et al., 1993) suggests that RPE is a primary fate.

In normal conditions RPE is among the first cell types to differentiate from the neuroepithelium. Moreover, the transcription factor MITF, that is essential for RPE development, is expressed by all hESC- or iPSC-derived neuroectodermal cells and is actively downregulated by retinal progenitor cells, but maintained in RPE cells (Meyer et al., 2009).

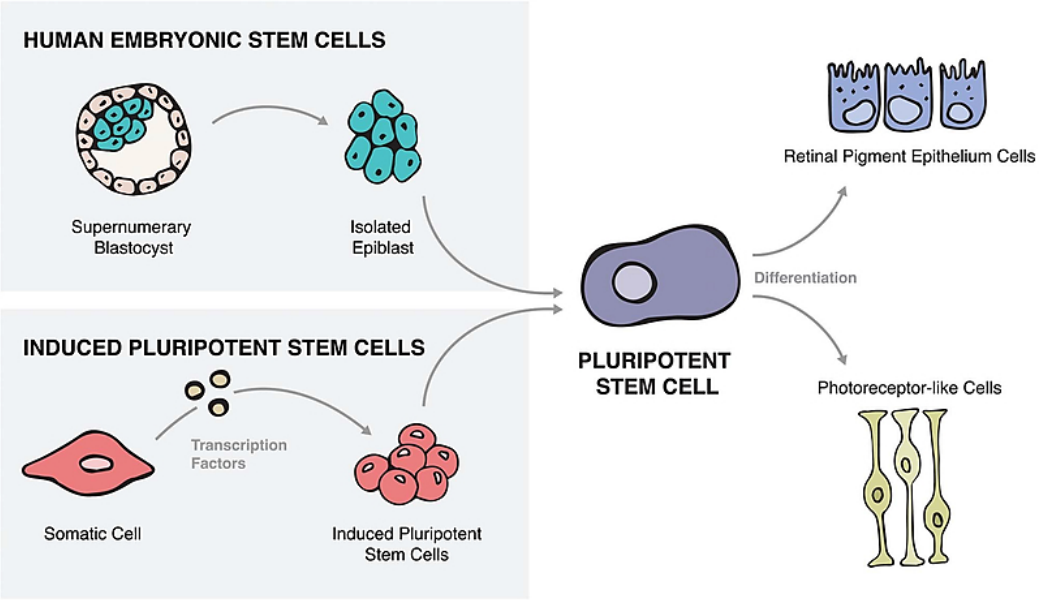

***Figure 4**: hPSCs for retinal degenerative diseases (Wood et al., 2019). hPSCs are most commonly derived from hESCs and/or iPSCs and may give rise to any assortment of retinal cell types including retinal pigment epithelial cells, photoreceptors, retinal organoids, and others.*

1.5 TISSUE-ENGINEERING FOR CELL TRANSPLANTATION TO THE SUBRETINAL SPACE

The generation of healthy RPE cells from stem cells leads the way to new investigations on how to deliver such cells to the subretinal space in order to maximize their therapeutic effect (Soto-Gutierrez et al., 2010). A bolus injection of RPE cell suspension has been for years at the forefront of the cell therapy (Schwartz et al., 2015, 2012). Despite the ease of logistic related to the injection of a cell suspension formulation, this approach engenders poor transplantation outcome, mainly due to insufficient cell survival and migration from the transplantation site. Initial benefits were referred to the ability of the suspended cells to secrete neuroprotective factors to protect photoreceptors from dying. Besides these initial results, pre-clinical animal data showed that suspended RPE

cells fail to form a polarized monolayer capable of performing several RPE functions and therefore providing a long-term engraftment of the cells (Carr et al., 2009; Diniz et al., 2013).

In contrast to the bolus injection, simultaneous and ongoing clinical trials have been investigating the safety and efficiency of transplanting a polarized monolayer of cells, which could overcome the issues related to injecting RPE in suspension. In this respect, the field of tissue-engineering has recently entered stem cell technology. The use of material carriers has been largely demonstrated to improve the stability and maintain cell polarization. By functioning as a synthetic analogue of the extracellular matrix, this approach facilitates RPE cell integration and functionality *in vivo*, setting the scene for a long-term implant after proper engrafting in the host BM (Ben M'Barek et al., 2017; Sharma et al., 2019). As alternative method for transplantation, the use of the scaffold enables to control the positioning of the transplanted cells *in vivo*, avoiding random migration of the cells to unwanted locations. Furthermore, the combination of this transplantation technique with advanced retinal imaging helps surgeons in locating the cells and evaluating any loss of cells from the implant.

Although not having any direct drug effect, scaffolds used for RPE-patch delivery are able to provide a therapeutic benefit by aiding RPE polarization and its delivery as a monolayer. Furthermore, the scaffold may be able to participate in disease etiology either in a positive or negative way. For example, non-biodegradable synthetic scaffold could shield hESC-RPE cells from the host immune system, but at the same time fibrotic alterations could accumulate around the scaffold and alter the functionality of the graft. Long-term studies are in need to rule out such event. Biologically compatible scaffolds such as natural or biodegradable synthetic scaffolds could be possible solutions for the problem of long-term fibrosis.

On the other hand, developing a substrate scaffold culture *in vitro* not only lengthens the product development timeline, but raises also new challenges to enter the clinical mainstream. For such cell formulations, specific delivery devices have to be designed to allow the insertion of the RPE monolayer cell sheets in the subretinal space, possibly avoiding potential surgical complications by decreasing the size of the retinotomy (Fernandes et al., 2017; Stanzel et al., 2012). In these conditions, the transplantation surgery becomes another limiting factor and it could greatly affect the fate of the cell therapy.

Scaffold-based approaches rely on the use of a support system that provides a suitable microenvironment for the development of living cells. Cells are expected to populate these matrices and build their own ECM. In the field of tissue engineering for retinal degenerative diseases, optimal graft formulation requires a close resemble of the scaffold with the BM in terms of biomechanical properties, considering the natural support that this membrane provides to the RPE cells *in vivo*.

The selection of a candidate scaffold should meet the following criteria (Ben M'Barek et al., 2018a; Hynes and Lavik, 2010; Kador et al., 2014; Nazari et al., 2015):

- Supporting the growth of the RPE monolayer;
- Compatibility with the host immune system;
- Permeability to allow free movement of water, nutrients and small molecules, but also of waste material;
- Mechanical resistance and flexibility for surgical manipulations;
- Thickness that allows subretinal implantation;
- Easy to transplant;
- If biodegradable, nontoxic byproducts.

Scaffold substrate culture of RPE can be classified as natural (derived from biological sources), synthetic (both degradable or nondegradable) or hybrid (containing elements of both natural and synthetic scaffolds) fiber formulations (Jha and Bharti, 2015). Table 1 shows a summary of some of the biological membranes and natural and synthetic polymers used for the fabrication of scaffolds employ in tissue engineering for retinal degeneration.

***Table 1**: Summary of tested RPE scaffolds.*

Material	Source	Cell type	Results
Anterior lens capsule	Animal or human	porcine RPE	*Pros*: biodegradable, high content of ECM molecules; *Cons*: 20 times thicker than BM, tendency to curl up
Amniotic membrane	Pig or human	haRPE, rabbit RPE	*Pros*: biodegradable, anti-inflammatory, antiangiogenic, flat shape, *in vitro* cells form epithelial phenotype, showed RPE-specific gene expression; *Cons*: hard to handle
Collagen	Commercial	haRPE, porcine RPE, ARPE-19	*Pros:* biodegradable fibrous structure, attractive mechanical properties, sufficient permeation of nutrients to RPE, xeno-transplant survived in rabbits and integrated with host RPE, ARPE19 showed good RPE attachment and viability
Cryoprecipitate membranes	human blood	hfRPE sheets	*Pros:* Cells retain cobblestone morphology and did not dedifferentiate, active POS phagocytosis
Descemet's membrane	Animal	porcine RPE, bovine RPE, porcine IPE, bovine IPE	*Pros:* biodegradable, easy to manipulate, *in vitro* monolayer formation, 10-12 µm thick
Gelatin	Porcine skin	porcine RPE sheets	*Pros:* nontoxic, biodegradable, hydrophilic, proper mechanical properties, controllable degradation time, survival of allo-transplants up to 3 months post-surgery, active POS phagocytosis
Inner limiting membrane	Adult human eyes	porcine RPE, haRPE, ARPE-19	*Pros: in vitro* cell proliferation and formation of RPE monolayer with cobblestone morphology, tight junctions and cell polarization
Pre-coated Bruch's membrane	Peripheral retinas of elderly donors	haRPE, hf RPE, ARPE-19, hESC-RPE	*Pros:* improved RPE adherence of pre-coated Bruch's membrane compared to non-coated versions.
PCL	Synthetic	haRPE	*Pros:* biocompatible, nontoxic, low cost, pore size and shape control, slow degradation rate, high porosity, promoted cell proliferation, *in vitro* cells expressed RPE-specific genes and show cobblestone morphology, PEDF secretion and phagocytic activity
PCL-treated plasma	Synthetic	haRPE	*Pros:* biocompatible, porous structure, good RPE adhesion and proliferation

PLGA	Synthetic	PSC-RPE	*Pros:* FDA approved, biodegradable, biocompatible, tailored degradation time, limited flexibility-, high porosity, controllable configuration and thickness, maintain high cell viability, high degree of porosity, uniform pore structure, controllable configuration and thickness; *Cons:* poor flexibility, bulk degradation resulted in non-uniform profile
PLDLA	Synthetic	hESC-RPE	*Pros:* hydrophilic, shorter degradation time than PLC, high porosity, enhance interaction between cells and tissues
PMMA	Synthetic	haRPE	*Pros:* limited support of cell growth, no foreign body response, *in vitro* RPE express RPE-specific genes and showed cobblestone morphology, PEDF secretion and POS phagocytosis, *in vivo* studies in rabbits showed no inflammation or rejection; *Cons:* toxic, nondegradable, high thickness
Parylene-C	Synthetic	PSC-RPE	*Pros:* biocompatible, nontoxic, good mechanical strength and biostability, semipermeable to macromolecules, mesh-supported submicron membrane, *in vitro* RPE showed epithelial phenotype, tight junctions, well-developed microvilli and good cell adherence

Abbreviations: ECM, extracellular matrix; FDA, Food and Drug Administration; haRPE, human adult RPE; hESC, human embryonic stem cell; hfRPE, human fetal RPE; IPE, iris pigment epithelium; PCL, polycaprolactone; PEDF, pigment epithelium-derived factor; PLDLA, poly(lactic acid); PLGA, poly(lactic-co-glycolic acid); PMMA, poly(methyl methacrylate); POS, photoreceptor outer segments; PSC, pluripotent stem cells; RPE, retinal pigment epithelium;

1.5.1 Biological scaffolds

Biological carriers are currently under investigations. Their unique structure resembles a native ECM composition and has shown to facilitate the constructive remodelling of many different tissues in both preclinical animal studies and in human clinical applications (Sheridan et al., 2004). These scaffolds have nanofibers that closely match the natural physiological properties of the BM in several key areas: concentration of protein, mechanical properties, morphological

properties, and biocompatibility. The approach of using natural scaffolds is to borrow materials that are already available in nature. For subretinal implantation, several membranes have been considered, such as native BM (Tezel et al., 2004), human amniotic membrane (hAM) (Capeáns et al., 2003; Ohno-Matsui et al., 2005; Singh et al., 2001; Stanzel et al., 2005), human lens capsule (Lee et al., 2007, 2002) and human Descemet's membrane (DM) (Thumann et al., 1997). These membranes and tissues can be isolated from donor tissue and then treated to remove any cellular components. However, they have remarkable disadvantages, including limitation of availability and concerns over possible transmission of diseases.

Human amniotic membrane

The hAM was first used in ophthalmology for reconstructing the ocular surface in patients with symblepharon (De Rotth, 1940). Since then, it has been widely used for ocular surface restoration in a variety of ocular pathologies. This membrane is the innermost layer of the placenta that surrounds the foetus during development. The hAM presents as a semi-transparent membrane and 0.2-0.5 mm of thickness. The structure consists of an epithelial monolayer, a thick basement membrane and an avascular stroma. Having no blood vessels or nerves, the nutrients are supplied directly by diffusion out of the amniotic fluid and/or from the underlying maternal *decidua* (Niknejad et al., 2008). The layer nearest to the foetus is called amniotic epithelium and consists of a single layer of metabolic active cuboidal cells with numerous microvilli uniformly arranged on the basement membrane. The latter is one of the thickest membranes found in all human tissue and it is mainly made of type IV and VII collage, fibronectin, laminins and hyaluronic acid. This basement membrane supports and protects the developing foetus throughout gestation. Lastly, the hAM has an avascular stroma that is itself divided into three layers based on their components: an inner compact layer which forms the main fibrous skeleton of the hAM, a middle fibroblast layer with a loose fibroblast network and an outermost almost acellular spongy layer with nonfibrillar meshwork of mostly type III collagen (Figure 5) (Niknejad et al., 2008; Parry and Strauss, 1998). The hAM is important for its ability in water and soluble compounds transportation and the production of several growth factors, as well as secretion of cytokines and vasoactive peptides.

Due to its biocomponents, the hAM has been considered as a scaffold for different types of cells. Indeed, the basement membrane and the stroma of the hAM resembles an ECM environment in terms of composition molecules and biomechanical structure. As a scaffold, the hAM has been used with or without the amniotic epithelium. Several protocols have been published for hAM de-epithelialization, but maintenance of its histoarchitecture and structural components.

To ensure consistent quality and correct preservation, various methods for processing and sterilisation of the tissue have been proposed. The choice of the appropriate hAM preparation for tissue engineering depends on multiple factors, such as the type of cells intended to be plated on.

The hAM has beneficial properties that stand behind the reason of its potential use as a scaffold for cells and tissues. Hao et al. (Hao et al., 2000) identified several anti-angiogenic and anti-inflammatory proteins in the hAM, along with anti-fibrotic and anti-microbial properties. These effects are exerted by: 1) Suppression of downregulation of TGF-β and its receptor (anti-fibrotic); 2) Inhibition of the expression of proinflammatory cytokines such as IL-1α and IL-1β and metalloproteinases (anti-inflammatory) (Jirsova and Jones, 2017); 3) Production of anti-angiogenic compounds including endostatin and thrombospondin-1; 4) Presence of bactricidin, lysozyme, transferrin and beta-lysin in the amniotic fluid (anti-microbial). These properties represent an asset in the use of the hAM as a support in tissue engineering constructs, which often provoke an inflammatory reaction upon implantation of the foreign body (Niknejad et al., 2008). Previous studies have demonstrated that the hAM has limited expression of major histocompatibility antigens, therefore having a low immunogenicity impact in view of transplantation (Hori et al., 2006; Houlihan et al., 1995).

In the field of RPE cell therapy, the hAM has been proposed as a scaffold for the RPE cells. Besides the abovementioned properties, advantages in the use of the hAM for the RPE cell therapy include the presence of a basement membrane that mimics the *in vivo* retinal environment and the availability of this membrane as cryopreserved small patches in tissue banks. Previous studies have reported that the hAM is well-tolerated in the subretinal space of pigs, causing limited inflammation and reducing CNV (Kiilgaard et al., 2012). Moreover, it has been used as a replacement for BM, since has shown to support RPE growth and functionality (Ben M'Barek et al., 2017; Ohno-Matsui et al., n.d.). M'Barek et al.

(Ben M'Barek et al., 2018b, 2017) developed a gelatin embedded hESC-RPE patch an amniotic membrane in patients with congenital retinal dystrophies that results in severe vision loss at an early age named Leber congenital amaurosis. The patch will be transplanted on top of dysfunctional native RPE cells and it is expected to integrate into the host RPE monolayer over the long term. In pre-clinical studies, the authors established a surgical approach to engraft this cell therapy product into the subretinal space of rat eyes with photoreceptor cell loss. They showed the rescue of photoreceptor cell death and improved visual acuity in the rats compared with the same cells delivered as cell suspension (Ben M'Barek et al., 2017). For the preparation and implantation of the proposed tissue-engineered product into the eyes of nonhuman primates, the authors manufactured two medical devices and demonstrated the graft integrity and the safety of the hESC-RPE sheet following transplantation (Ben M'Barek et al., 2020). These results have opened the way for the first clinical trial.

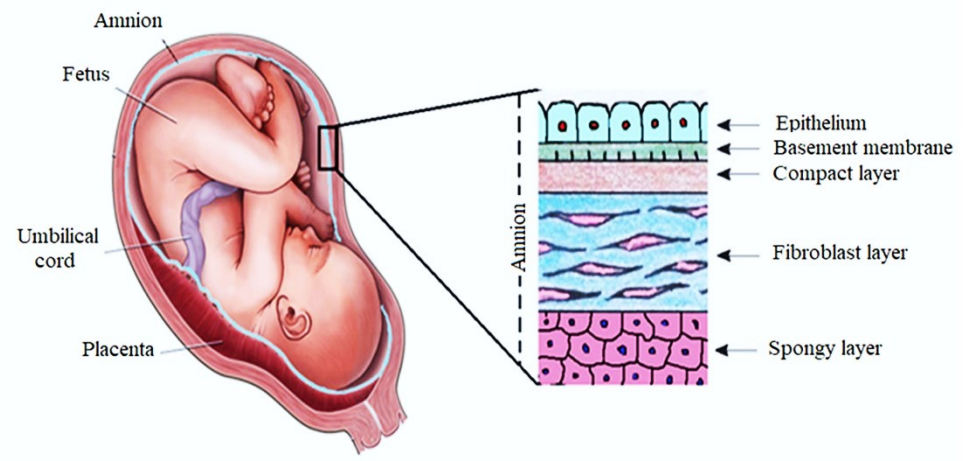

***Figure 5**: Schematic structure of the hAM (Jafari et al., 2021).*

Human Descemet's membrane

The human Descemet's membrane is a perfect example of basement membrane produced by the corneal endothelium (Ed, 1980; Van Cruchten et al., 2017). This membrane thickens during development until fully differentiate into a striated ultrastructure of distinct layers that accumulate during lifetime (C et al., 1984; de Oliveira and Wilson, 2020). Mature DM (Figure 6) is composed of an anterior banded layer (ABL) located posterior to the corneal stroma and a posterior non-banded layer (PNBL) situated beneath the endothelium (Eghrari et al., 2020). The ABL has found to be 3 µm at birth, while the PNBL keeps thickening during adult

life as it is deposited by the endothelial cells. The collagen composition of this membrane is complex. The ABL is mainly made of type IV and VIII collagen. The latter gives the ABL its typical banded pattern and it is described as relatively specific to the DM (Gottsch et al., 2005; Saikia et al., 2018). With the transition to a non-replicating state after birth, the endothelial cells diminish the secretion of type VIII collagen, while continuing to secrete type IV collagen. This deposition lead to PNBL formation and an increase in DM overall thickness that can reach >10 µm in old age (C et al., 1984; Lesueur et al., 1994). Besides collagen, the DM contains non-collagenous components including laminins, nidogens and perlecan, and other constituents typically found on basement membranes such as fibronectin and keratan and dermatan sulfate (Eghrari et al., 2020; Saikia et al., 2018). Fibronectin is found along DM's interfaces and it plays a crucial role in the adhesion of the endothelial cells to the DM (Gordon, 2014). This arrangement of components makes the DM unique compared with other basement membranes and contributes to its function. As an example, the hexagonal lattice structure of the type VIII collagen creates an array of open porous (average size of 38 nm) that allows the nourishment of the corneal stroma (Last et al., 2009; Shuttleworth, 1997).

The DM is crucial for the maintenance of corneal transparency and homeostasis. By providing adhesion for the endothelium, the DM has a direct association with this monolayer of cells, known as "dynamic reciprocity" (Ali et al., 2016; Bissell and Barcellos-Hoff, 1987). This relationship bidirectionally regulates the passage of nutrients, macromolecules and growth factors. Investigations on the mechanical properties of human corneal basement membranes found that the DM represents the stiffest layer of the cornea and therefore vital for corneal integrity (Last et al., 2012, 2009).

The DM has been explored as a scaffold for porcine RPE and iris pigment epithelium cells. On this substrate, the cells formed *in vitro* an intact monolayer with defined apical microvilli (Thumann et al., 1997). Nonetheless, the potential use of this scaffold in subretinal implantation remains unknown.

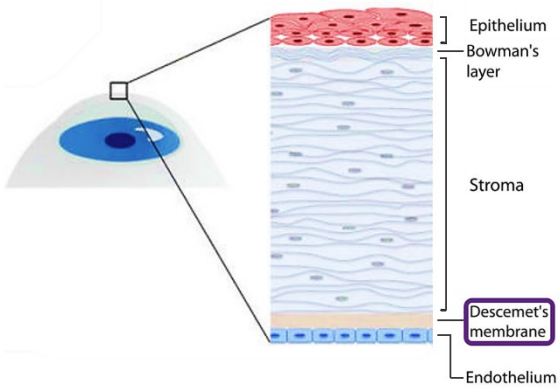

***Figure 6**: Schematic image of human cornea layers (Ghezzi et al., 2015). The corneal stratified squamous epithelium with underlying the Bowman's layer, the stroma with keratocytes for the maintenance and production of extracellular matrix, the Descemet's membrane, and the single layer endothelium*

Human Bruch's membrane

The pentalaminar BM is a thin (2 – 4 µm) acellular ECM located strategically between the retina and the choroid, functioning simultaneously as RPE substratum and a vessel wall (Johnson et al., 2007). This five-layered structure plays a major role in cell-cell communication, cellular differentiation, proliferation and tissue remodelling (Campochiaro et al., 1986; Guymer et al., 1999). From the RPE toward the choroid five layers can be distinguished histologically, each of them undergoing structural and functional changes during retinal disease development (Figure 7).

- **RPE basal lamina (RPE-BL)**: this 0.14 – 0.15 µm thick layer resembles other basement membranes in the body, with a mesh of fibers similar to those of the choriocapillaris endothelium, but without the presence of type IV collagen (Guymer et al., 1999; Lamme et al., 1996).
- **Inner collagenous layer (ICL):** in the 1.4 µm thick of this layer there are striated collagen fibers type I, III and V that form a multi-layered collagen grid embedded in a bunch of interacting molecules such as proteoglycans.
- **Elastin layer (EL):** this layer consists of several stacked layers of linear elastin fibers different in shape and sizes which form a 0.8 mm sheet with interfibrillary spaces of ~ 1 µm. A variety of other structural proteins such as type VI collagen and fibronectin are present in this layer. The EL is responsible for biomechanical support, antiangiogenic barrier and vascular compliance (Chong

et al., 2005). In addition, it has been shown that this layer is several times thinner in the macula than in the periphery.

- **Outer collagenous layer (OCL):** similar in molecular components to the ICL, this layer is ~ 0.7 μm in the young donors.
- **Choriocapillaris basal lamina (ChC-BL):** this 0.07 μm thick layer is discontinuous with the BM due to the interruptions of the intercapillary columns of the choroid. It is mainly composed of heparan sulfate, laminin and types IV, V and VI collagen. Its collagen composition should prevent endothelial cells to migrate into the BM (Roberts and Forrester, 1990).

Significant changes occur in the BM during aging. These age-related modifications affect structural and functional features of the BM, including overall increase in thickness and reduced filtration capacity due to molecular modification and reconfiguration (Moore and Clover, 2001; Ramrattan et al., 1994).

The BM is responsible for regulating the diffusion of biomolecules between the choroid and the RPE, providing physical support for the RPE cells, and acting as a wall by limiting choroidal and retinal cellular migration (Booij et al., 2010).

Despite recent trends in tissue engineering for retinal regeneration aim to design and develop scaffolds that mirror the structural and biomechanical composition of the human BM, the refurbish of this membrane itself as a matrix for RPE cells has been attempted in the years (Ho and Del Priore, 1997; Tezel et al., 1999; Tezel and Del Priore, 1997). In earlier studies, RPE cells were cultured on explants of human BM or its constituent layers. These studies found that the basal layer of the BM was critical for RPE physiology. Moreover, the level of support from the different layers of the BM to RPE cell growth decreased in relation to the distance of the layer from the basal lamina of the RPE (Tezel et al., 1999; Tezel and Priore, 1999). In explants of aged BM, the RPE had impaired survival and this was correlated with decreased prevalence of typical basal layer proteins (Gullapalli et al., 2005; Sugino et al., 2011a; Tezel et al., 2004). Reengineering the lower layers of the BM or aged BM with laminin or other ECM proteins was shown to recover some functionality in the RPE cells (Del Priore et al., 2001; Sugino et al., 2011a; Tezel et al., 2004). In view of RPE transplantation, main disadvantages in the use of native BM are limited donor tissue availability and risk of disease transmission. These factors have prevented its use as a possible source for clinical-grade applications (Hotaling et al., 2016).

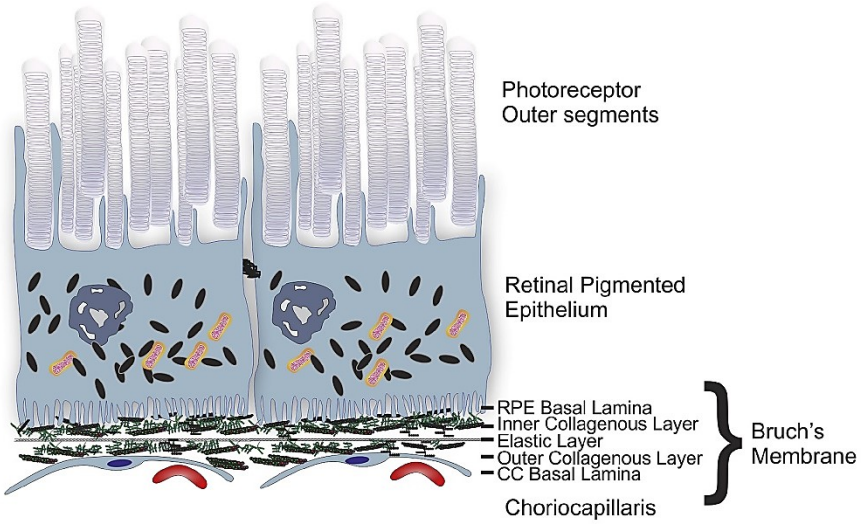

***Figure 7**: Bruch's membrane layers (adapted from Toomey et al., 2018). Schematic of photoreceptor outer segments, RPE, BM, and choriocapillaris. BM layers: basal lamina of the RPE, inner collagenous layer, elastic layer, outer collagenous layer and basal lamina of the choriocapillaris endothelial cells. BM, Bruch's membrane; CC, choriocapillaris; RPE, retinal pigment epithelium.*

1.5.2 Artificial scaffolds

Scaffolds based on synthetic biomaterials have been designed in a reproducible and predictable manner with the aim of providing consistency to generate structures with optimized mechanical strength, degradation rate, and microstructure. Additionally, these matrices can be produced in large quantities, and have a longer shelf-life. Given that synthetic scaffolds are easy to produce, they can potentially be used to prepare treatment doses for millions of patients. The manufacturing under controlled conditions assures high purity and tailoring the composition of the polymers with specific physiochemical and biological properties that could match the intended host tissue. All these factors make them promising candidates for clinical translation. The major concern in the use of these polymers is the potential toxicity, that needs to be carefully evaluated when implanted into the eye of animal model.

Polymers can be selected to be either non-degradable or degradable under certain conditions and a desired time course. Nonbiodegradable synthetic polymers like the ultrathin parylene or the porous polyester are currently tested as scaffolds for the RPE tissue preparation in ongoing clinical trials.

Different types of synthetic scaffolds have been used for RPE culture and are being tested as potential scaffolds for transplantation in patients. Unmodified poly(D-L-lactic acid) (PDLLA) nanofibers supported by a poly(4-dioxanone) frame were shown to improve RPE tight junction formation and increase expression of retinoid isomerohydrolase (RPE65). The construct was shown to maintain cell viability into the subretinal space of porcine eyes and could be easily implanted as an unfolded monolayer. Liu et al. also showed that either polyethylene terephthalate (PET) or poly(L-lactide-co-ecaprolactone) (PLCL)-uncoated nanofiber scaffolds were able to promote functional RPE growth, besides developing pigmentation and proper tight junction formation. Based on the outcomes, RPE on nanofibers with a mean diameter of 200 nm had the highest performance, regardless of starting material. Unfortunately, for transplantation purposes into rabbit eyes the authors had to provide these nanofiber scaffold with mechanical support by attaching the scaffolds to porous PET membranes. PET membranes can successfully incorporate into native tissue. However, the lack of biodegradability and the limited porosity could eventually inhibit functionality of the tissue-engineered construct. To address this concern, Warnke et al. fabricated three-dimensional nanofibrous membranes from poly(lactic-co-glycolic acid) (PLGA) or type I collagen. RPE cell morphology and functionality were evaluated on both scaffolds and compared with PLGA and collagen films. They found out that either fiber formulation supported RPE biofunctional characteristics and exhibited a correctly orientated monolayer with a polygonal cell shape and abundant sheet-like microvilli on their apical surfaces. Furthermore, the nanofiber samples could provide an artificial niche for the RPE cells. This environment allowed such cells to mature in a well-organized *in vivo*-like monolayer, superior on either of the nanofiber samples than on the films. However, no *in vivo* studies of RPE cells on these scaffolds were carried out, leaving unknown their impact on the RPE cells post-transplantation (Warnke et al., 2013).

Surface modification of nanofibers has been shown to have higher benefits compared with seeding RPE onto nanofibers alone (Ha et al., 2011). For instance, plasma treatments of polytetrafluoroethylene fibrous membranes were shown to improve RPE attachment, formation of tight junctions, and increase phagocytosis of POS (Krishna et al., 2011). In a similar study, cell attachment molecules were attached to the backbone of polyamide fibers. On this substrate, RPE cells improved viability and proliferation over that of polyamide fibers alone (Treharne et

al., 2012). Plasma treatment of fibers and type IV collagen adsorption onto PLCL were also shown to enhance the growth, maturation and functionality of hESC-RPE cells in serum-free culture conditions to a greater extent than untreated fibers (Sorkio et al., 2015). Further research supported the premise that the adsorption of ECM proteins could enhance RPE cell. Thomson et al. showed that adsorption of laminin onto poly(L-lactic acid) (PLLA)/PLGA polymer blend nanofiber scaffolds boosted cell viability and proliferation (Thomson et al., 2011). The asset of these coating techniques is that the nanofiber scaffolds are not altered in their bulk size and mechanical properties, but only improved in their cell culture supporting properties. When produced under Good Manufacturing Practices (GMP) conditions and with the use of xeno-free materials, these modifications will not deny the scaffolds' translatability to the clinic.

Poly(lactide-co-glycolide) scaffold

The PLGA is one of the most common synthetic polymers explored and used in scaffolding for tissue engineering (Gunatillake et al., 2006). The polymer is US Food and Drug Administration (FDA) approved, biocompatible and biodegradable (Makadia and Siegel, 2011). This latter property owes to hydrolysis of the ester linkage into lactic and glycolic acids, which are subsequently metabolized by the body. By varying the ratio of lactic to glycolic acid subunits, the initial thickness and degradation profile of PLGA can be controlled (Gunatillake et al., 2006). PLGA can be blended with other synthetic polymers such as PLLA to form scaffolds with different mechanical properties (Lim et al., 2004).

RPE cells have been successfully cultivated on the PLGA scaffold, with the advantage that PLGA degradation rate can be tailored with the formation and maturation of the RPE monolayer (Giordano et al., 1997). Lu et al. manufactured thin films of PLGA with a controlled thickness of less than 10 µm. These thin films of biodegradable PLGA could provide suitable substrates for the RPE cells and may serve as temporary carriers for subretinal implantation of organized sheets of RPE (Lu et al., 2001, 1998). Further research revealed that over this scaffold, the RPE cells are able to secrete their own ECM and form a BM-equivalent structure (). In preclinical studies, it has been demonstrated that the subretinal implantation of the RPE monolayer onto PLGA scaffold allowed the integration of the cells in the pig eye following a complete degradation of the PLGA (Sharma et al., 2019).

1.6 PRODUCTION OF AN ADVANCED THERAPY MEDICINAL PRODUCT

In the progress toward a stem cell based RPE therapy there are critical steps that must be undertaken for a successful transition from bench to bench side. These steps have many challenges, all of them aiming to validate the quality of the transplanted cells, along with their purity, functionality and survival. The effectiveness of the cell therapy is dependent on a whole-of-problem strategy involving a compliant GMP manufacturing process that ensures the safety and long-term integration of the cell therapy product. I*n vitro* and *in vivo* studies in animal models are then mandatory to demonstrate the safety and efficacy of this product. Lastly, the development of surgical delivery and follow up approach to assess subretinal integration and efficacy in AMD patients represent further steps in the long pathway toward the clinic.

1.6.1 Regulations

With the onset of cell replacement-based products as novel treatment options for these unmet clinical conditions, the regulatory bodies have met significant challenges to guarantee patient safety as the foremost priority.

Within Europe, the European Medicines Agency (EMA) is the competent agency responsible for the issue of European regulations on the production of medicines for human use. For their approval, regenerative medicine therapies must adhere to Regulation n° 1394/2007/EC, outlining the requirements to reassure high standards of quality and safety of the medicinal products.

Conventional medicinal products have been developed following GMP guidelines. These guidelines describe special aspects throughout the manufacturing process and quality control that aim to minimize or eliminate any hazardous to the final product and define general measures to ensure that all the processes necessary for production and testing are clearly defined, validated, reviewed, and documented (World Health Organisation (WHO), 2014). In the Regulation n° 1394/2007/EC, the European Parliament reclassified gene therapy, somatic cell therapies (including stem cell therapies), and tissue-engineered products as advanced therapy medicinal products (ATMPs), requiring for their manufacturing the same GMP standards as for conventional medicinal products. Facing the need

of a safely regulation of these ATMPs development put significant effort to the regulatory bodies, who had to keep up to date and amend/implement relevant legislation to apply to their production and provide the appropriate quality assurance (Pearce et al., 2014). In Italy, the Italian Medicines Agency (AIFA) is the competent authority regulating ATMPs and their safe manufacture to GMP standards, as well as approving investigational medicinal products in clinical studies. The same AIFA authorizes their use as investigational new drug in clinical studies. In order to be marketed in Italy, a medicinal product must be granted a Marketing Authorisation (MA) by AIFA or the European Commission. The MA is issued following proper application submission consisting of a dossier containing information on chemical-pharmaceutical, preclinical and clinical aspects. All the data and studies provide to support the application for MAs shall comply with guidelines defined by EMA.

Stem cell-based therapies have stringent regulatory requirements because of the nature of the therapeutic unit as a complex biological entity. The roadmaps established by the regulatory bodies are necessary to achieve successful clinical outcomes and useful in facilitating the widespread delivery of these products in the field of retinal regenerative medicine (Bharti et al., 2014).

1.6.2 Preclinical studies

The production of a cell therapy product in a GMP-compliant clinical trial setting can be extremely challenging. GMP standards require an extensive workload in which multiple areas of expertise must cooperate into an extensive network to fulfil every step of the process (Hartmann-Fritsch et al., 2016). Several disciplines are involved in the transition from the research stage to clinical and commercial applications including cell biology, microbiology, engineering, quality assurance and clinical operations. The common endpoint among these areas is to ensure the safety and the efficacy of the candidate therapeutic.

Extensive basic research is mandatory during the collection of preclinical data, which include *in vitro* and *in vivo* studies. During this stage, the development and implementation of quality control assays are mandatory to ensure the compliance of the product within appropriate parameters and to support the following manufacturing process. Preclinical *in vitro* studies are used to qualify

reproducibility, product purity and safety, functional characteristics and stability. These tests are critical to confirm consistency of the final product and can be helpful in predicting poor manufacturing runs in real time (Campbell et al., 2015). *In vivo* studies are performed to assess toxicity, tumorigenicity and biodistribution. For iPSC-RPE cells, *in vivo* genotoxicity assay has been used to verify *in vitro* assay. Using a disease-relevant animal model or a model mimicking disease, *in vivo* studies add important information on the efficacy of the RPE transplant.

The progress in the field of regenerative medicine with pluripotent stem cells unveils serious concerns for their clinical translation that need to be addressed. Preclinical prerequisites include contaminant tumorigenic or residual undifferentiated cells in the final product that could cause tumor or teratoma, lack of any therapeutic benefit due to the presence of contaminating cell types originating from undesired differentiation, potential immune reactions (especially with hESC-derived RPE) or any accidental agents that could impact the purity of the pluripotent stem cells originating from cell banks (Jha and Bharti, 2015; Whiting et al., 2015). These risks put a considerable threat on the final product and are among the first factors that must be investigate and eventually mitigate to acceptable levels prior to continue the manufacturing process.

1.6.2.1 Toxicology

Cell therapy products carry five main safety concerns, including: (1) the presence of infectious agents such as bacteria, fungus, mycoplasma, and virus; (2) the presence of foreign substances (endotoxin and animal products); (3) the presence of contaminating hPSCs; (4) the presence of cells with undesired cell lineages; and (5) the generation of cell therapy products which are genomically unstable (Sharma et al., 2020). For the clinical study, addressing these concerns play a crucial part in ensuring the recipient of the cells will gain the best outcome. Most preclinical studies have tested tumorigenic, toxicity, and migratory profile of hPSC-derived RPE cells, in addition to confirming their sterility and lacking endotoxins. To this aim, the use of immuno-compromised animals has helped to ensure that transplanted cells survive long enough to reveal their tumorigenic potential.

1. Sterility tests of cell therapy product and all its animal origin reagents are used to confirm the absence of bacteria, fungi and mycoplasma. Sterility is

monitored at cryopreservation stages and in the final formulation. For iPSC-RPE transplant, an additional time point is due after the introduction of reprogramming factors in the starting cells. One fundamental difference exists between allogeneic and autologous cell therapy products for testing of adventitious viruses. All allogeneic products must be tested for the entire panel of adventitious viruses to rule out the possibility that a virus from a contaminated product spreads to patients that receive a contaminated allogeneic transplant (Schwartz et al., 2012). Because autologous products are delivered back to the patients they are derived from, they do not require this extensive viral testing.

2. Presence of endotoxins or animal proteins could induce an immune response against the cell therapy product leading to transplant rejection and severe adverse events. Bacterial endotoxins are lipopolysaccharide components in the cell walls of Gram-negative bacteria. They can contaminate the cell therapy product through plasticware, reagents, serum, or even water, causing inflammatory reactions if introduced with the transplant (Magalhães et al., 2007).

3. Using pluripotent stem cell-derived RPE as a cellular therapy, it is mandatory to rule out the possible formation of teratomas coming from contaminating hPSCs in the final product that can proliferate and differentiate unchecked. In mice it has been showed that a minimum of 500 hESCs is required to form teratoma when injected as pure cells subcutaneously (Cao et al., 1997). This amount corresponds to 0.5% of a clinical dose of 100,000 cells that are currently being used in most RPE transplants. In comparison, Schwartz et al. demonstrated that even 1% ESCs mixed with RPE cells in immunocompromised mice do not lead to any teratoma formation in the sub-retinal space (Schwartz et al., 2015, 2012). I*n vitro* spiking study demonstrated that hPSCs cannot survive the culture conditions used for RPE differentiation (Sharma et al., 2019). In this study, 0.01%, 0.1%, 1%, 10% iPSCs mixed with PSC derived-RPE cells were seeded on PLGA scaffolds under RPE maturation conditions. In less than 14 days, all iPSCs died, as determined by flow cytometry and gene expression analysis, confirming the notion that hPSCs cannot survive RPE differentiation conditions. Other groups confirmed similar evidence,

supporting the absence of hPSCs in the final RPE transplant (da Cruz et al., 2018; Kashani et al., 2018; Song et al., 2015). Toxicity and tumorigenicity studies are investigated *in vivo* in animals such as immune-compromised rats to assess lack of teratoma formation and viability of the transplanted cells (Khristov et al., 2018). Moreover, teratoma concern can be addressed by surgeons: by using ophthalmic instruments, they will be able to track cells within the eye. In the case of teratoma formation, the transplanted tissue could be treated with laser ablation or, as a last resort, the eye could be removed from a patient who, without the transplant, would have been rendered blind by the disease (Whiting et al., 2015).

4. Cells other than RPE and non-hPSCs that may contaminate the RPE transplant or RPE cells that change phenotype after transplantation both can be detrimental for an RPE transplant. For instance, in the case of RPE cell suspension transplants, exposure to inflammatory cytokines in a diseased environment can induce Epithelial-to-Mesenchymal Transition (EMT) in RPE transplanted cells. EMT transition causes RPE cells to lose their phenotype, become fibroblastic and form membranous scars that can lead to severe vision loss. These membranes were detected in some patients that received a suspension of RPE cells (Schwartz et al., 2015, 2012). EMT is not a prominent concern for RPE monolayer graft patch, because cells are able to exit the cell cycle when cultured on the patch structure and become fully-polarized, thus reducing the possibility of EMT.

5. Previous publications have suggested the issue of hPSC genomic instability when maintained for extended time in culture, and/or during cell passaging process. In the case of iPSCs, genomic alterations can be acquired during reprogramming process or can be enriched from pre-existing genetic mosaicisms in source cells (Turinetto et al., 2017). If this happens, hPSCs may become genomically unstable and acquire karyotypic abnormalities, and/or copy-number variations and mutations. These events can cause the final product to become tumorigenic or acquire unstable or incomplete phenotype (Mandai et al., 2017; Merkle et al., 2017; Peterson and Loring, 2014). The proof of hPSCs genomic imbalance was highlighted in two recent publications. Merkel et al. showed that when hESCs and iPSCs were cultured for extended periods, they enriched p53 mutations (Merkle et al.,

2017). Although most cell lines tested in this study were generated under non-GMP environment, this observation is supported by previous work showing that cells in culture tend to accumulate genomic alterations that provide survival advantage (Avery et al., 2013; Rutledge et al., 2016). Copy number variations in clinical-grade iPSCs reprogramed from AMD patient's skin fibroblasts were reported my Mandai et al (Mandai et al., 2017). To reduce and control the likelihood of these changes in the cell therapy product, some measures must be taken. Regular metaphasic karyology checks throughout the process and oncogene exome sequencing can help in detecting any chromosomal abnormalities and provide information about the safety of the cell therapies derived from hPSCs. For iPSCs, recent work reported that oncogenic mutations may be avoided by using CD34+ cells as a starting source for iPSCs, since CD34+ cells are progenitor in nature and continue to retain their proliferative potential when expanded *in vitro* (Sharma et al., 2019; Sidney et al., 2014).

1.6.2.2 Functionality

The functionality of a cell therapy product is another critical quality attribute that competes for its success. The first step must be to ensure that the RPE cells derived *in vitro* are as comparable to the native RPE tissue as possible The RPE presents several functional properties that can be assessed *in vitro* to validate an RPE monolayer graft patch. Structural and functional validation assays have been used in preclinical and clinical studies. Among these, there is the morphology evaluation of the RPE monolayer, confluency and pigmentation (da Cruz et al., 2018), expression of typical RPE markers (Sharma et al., 2019; Souied et al., 2017), measurement of barrier function (Miyagishima et al., 2016; Sharma et al., 2019), polarized cytokine expression (Miyagishima et al., 2016), functional intracellular calcium signalling (Kashani et al., 2018; Sharma et al., 2019), POS phagocytosis (Kashani et al., 2018; Sharma et al., 2019), maintenance of ion balance in the sub-retinal space () and water transport from the apical to basal sides (Miyagishima et al., 2016; Sharma et al., 2019).

Functional features of the RPE transplant depend upon its monolayer properties. Thus, testing the ability of the cells to perform these functions represents also a way to evaluate structural hallmarks of the RPE monolayer such as tight junction

complexes between neighboring cells, appropriate apical-basal polarization of the cells and integrity of signalling pathways that occur into the cells.
Furthermore, addressing functional capabilities of the RPE transplant is important to show the ability of the cell therapy product to consistently recapitulate native RPE cell functions *in vitro* and to investigate batch-to-batch or donor-to-donor variability in manufacturing runs. Measurements of global gene expression patterns or visual inspection of the RPE monolayer alone, although simple, may not be sufficient to provide complete insight into RPE physiology or be able to address batch-to-batch or donor-to-donor variability in manufacturing runs (Sharma et al., 2019). The presence of this variability can provide insight into the potential safety of the transplant and distinguish among transplantable and non-transplantable patches. This functional validation becomes imperative as a required readout before commercial approval of the cell therapy product.
In vivo, retinal imaging and functional testing techniques allow researchers to track the survival and measure the functional capacity of the transplanted cells.

1.6.2.3 Efficacy

In vivo studies are performed to investigate the efficacy of the transplanted healthy hPSC-derived RPE cells to replace the damaged RPE. The efficacy of the candidate cell therapy product is tested in a disease-relevant animal model or a model that mimics disease conditions. An ideal animal model able to replicate disease pathology of AMD do not exist at the moment. As mentioned before, most efficacy studies have used the RCS rat model. A limitation in the use of the RCS rat is that the RPE does not generate and the therapeutic benefit owed to the transplant is its ability to clear out POS debris that accumulates in this model. In addition, even only a surgical intervention can provide photoreceptor protection in this mutant rat (Silverman and Hughes, 1990). Despite these premises, studies showed that these effects do not last over the long term (McGill et al., 2017, 2012), leaving the reliability of using these rats for testing RPE transplant activity at longer timepoints.

Feasibility and safe-delivery of the RPE-patch have been investigated in pigs and monkeys using a surgical procedure and delivery tools similar to those planned for human surgeries (da Cruz et al., 2018; Fernandes et al., 2017; Kashani et al.,

2018; Mandai et al., 2017; Sharma et al., 2019). Sharma et al. published the first study on the use of a large animal model for testing the efficacy of a human clinical dose of an RPE transplant. A 2×4 mm human iPSC-RPE patch was implanted into an acute RPE injury model pig eye. This model displayed photoreceptor degeneration triggered by laser induced RPE-cell death and recapitulates some features of AMD pathology (Sharma et al., 2019). In the study, the implant was transplanted into the pig eye before the photoreceptors degenerate. Ten weeks later, the graft was shown to integrate into the subretinal space, along with improved indicators of retina health and gradual recovery of retinal function assessed by multifocal electroretinograms (mfERG). As a comparison, Sharma et al. found that the same number of iPSC-RPE cells did not achieve the same outcome in rescuing laser-damaged pig photoreceptors when injected as a suspension of cells, supporting the superiority of the RPE monolayer over a RPE suspension in rescuing photoreceptor degeneration.

1.6.2.4 Clinical dose and delivery

The clinical dose and the surgical tool used in the transplantation studies are another critical variable. In this regard, various approaches have been tested for delivery of RPE cells in suspension or as a patch. The injection of cell suspension depends upon an injection cannula, while the transplantation of a patch is more complicated, given the fact that in many cases requires folding a large in size RPE patch and unrolling it in the sub-retinal space (da Cruz et al., 2018), or embedding an amniotic membrane patch in gelatin to provide strength during surgery (Ben M'Barek et al., 2017), or a large sclerotomy (2.5 mm) (Sharma et al., 2019). The design of the device significantly differs between procedures depending upon the delivery approach. A well-designed injector should allow a safe and reproducible transplantation procedure, together with minimal damage to the host retina and preventing significant cell loss during implantation (Fernandes et al., 2017). Overall, transplantation tools can be classified based on type of transplant (suspension versus rolled or flat RPE-patch), the sizes of the cannula and of the implant (dosage) and type of tool operation such as viscous fluid injector or manual (push button, plunger, rotary control) (Sharma et al., 2020). In any case, the patch transplant procedure is surgically more invasive, may require longer recovery times, and often also result in a scar on the retina. At this stage, longer-

term studies with more patients for each category will provide useful data to understand if the advantages of transplanting an RPE-patch can outweigh the disadvantages of a more invasive surgical procedure.

1.6.3 Manufacturing

Once the preclinical work has completed and the regulatory and ethical approval have been obtained, the manufacturing of the ATMP can begin. The whole process must be performed in a GMP environment holding a manufacturing license for investigational new medicine products. The translation of the cell therapy production to a GMP compliant manufacturing process can be though based on the complexity of the initial model. Therefore, the long differentiation methods to derive RPE cells bring considerable challenges to the whole process, especially in the case of direct differentiation approaches involving the use of multiple exogeneous growth factors aiming to reproduce the neuroectoderm developmental biology of the eye.

The manufacturing timelines of hPSC-derived therapies are relatively long compared to conventional medicines, particularly if they required a maturation phase at the end of the differentiation process. During long manufacturing protocols, intermediate quality control breakpoints are desirable in order to avoid issues that might end up with a failure of the manufacturing run and the inevitable loss of resources. In the case of sterility for example, if the manufacturing run is not terminated, the contamination can spread to other runs.

The inclusion of cryopreservation steps is strongly recommended at appropriate stages of the process. The cryopreservation steps also allow to perform quality tests to be done on the batch of cells that will be transplanted. These steps allow This facilitate the distribution of the product to additional facilities, as well as reducing the costs of ongoing cell cultures and the loss of material if a patient is not recruited in time.

Before manufacturing under GMP conditions starts, it is of utmost importance to define the reagents intended to be used. All the ancillary materials choose for cell culture must meet regulatory standards for clinical-grade manufacturing and diminishing concerns about purity and quality. Thus, change of suppliers and batch variation are undesirable.

Clean areas for operations are controlled for particulates and microbial contamination, that have to be kept to a minimum level. The same areas are classified according to specified particle limits. RPE cells production occurs out in Grade A, intended as the most critical area where the cell product is manipulated and particle limits are at a minimum. To control these levels, air-handling unit are in charge of maintaining temperature, humidity and different pressures between the rooms. Particles and contaminant are removed with the outward airflow created by a positive pressure gradient throughout the facility (Sheth-Shah et al., 2016).

The policies, procedures and controls in need to create and deliver high-quality product specification are documented by a quality management system (QMS). The main goal of this entity is to help a facility to meet its regulatory requirements throughout the manufacturing process. The QMS includes all of the activities an organization does to verify the suitability of the product for its purpose. Employment of the QMS should work in limiting significant risks that might affect the manufacturing runs.

Validations and service-level agreements are two key quality assurance aspects that influence the manufacturing process. Validating the function of the cleanroom, equipment, reagents, and processes according to their own purpose ensure product safety and function. A service-level agreement defines the level of service expected from a vendor and in this case is related to the traceability of every material and reagent used during the manufacturing process. The agreement ensures the requirements of both parties are maintained and the quality and specification of each item used for manufacturing is consistent every time.

Operators working in a cleanroom are obliged to strictly follow standard operating procedures and protocols agreed with the quality assurance manager. From these measures, it is imperative they cannot deviate.
Even if under restricted protocols, certain stages during the manufacturing process require some flexibility, especially while working with living cells. To avoid additional risks when a variation to the stipulated protocol must be performed, production “windows” are established during the process validation of each step with the aim of demonstrating that the safety and efficacy of the product is accurately preserved.

Even in the presence of considerable challenges, the accurate awareness of the entire process and the compliance of the regulatory requirements pave the way for regulatory approval and the translation of these cell-replacement therapies into the clinic.

1.7 CLINICAL TRIALS

Multiple therapies with different rationales and mechanistic approaches have moved forward to the clinic. An outline on the most debated clinical trials of the last years concerning hPSC-RPE cell transplantation is reviewed below. Table 2 reports keys information of ongoing clinical trials involving hPSC-RPE cells. Figure 8 shows a cartoon of the mentioned clinical study.

Astellas Institute for regenerative Medicine, Astellas Pharma Inc.

Schwartz et al. were the first to transplant a hESC-derived RPE cell suspension into the subretinal space of human patients having dry AMD and Stargardt disease in a phase I/IIa trial (Schwartz et al., 2015, 2012). In this landmark study, the authors used the MA09 hESC line and allowed them to differentiate into embryoid bodies with pigmented RPE cells. Pre-clinical studies were performed in three animal models (small rodents) by injection of a dose of hESC-RPE cells subretinally to confirm integration of the transplanted cells. No evidence of teratoma formation was shown and visual function as well as light sensitivity thresholds improved compared to controls.

The study in human included nine patients with dry AMD (median age: 77 years) and nine patients with Stargardt disease (median age: 50 years), who were divided in three dose cohorts ranging from 50.000 to 150.000 cells. First endpoint was the safety of the injected cells in the patients. After a two-year patient follow up, hESC-RPE cells were safe and did not cause any serious adverse events. There was no evidence of teratoma formation or hyperproliferation and the immunosuppression administered did not lead to any subretinal inflammation in the treated eyes. Second endpoint was efficacy of the transplanted cells. Enrolled patients were examined for visual acuity, visual fields, OCT, fundus autofluorescence, FA and electroretinography. Main limitations of the study were

the small number of patients that did not allow a statistical analysis, and the complexity of visual acuity measurements in patients with advanced GA. However, best corrected visual acuity (BCVA) improved or remained stable and 13 out of 18 patients showed subretinal pigmentation at the border of the transition zone as a possible sign of cellular integration and survival.

Patients with Stargardt disease were included in the study in order to investigate the relative effect of a diseased Bruch/choriocapillaris complex to the transplanted cells. These patients are younger than patients with dry AMD and they should not show a senescence BM along with thin choriocapillaris, which may instead affect the survival and engraftment of the transplanted cells in relatively older dry AMD patients. The treated area was an area close to the macula. This transition zone between healthy retina and an area of severe atrophy could recapitulate an early disease stage and represents therefore an optimal target for the cell therapy approach.

This study was the first-in human safety study and it laid the foundation for the next generation of RPE cell therapies in terms of identification of the optimal state of the disease in which intervene, appropriate study design and accurate methods to measure efficacy.

RIKEN Laboratory of retinal regeneration, Kobe, Hyogo, Japan

This was the first study involving iPSC-RPE cells, which were delivered as a patch of cells without any additional substrate in a 77-year-old Japanese woman patient with non-treatable form of CNV (neovascular AMD) (Mandai et al., 2017). For this study, the primary endpoint was proving the safety of the iPSC-RPE sheet prepared *in vitro*, along with the assessment of the transplantation procedure. The clinical efficiency (retinal morphology and visual function) was considered as second endpoint after surgery. After initial removal of the neovascular membrane, the surgery was performed with a custom-designed hand piece and a cannula (Kamao et al., 2017) and the iPSC-RPE cell sheet was delivered under the macular area. No adverse events were observed after surgery. Fundus photography and OCT revealed the presence of an intact transplanted sheet of cells after 2 years follow up, indicating successful engraftment and lack of rejection (Mandai et al., 2017). Nevertheless, there was not any evidence of BCVA improvement during the follow up period. The patience experienced “brighter

vision” probably due to the CNV membrane removal and stopped the anti-VEGF injections. After 1 year follow up, the OCT showed good retinal integrity over the graft and there was not any sign of recurrence CNV. The transplanted cell sheet survived up to 3 years after surgery, with no tumor formation nor rejection. Photoreceptors were maintained only in the are adjacent to the graft.

A second patient (68-year-old male) with polypoidal choroidal vasculopathy was enrolled in the study. Whole genome and exome sequencing performed on this patient’s iPSC and iPSC-RPE unveiled the presence of two driver mutations that occurred during the reprogramming process. Owing to these genetic alterations, the ethical committee recommended to halt the study, even if all the *in vivo* tumorigenicity tests were negative. The transplantation was still suspended in view of the moderate activity of the neovascular membrane and the stability of the visual acuity under the anti-VEGF treatment.

This study was considered a pilot study in the field of autologous transplantation of iPSC-RPE. It also pointed out the need for a consensus on the criteria for genome integrity and the possible large-scale limitations of the feasibility of this type of transplantation related to this issue (Singh et al., 2020).

Regenerative Patch Technologies, LLC

Following the example of the RPE monolayer, other research groups developed an ideal therapeutic substrate to use in the clinical trials. The patch of RPE cells could therefore address degenerative changes in the native BM of the AMD patients and provide correct cell functionality to ensure the long-term efficacy of the cell therapy.

hESC-RPE cultured on ultrathin parylene membrane has been transplanted as part of a Phase I/IIa clinical trial held by Kashani and colleagues at the University of Southern California Roski Eye Institute (NCT02590692) and sponsored by Regenerative Patch Technologies (Kashani et al., 2018; Lu et al., 2012). The investigators of the study, named the California Project to Cure Blindness-Retinal Pigment Epithelium 1 (CPCB-RPE1), implanted a patch of RPE cells derived from hESCs (NIH-H09 line) coupled with a synthetic parylene membrane scaffold in the worse-seeing eye of 16 subjects with advanced dry AMD. The trial aimed to assess the safety and tolerability of the transplanted monolayer. With six microns thickness and a nonporous anterior surface which enabled the adherence of the

overlying hESC-RPE cell sheet, the parylene membrane mimicked BM in its molecular exclusion characteristics (Singh et al., 2020). A pattern of circular indentations (50 microns in diameter) were designed to allow bidirectional diffusion of solutes such as nutrients and growth factors for supporting cell survival after transplantation. Membrane dimension was 3.5mm x 6.25 mm and supported nearly 100.000 mature hESC-RPE cells on top. For delivery purpose, a custom-designed surgical insertion forceps was manufactured and FDA-approved for the trial.

A subretinal haemorrhage event was reported during routine follow up, but it was considered to be related to the surgical procedure (Kashani et al., 2018) and the authors confirmed its resolution during the last follow up visit at 180 days. In addition to this adverse event, mild or moderate intraoperative or postoperative haemorrhages were reported in all other subjects, but they resolved spontaneously. Not any uncontrolled proliferation or off target cell delivery was documented, indicating that the hESC-RPE cells remained attached on the parylene substrate during and after the surgical implantation procedure. Kashani et al. reported a gain in visual acuity of 17 letters and visual fixation ability improvement in one patient (Kashani et al., 2018) and stability of visual acuity in other subjects over the study period. In some subjects, signs of outer retinal lamina restoration in areas overlying the graft were detected by high resolution *in vivo* imaging. Even in the absence of histological data, these observations were taken as possible photoreceptor layer restoration and/or integration with the ESC-RPE cells of the implant.

Pfizer

The London Project to Cure Blindness collaborated with Pfizer (London, UK) for the treatment of 2 patients out of a planned 10 in a Phase I/II clinical trial (NCT01691261) (Carr et al., 2013). Patients with severe exudative wet AMD were treated with a patch of hESC–RPE immobilized on a polyester membrane. The RPE patch measured 6 x 3 mm (total area 17 mm^2) and covered with approximately 100.000 cells which overlaid most part of the macula (da Cruz et al., 2018). RPE cells were generated from SHEF-1.3 hESC line using a spontaneous differentiation protocol. The synthetic membrane was made of PET), coated with human vitronectin and characterized by a thickness of 10 microns and pores of 0.4

microns (pore density 1 x 10^8 pores per cm^2). For grafting, the patch was cut with a purpose-built punch prior to implantation. The surgical tool was designed to avoid damage of the cellular patch. The clinical study aimed to address safety issues (primary outcomes) and long-term survival and functionality of hESC–RPE (secondary outcomes).

To rule out the potential intraocular neoplasm formation, the authors performed *in vitro* cell-spiking studies and mouse teratoma during preclinical safety assays (da Cruz et al., 2018). NIH III mice were injected with hESCs or hESC-RPE cells in suspension. Only the mice that received the undifferentiated cells formed teratomas. After 26 weeks, pigmented hESC-RPE cells were detected on the vitreous cavity. However, these non-subretinal cells did not form tumors and the cells retain their RPE phenotype. As for the spiking studies, the addition of undifferentiated hESCs (from 1% to 50% dose of the total cells) into the RPE cell culture did not show any negative effect on the resulting RPE cultures, supporting the hypothesis that hESCs are not able to survive RPE cell culture conditions.

In-vivo imaging modalities were used to assess anatomical outcomes following transplantation. In the first patient, OCT showed an overlapping between the native RPE and the patch in one area of the implant. The latter remained covered by the hESC–RPE cells for 12 months. Over six months, darker pigmented areas were seen to grow into areas that were contiguous with the patch, representing a possible migration of the cells out of the PET membrane. Long term data will be needed to verify that these cells would not change if not lying on the PET membrane and vitronectin coating. One patient gained visual recovery of 29 letters after 12 months, while second patients showed +21 letters. Nevertheless, the absence of control eyes did not allow for any direct comparison.

Full field electroretinography (FF-ERG), which measures the summed function of all retinal photoreceptor cells, showed a reduction in global photoreceptor function at six months in both patients that recovered only in the second patient by the end of the observation period of 12 months. The exact cause of this disorder was unclear. The majority of the photoreceptor cells were not affected by wet AMD and were located distant from the implant and outside the macula, and by this result have shown a possible reduction in functionality. On the contrary, the macular photoreceptors over the implant, demonstrated functional improvements from baseline. It could be that the global reduction in photoreceptor function blunted the functional improvements detected in the macular photoreceptors.

Three serious adverse events were described by the authors, including suture exposure in patient one and a retinal detachment in patient two and an epiretinal band causing focal traction on the macular surface. The detachment was associated with proliferative vitreoretinopathy (PVR) and specified as a tractional retinal detachment that was distant from the implant. In the case of PVR development, a possible explanation could be the presence of the hESC-RPE cells on PET membrane or at off-target locations.

All the concerns highlighted in this study (retinal detachment, PVR, macular traction, unanticipated cellular proliferation or migration) will need more evaluation in longer than 12 months follow up period. In light of these initial data, manufacturing and delivering a hESC-RPE monolayer supported on a synthetic basement membrane in patients with recent-onset exudative AMD could represent a viable alternative to the typical current medications with intraocular anti-VEGF therapies.

National Institutes of Health, Bethesda, MD, USA

The clinical study carried out at the National Eye Institute and the National Institutes of Health (Bethesda, MD, USA) aimed to transplant iPSC-RPE paired with PLGA membrane for autologous cell therapy. This has been the first trial using a biodegradable scaffold made of PLGA with the aim of providing a temporary substrate for implantation, but ultimately allowing the RPE monolayer to interact with patient's existing BM (Liu et al., 2014). Sharma et al. described a safe and efficient protocol to generate iPSC-derived-RPE (Sharma et al., 2022). This RPE derivation method was translated into a GMP-compliant manufacturing protocol. The obtained iPSC-RPE cells were grown on the PLGA scaffold to create a polarized RPE tissue that was functionally tested *in vitro* and *in vivo* preclinical studies (Bharti et al., 2014; Sharma et al., 2019). The first patient having wet AMD with advance GA underwent surgery on summer 2022. Follow up with reported outcomes are not yet available.

***Table 2**: Summary of ongoing stem cell-derived RPE tran*

Author	Clinical trial number	Phase	Condition	hPSC source	Follow-up period	Patient population	Sponsor/collaborators
Schwartz et al., 2012; **2015a**; **2015b**; Song et al., 2015	NCT01345006	I, IIa	Stargardt macular degeneration	hESCs (MA09), allogenic	Median 22 Months	11 (20-71 years)	Astellas Institute for Regenerative Medicine
	NCT01344993	I, IIa	Dry AMD	hESCs (MA09), allogenic	Median 22 Months	11 (70-88 years)	Astellas Institute for Regenerative Medicine
	NCT02463344	Long term follow-up of phase I/IIa trial	AMD	hESCs (MA09), allogenic	60 Months	11 (55 years and older)	Astellas Pharma Inc
Mandai et al., **2017**	Not available	I, IIa	Wet AMD	Autologous iPSCs	12 Months	1 (77 years)	RIKEN Laboratory of Retinal Regeneration
Kashani et al., **2018**	NCT02590692	I, IIa	Dry AMD	hESCs (H09), allogenic	4 - 12 Months	5 (69-85 years)	Regenerative patch technologies, LLC
da Cruz et al., **2018**	NCT01691261	I, IIa	Acute wet AMD	hESCs (CSHEF01), allogenic	4 - 12 Months	2 (60 years and older)	Pfizerl University College, London
Sharma et al., **2019**	NCT02903576	I, IIa	Dry AMD with GA, Stargardt's, RP	Autologous iPSCs	12 - 60 Months	1 (55 years and older)	National Eye Institute/NIH

neration; GA, geographic atrophy; hESCs, human embryonic stem cells; iPSCs, induced
al; RP, retinitis pigmentosa.

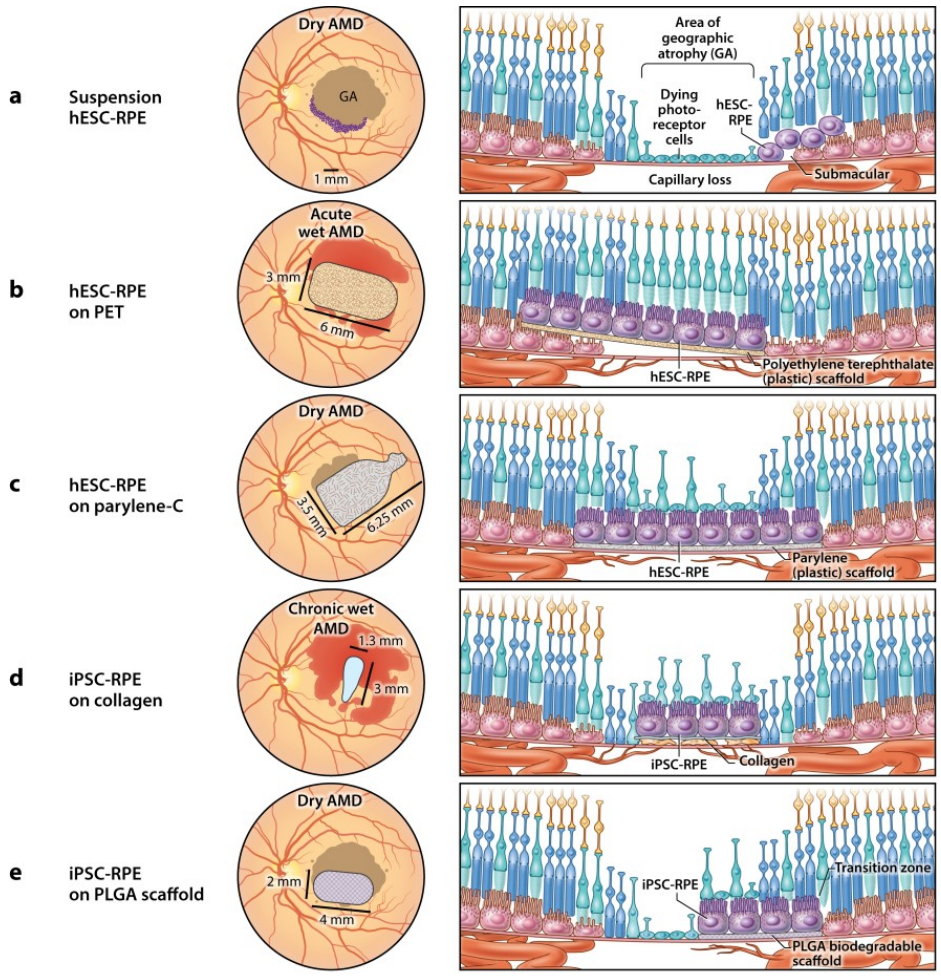

***Figure 8**: Schematic of various ongoing and planned retinal pigment epithelium transplant approaches (Sharma et al., 2020), showing fundus views of the transplants (left) and how the transplants (purple) would be integrated into the subretinal space, their possible impact on retina and choroid, and the various scaffold materials involved (right). (**a**) Schwartz et al. (Schwartz et al., 2012) injected hESC-RPE cell suspension in the submacular region. hESC-RPE cells in suspension do not form a polarized monolayer but stay as a bolus of rounded nonpolarized cells in the submacular region. (**b**) da Cruz et al. (da Cruz et al., 2018) transplanted a hESC-RPE patch over the area of acute choroidal neovascularization. This 3 × 6-mm transplant was intended as an actual patch over the area of acute CNV. The RPE patch helps stop CNV and rescues photoreceptors that may not have degenerated in these specific patients. (**c**) Kashani et al. (Kashani et al., 2018) used a hESC-RPE patch on a parylene scaffold, transplanted in the area of GA. Change in fixation point to over the area of the hESC-RPE patch was observed in three patients, suggesting that the RPE patch was able to recover the activity of a few photoreceptors in the transplanted region. (**d**) Mandai et al. (Mandai et al., 2017) tested the first autologous iPSC-RPE patch in an acute wet AMD patient. This patch was transplanted in a macular region that was fibrotic due to chronic vessel leakage. One-year follow-up in this patient revealed the absence of new leaks. (**e**) Sharma et al. (Sharma et al., 2019) propose to transplant an autologous iPSC-RPE patch using a PLGA scaffold at the border of the GA lesion. This patch is intended to cover parts of the transition zone where the photoreceptors are still alive to slow down or halt the expansion of the GA lesion (adapted from Sharma et al., 2020). AMD, age-related macular degeneration; hESC,*

human embryonic stem cell; iPSC, induced pluripotent stem cell; PET, polyethylene terephthalate; PLGA, poly(lactic-co-glycolic acid); RPE, retinal pigment epithelium.

2. STUDY DESIGN

Several RPE-transplant approaches are currently ongoing and planned for the treatment of a wide range of retinal degenerative diseases. Although the RPE cell therapies investigated may have distinct formulation, they share common principles, challenges and issues across the clinical development pipeline.
To date, safety data from Phase I/II clinical trials of RPE stem cell transplantation have been published. However, evidence of serious adverse events has emerged from these studies, leaving a deep gap in the establishment of an effective and harmless treatment for these blinding conditions.

The main goal of this study was to generate an alternative allogenic hESC cell-based cell therapy product for the dry form of AMD. For developing the hESC-RPE patch, different scaffolds have been tested (both biological and synthetic). The pluripotent- derived RPE cells on scaffold underwent morphological and functional characterization prior to transplantation into the subretinal space of rats. Predefined end point criteria included RPE monolayer viability and functionality over the investigated scaffolds, biomechanical characterization of define substrates, histological evaluation and OCT analysis.

3. METHODS

3.1 DIFFERENTIATION OF PLURIPOTENT STEM CELLS TO RPE LIKE CELLS

The hESC line H09 from WiCell Research Institute (Madison, WI, USA) was used for the entire research and subjected to both methods of differentiation described below. The iPSC line AMDCD was used later in the project. The addition of this cell line to the study aided data for comparison and consistency of the results.

3.1.1 Pluripotent stem cell culture system

The state of the hPSC culture is one of the critical factors determining the efficiency of RPE differentiation. Therefore, ensuring a good hPSC culture's health is mandatory for further differentiation.

H09 hESC line was derived, banked and provided by WiCell (WiCell Research Institute). These cells were cultured for 29 passages prior to freeze. Genetic profile (including G-band karyotyping and Short Tandem Repeat analysis) and sterility of the cells was established by the WiCell Research Institute Quality Department (Madison, WI, USA). Initially, H09 cells were maintained in a feeder-independent culture system on well plates coated with 1.09 µg/cm^2 human recombinant laminin-521 (LN-521; BioLamina, Sweden) in Essential 8™ Flex Medium (E8; Thermo Fisher Scientific, Waltham, MA, USA) supplemented with 50 U/ml penicillin-streptomycin (Thermo Fisher Scientific). Single cell passaging with xeno-free TrypLE™ Select Enzyme (Thermo Fisher Scientific) was carried out twice a week onto 0.55 µg/cm^2 LN-521, using a plating density of 0.4 - 0.5 x 10^5 cells/cm^2.

The iPSC line used later in the experiments was generated by the National Institute of Health Center for Regenerative Medicine (NIH CRM; Bethesda, MD, USA). The line, referred as AMDCD, was derived from the fibroblasts of an 83 years old woman by episosomal reprogramming. The AMDCD cell line is considered a control line routinely used in Dr. Kapil Bharti's laboratory.

With the aim of optimizing the research-grade differentiation protocol of these two hPSC lines, a new hPSC culture platform was tested for both cell lines.
hPSCs were thawed and cultured under feeder-free conditions on Vitronectin (Thermo Fisher Scientific) coated (2.5 mg/mL) well plates. The medium (changed daily) was still E8, but without further addition of antibiotics. For passaging, the hPSCs were split as small clumps using Versene (Thermo Fisher Scientific) when culture reached 70%–80% confluency (to avoid spontaneous differentiation). After thawing, first split was at a 1:3 ratio, whereas subsequent splits could be at a 1:6 - 1:12 ratio to get the confluency of 70% - 80% by day 4–5.

3.1.1.1 Pluripotent stem cell characterization

Immunofluorescence

H09 cell culture was monitored for attachment, growth, and morphology.
Immunofluorescence labelling for pluripotency markers was done using the following antibodies: NANOG (1:200, AF1997), OCT-3/4 (1:200, AF1759), SSEA-4 (1:200, NL1435V) (all from R&D Systems, Minneapolis, MN, USA), TRA-1-81 (1:200, Sc-21706, Santa Cruz Biotechnology, Dallas, TX, USA) and LIN-28 (1:400, MA1 – 016, Thermo Fisher Scientific). The following Alexa Fluor 488- or 594-conjugated secondary antibodies were used: 1:800 donkey anti-goat IgG (A11055), goat anti-Mouse IgM (A21044), donkey anti-mouse IgG (A21202) (all from Thermo Fisher Scientific) (Table 4). Nuclei were counterstained with 4´, 6´ diamidino-2-phenylidole (DAPI) included in Fluoromount-G™ Mounting Medium (Thermo Fisher Scientific). Images were captured with Nikon Eclipse Ti-E fluorescent microscope (Nikon, Tokyo, Japan) using 40x oil immersion objective.

In vitro pluripotency assay

To assess the potency of forming the three germ layers, H09 hESCs were allowed to differentiate as embryoid bodies (EBs), followed by immunofluorescence labelling for derivative cells of the three embryonic germ lineages. Cells were detached with TrypLE™ Select Enzyme and transferred to Corning® Costar® Ultra-Low attachment plates (Corning, New York, NY, USA) in KnockOut™ Dulbecco's Modified Eagle's Medium (KO-DMEM) supplemented with 10% fetal

bovine serum (FBS), 2 mM GlutaMAX™ Supplement, 0.1 mM 2-Mercaptoethanol, 1% MEM Non-Essential Amino Acids Solution, and 50 U/ml Penicillin-Streptomycin (all from Thermo Fisher Scientific). Blebbistatin (Sigma-Aldrich, St. Louis, MO, USA) was added 10 µM for the first 24 hours. EBs-medium was changed the following day and three times a week there after. After 14 days of differentiation, the EBs were plated onto LN-521 coated plates and cultured for 7 days. The cells were then washed, fixed with 4% paraformaldehyde (PFA; Santa Cruz Biotechnology) and labelled with the following primary antibodies: alpha-smooth muscle actin (α-SMA, 1:400; MAB1420, R&D Systems) for mesoderm, SOX17 (1:200; AF1924, R&D Systems) for endoderm, and OTX2 (1:200; AF1979, R&D Systems) for ectoderm. Secondary antibodies included 1:800 A594 donkey anti-mouse IgG (A21203) and 1:800 A488 donkey anti-goat IgG (A11055) (both from Thermo Fisher Scientific). Images were acquired with Nikon Eclipse Ti-E fluorescent microscope.

3.1.2 Differentiation strategies

The hESC line H09 was derived using the two different methods of RPE derivation described below, whereas the AMDCD iPSC line was differentiated into RPE cells using only the direct differentiation protocol.

3.1.2.1 Spontaneous RPE differentiation

Differentiation of H09 hESCs into RPE cells using the spontaneous method was carried out following the protocol outlined by Hongisto et al. (Hongisto et al., 2017). Undifferentiated H09 hESCs were single-cell detached and transferred to Ultra-Low attachment plates (Corning) in 15% KnockOut Serum Replacement (KO-SR) medium, consisting of KO-DMEM supplemented with 15% Serum Replacement, 2 mM GlutaMAX™, 0.1 mM 2-mercaptoethanol, 1% MEM non-essential amino acids, and 50 U/ml penicillin-streptomycin (all from Thermo Fisher Scientific). Blebbistatin was added 10 µM to EBs formation overnight at +37 °C. For RPE differentiation, EBs underwent spontaneous differentiation in 15% KO-SR medium for approximately 4 weeks. During the first 4 days of induction the medium was changed daily, after which the EBs were transferred onto well plates coated with

0.75 µg/cm^2 LN-521 and 10 µg/cm^2 human placental type IV collagen (CIV; Sigma) in 15% KO-SR medium. The medium was changed three times a week. After this time, pigmented foci were manually separated with a scalpel and dissociated with TrypLe Select Enzyme (Thermo Fisher Scientific). The resulting singe-cell suspension was seeded to culture wells coated with LN-521 and CIV. For further passaging, the RPE cells were detached with TrypLe Select Enzyme. For phenotypic analysis, the derived RPE cells were replated 2.5 x 10^5 cells /cm^2 on similarly coated polyethylene terephthalate – tissue culture inserts (also known as Transwell inserts) with a 1.0 µm pore size (Corning) in a 24-well plate until full maturation, which occurred after nearly 12 weeks on the inserts (Figure 9). H09-derived RPE cells were characterized after approximately 9 weeks of maturation on Transwell inserts. Key RPE protein expression and localization was verified with immunofluorescence labelling as previously described. The functional capacity of the h09-RPE to phagocytose POS was assessed *in vitro* and porcine POS were kindly donated by Heli's Skottman laboratory (Tampere University, Tampere, Finland).

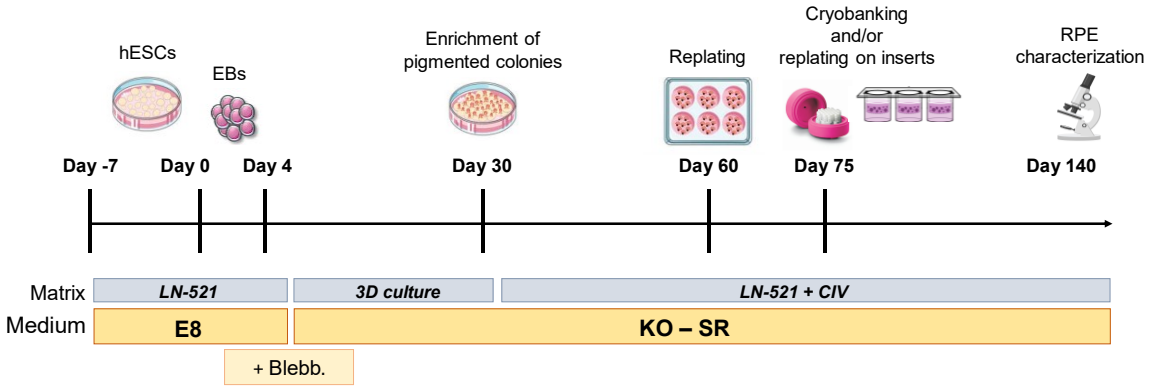

***Figure 9**: Schematic view of the initial spontaneous differentiation process carried out to generate H09 hESC-RPE cells. Blebb, blebbistatin; CIV, type IV collagen; E8, Essential 8TM Flex Medium; EBs, embryoid bodies; hESC, human embryonic stem cell; KO-SR, Knock-outTM serum replacement; LN-521, recombinant laminin-521; RPE, retinal pigment epithelium.*

3.1.2.2 Triphasic RPE differentiation

The AMDCD iPSC line was differentiated into RPE cells using a protocol developed by Sharma et al. (Sharma et al., 2019). The same derivation methodology was tested simultaneously on the H09 hESC line.

Previous studies showed that RPE differentiation from stem cells can be induced by activation of TGF and WNT pathways at the neuroectodermal stage (Idelson et al., 2009; Lamba et al., 2006; Leach et al., 2015; Reh et al., 2010). This direct differentiation approach consists of a triphasic protocol that further improves the efficiency and reproducibility of differentiation (Sharma et al., 2022) (Figure 10). First, dual-SMAD inhibition was combined with FGF inhibition to induce the formation of neuroectoderm cells from hPSCs. This decision was based on previous observations that showed that dual-SMAD inhibition promotes neuronal fate and that FGF pathway activation inhibits differentiation of the eye field into RPE (Bharti et al., 2012; Chambers et al., 2009; Fuhrmann, 2010; Meyer et al., 2009). Second, TGF-β and WNT pathways were activated to promote the commitment of neuroectodermal cells to RPE fate, as reported in literature (Carr et al., 2009; Fuhrmann, 2010; Idelson et al., 2009). Third, committed RPE were matured by treatment with prostaglandin E2 to actively suppress canonical WNT pathway through stimulation of primary cilium (May-Simera et al., 2018).

For differentiation, the two hPSC lines were seeded on Vitronectin coated 6-well plates. After 2 days in E8 medium, cells were treated for 2 days with neuroectoderm induction medium (named NEIM), which is composed by basal differentiation medium DMEM/F12, N2 supplement, B27, KO-SR (all from Thermo Fisher Scientific), 200 µM ascorbic acid (Sigma) with the addition of 10 nM LDN (Stemgent, ReproCell, Yokohama, Japan), 0.5 µM CK1-7 Dihydrochloride (Sigma), 1 µM SB 431542 hydrate (Sigma), and 1 ng/ml IGF-1 (R&D Systems). Neuroectodermal cells were next cultured in RPE induction medium for 10 days (named RPEIM), a basal differentiation medium with 100 nM LDN (Stemgent), 5 µM CK1-7 Dihydrochloride (Sigma), 10 µM SB 431542 hydrate (Sigma), and 10 ng/ml IGF-1 (R&D Systems), 1 µM PD0325901 (Sigma). Cells were cultured for 10 days in RPE commitment medium (named RPECM), composed of a basal differentiation medium containing 10mM Nicotinamide (Sigma), 150 ng/ml Activin A (R&D Systems). Committed RPE were maintained in RPE growth medium for 5 days and then reseeded to remove neuronal formations in a medium named RPEGM and containing MEM α, GlutaMAX Supplement, 5%FBS (both from Thermo Fisher Scientific), Taurine (Sigma), Thyronine (Sigma), Hydrocortisone (Sigma). Subsequently, immature RPE were cultured for 15 days in RPE growth medium (named RPEGM) and then enriched by negative selection using anti-CD24 and anti-CD56 (both Miltenyi Biotec, North Rhine-Westphalia, Germany)

antibodies. Finally, immature RPE cells were seeded onto Vitronectin coated Transwell inserts and cultured in RPE maturation medium (named RPEMM, formulated with RPEGM containing 50 µM PGE2 (Tocris, Bristol, UK) for 6 weeks to obtain fully mature hPSC-derived RPE.

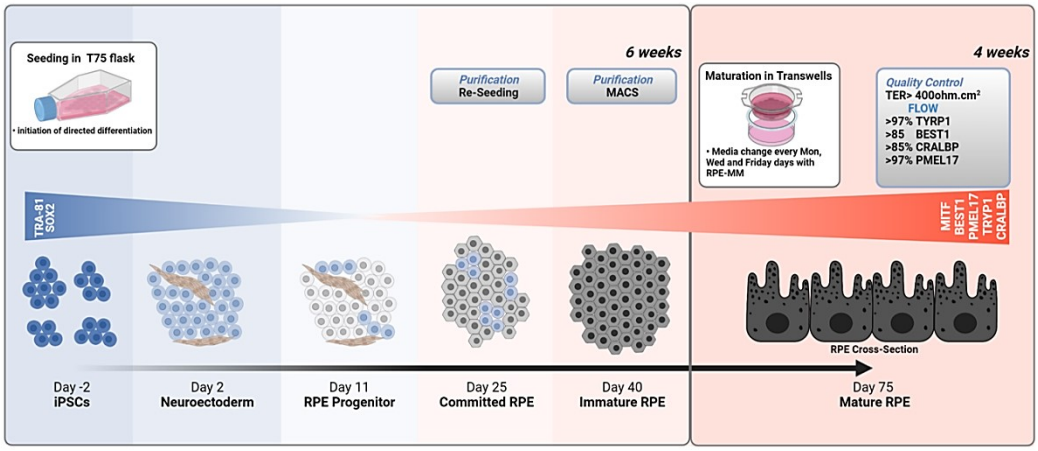

***Figure 10**: Timeline of iPSC-RPE differentiation (Sharma et al., 2022). In the first phase, an adherent monolayer of iPSCs is primed to neuroectoderm by dual-SMAD and FGF inhibition. Committed RPE cells are induced by TGF and WNT activation. RPE maturation is promoted by canonical WNT inhibition through primary cilium induction with PGE2. This protocol of RPE derivation from iPSCs takes about 10 weeks. BEST1, bestrophin 1; iPSCs, induced pluripotent stem cells; MACS, Magnetic activated cell sorting; RPE, retinal pigment epithelium; RPE-MM, RPE maturation medium; TER, transepithelial electrical resistance.*

3.1.3 Quality check

First checkpoint aimed to target the RPE cell population throughout the differentiation process, as a way to verify the production of a pure RPE cell population. These assays were established to confirm the identity and purity of the derived RPE cell population.

3.1.3.1 Flow cytometry analysis

Flow cytometry was performed on day 25 and day 40 timepoints during direct RPE differentiation to assess the % of committed hPSCs to RPE cell fate. For research grade cells, two antibodies were used at each timepoints to investigate the enrichment of RPE markers expression along the differentiation. Cells were

dissociated with Versene and counted with a hemocytometer using trypan blue exclusion. At day 25, 3.5 x 10^6 cells were washed twice with wash buffer containing 2% FBS and fixed with 4% PFA for 15 minutes at room temperature (RT). After additional washing step, the cells were put at +4 °C for further staining. The cells were then labelled overnight with primary antibodies CRALBP (1:500, MA1-813, Thermo Fisher Scientific) and TYRP1 (1:500; NBP2-32901, Novus Biologicals, Centennial, CO, USA) diluted in permeabilization buffer containing phosphate-buffered saline (PBS; Thermo Fisher Scientific) + 2%FBS + 0.2% Triton X-100 (Sigma). For day 40 labelling, 2.0 x 10^6 cells per sample were stained with the same primary antibodies. The following day, the cells were counterstained with A488 donkey anti-mouse IgG (1:1000; A21202, Thermo Fisher Scientific) in permeabilization buffer. All samples were analyzed with Becton-Dickinson FACS Calibur analyzer (Becton-Dickinson, Franklin Lakes, NJ, USA) with acquisition set to at least 10000 events per sample and gating performed with unlabelled sample. FlowJo™ software (BD Biosciences, Becton-Dickinson) was used for data interpretation.

3.1.3.2 Purity of hPSC-RPE cells

Quantitative real-time polymerase chain reaction (RT-PCR) were used to confirm the purity of the H09 cell culture. Undifferentiated H09 hESC line was taken as positive control. For gene expression analysis, total RNA was extracted with miRNeasy Tissue/Cells Advanced Mini Kit (Qiagen, Hilden, Germany) following manufacturer's instructions and RNA concentration was calculated with Qubit 2.0 Fluorometer (Thermo Fisher Scientific). cDNA was synthesized using the High Capacity cDNA Reverse Transcription Kit (Thermo Fisher Scientific), according to the kit protocol. Quantitative RT-PCR was performed with TaqMan Universal Matermix and predesigned TaqMan assays with FAM-labels (all from Thermo Fisher Scientific). The reactions were carried out on ABI Prism 7900HT Sequence Detection System (Thermo Fisher Scientific). Relative gene quantification was measured by using the $2^{-\Delta\Delta Ct}$ method. GAPDH was the internal housekeeping gene reference for normalization. Stem cell markers OCT-3/4 and NANOG were not expressed in derived RPE cells, while high expression levels could be detected in H09 cell line.

3.2 TISSUES

The following paragraph described the procurement and further manipulation of each biological membrane used in this study. No distinction was made on the basis of donor age, race, or gender.

3.2.1 hAM

All the hAMs within this study were subjected to cryopreservation and used after thawing. No fresh tissues were considered for the experiments. The impact of the cryopreservation methodology on the resulting cell cultures was not evaluated.

3.2.1.1 Procurement and banking

hAMs were obtained from the Treviso Tissue Bank (Treviso, Italy). The tissues were procured under sterile conditions during a cesarean section in mothers who signed an informed consent for placenta donation for the use either in clinic or research. Only chorion-free tissue samples negative for serologically detectable pathogens (HIV-1/2; hepatitis B, C; HTLV-I/II; syphilis; CMV) were prepared in a clean room and packed in a sterile environment. Microbiological controls were carried out during the preparation process to assess the sterility of hAMs. Patches of hAMs were fixed to a paper to maintain polarity and were cryopreserved and stored at -80°C in cryopreservation medium containing 10% dimethyl sulfoxide (DMSO) and 10% human albumin. hAMs were thawed at 37°C immediately before use and washed three times with PBS. The samples were then locked in an Amnio Ring (Harkin et al., 2017), with the epithelial side facing up, to prevent the hAMs from slipping or detaching during the treatment (Figure 11A).

3.2.1.2 De-epithelialization

Three different protocols were followed for hAM de-epithelialization: 1.) incubation with 1.2 U/mL Dispase II (Sigma) in PBS for 30 min at RT; 2.) treatment with 0.25% trypsin-EDTA (Thermo Fisher Scientific) in PBS for 30 min at 37°C; 3.) incubation with 3.75 U/mL thermolysin (Sigma) for 9 min at 37°C (Hopkinson et al.,

2006). The treated hAMs were gently brushed with an absorbent surgical sponge to remove the remaining epithelial cells. The brushing was performed under a stereomicroscope to guarantee a complete removal of the remaining hAM epithelium. Intact hAMs were retained as controls. The patches of hAM used in this study measured 10 X 10 cm. Each of these 10 X 10 cm pieces was then cut into twelve smaller pieces, in order to randomly test each de-epithelialization method in triplicate on the same donor (plus the untreated control condition).

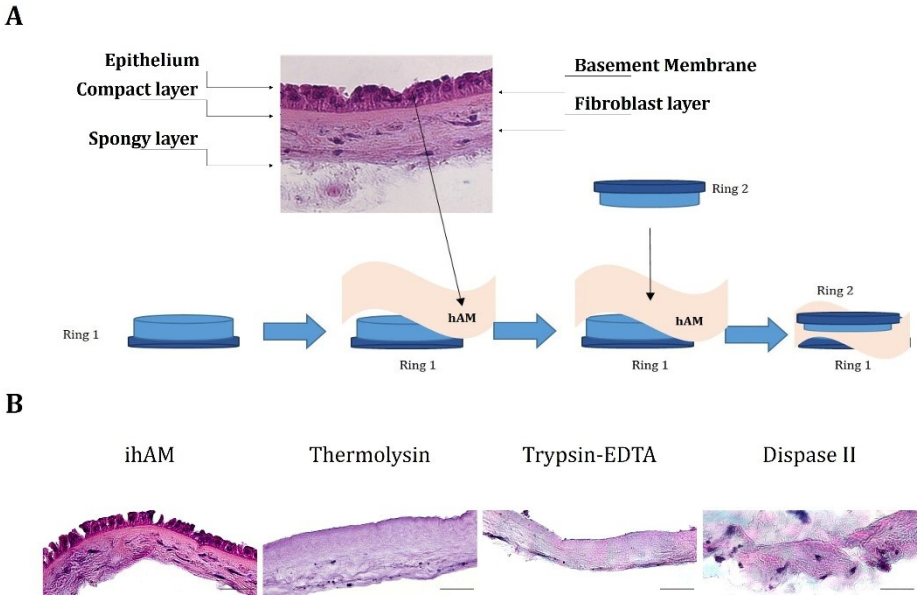

***Figure 11**: hAM preparation and de-epithelialization. (**A**) Schematic presentation of the locking of the hAM: the hAM is placed on the Ring 1 of the Amnio-Ring with the epithelial layer facing upwards. Ring 2 is placed inside to block it. (**B**) Hematoxylin-eosin staining of intact hAM and de-epithelialized hAMs after thermolysin, trypsin-EDTA and Dispase II treatment, respectively. Scale bars = 50 µm. hAM, human amniotic membrane; ihAM, intact human amniotic membrane.*

3.2.1.3 hESC-RPE cell culture on hAM

hAMs were locked into the silicon ring and treated with thermolysin enzyme as described earlier. Immobilized hAMs were placed in a 12 well tissue culture plate. H09 hESC-derived RPE cells were seeded either straight after differentiation or following thawing at a density of 2.75 X 10^5 cells/cm^2 over the epithelial-side surface of locked hAMs. The cultures were then filled with KO-DMEM supplemented with 10% FBS for its adhesion-promoting properties. Medium was changed three times a week. Cultures were maintained for up to 4 weeks. Some

H09-RPE cells derived from the same batch were cultured on LN-521+CIV-coated Transwell inserts in 15% KO-SR medium and used as controls.

3.2.2 Human Descemet's membrane

The so-called "stripping" of the corneal endothelium is a routinely practice in the Veneto Eye Bank Foundation (Venice, Italy). This procedure aims to retrieve the endothelium and the DM of donor corneas. The resulting tissue is used as a replacement of the host DM and endothelium during Descemet's membrane endothelial keratoplasty (DMEK).

3.2.2.1 Procurement and isolation

Cadaveric human corneal specimens were obtained from Eversight (Ann Arbor, MI, USA). Briefly, corneal tissues unsuitable for clinical use were assigned for research purposes with written informed consent signed by the next-of-kin on a 'Donation Disclosure and Acknowledgement' form. Donor corneas were delivered in corneal storage hypothermic medium at 4°C to the laboratory. Each cornea was placed on a vacuum block and a gentle cut was applied with a 9.5 mm Moria punch (Moria Surgical, Antony, France). The endothelium was stained with Trypan blue, in order to recognize the peripheral edge of the cut. Few drops of PBS were added on the top of the endothelium before proceeding with the following step. Using sterile forceps, a gentle stripping of the endothelium was performed from one end to the other with a longitudinal movement. The membrane was then peeled off from its original site, ensuring a complete detachment. Only a small hinge at one peripheral edge was left, thus allowing the labelling of the endothelial side of the membrane with an inverted "F" letter.

3.2.2.2 Decellularization

For decellularization, the DM was placed in a 15 mL Falcon tube containing a 1 U/mL working solution of thermolysin. The bottle was placed at 37°C for 5 minutes. The treated membrane was then placed in PBS and subjected to fast shaking for 5 more minutes to remove cellular debris. Afterwards, the DM was spread over a 24-

well culture plate or on Transwell inserts, 12-well format. DM samples were dried out and terminally sterilized using UV-C irradiation for at least 30 minutes prior to use.

3.2.2.3 Atomic force microscope analysis

For atomic force microscopy (AFM) analysis, denuded DMs were rinsed with deionized water. They were spread on top of a thin layer of 2% agarose gel and allowed to dry completely. To avoid any drift of the samples during measurements, they were firmly mounted onto a Superfrost-plus glass slide (Thermo Fisher Scientific) by slightly melting of the gel. Surface topography analysis was performed by static force mode with an Easyscan 2-controlled FlexAFM (Nanosurf, Liestal, Switzerland) equipped with a contact mode cantilever (ContAl-G, Budget Sensors, Sofia, Bulgaria) with a tip radius of 10 nm and nominal spring constant of 0.2 N/m. The nanostructures of enzymatic-treated DM and intact corneal endothelium were characterized from four randomly regions within each sample, with 256 x two-direction lines scanned at 2 µm/s. Surface roughness was calculated with Mountains SPIP 9 software (Image Metrology A/S, Copenhagen, Denmark) by means of root mean square (Sq) values of the surfaces within selected areas.

3.2.2.4 hPSC-RPE cell culture on decellularized DM

Once obtained a confluent RPE monolayer, cells were replated on top of decellularized DM (dDM). dDM samples were plated inside a 24-well culture plate (Corning) at a density of 1.6 x 10^5 cells/cm^2. To allow further phenotypic analysis of derived RPE cells, dDMs were unfolded over Transwell inserts. Similarly, H09-RPE cells cultured on LN-521+CIV-coated Transwell inserts were used as controls, since this formulation of proteins was previously used for the enrichment and the maturation of H09-RPE cells.

A new culture platform was used during the comparison study. In this case, the dDMs were stretched over Snapwell™ Inserts (Corning). An O-ring was fixed on top of the dDM to hold the membrane and allow proper tension to be achieved for further measurement of electrical resistance.

3.2.2.5 Cell adhesion and proliferation assays

H09-RPE cells seeded onto the endothelial-side surface of acellular DM were cultivated for 4 weeks with fresh medium change every 3 days. To test adhesion of viable cells, H09-RPE cells were incubated in the dark with 1 µM of calcein-acetoxymethyl ester (Calcein-AM) at 24 hours post-seeding for 35 minutes at RT. The cells were visualized with Nikon Eclipse Ti-E fluorescence microscope. ImageJ was used to quantify the number of attached cells at 24 hours. Data were obtained from four independent experiments.

The 5-Bromo-2'-deoxy-uridine Labelling and Detection Kit I (Roche, Indianapolis, IN, USA) was used to detect cell proliferation following the manufacturer's instructions. The proliferation capacity was assessed at 1-week interval. At each time point, the cells were incubated with 10 µM of bromodeoxyuridine (BrdU; Roche) for 45 minutes. After fixation with ethanol for 20 minutes at – 20°C, the cells were covered with an Anti-BrdU solution (Roche) for 30 minutes at 37°C, followed by incubation with Anti-mouse-Ig-fluorescein solution (Roche) for 30 minutes at 37°C and nuclei stained with Hoechst (1:3000; 33342, Thermo Fisher Scientific). Cells were then examined using Nikon Eclipse Ti-E fluorescence microscope. Total and positive BrdU cells were quantified from four random visual fields (20X magnification). The data were generated from three independent experiments and all experiments performed in triplicate at each time point.

3.2.2.6 Phagocytosis of labelled beads

In vitro phagocytic activity of H09-RPE cells was assessed when cultured on the dDM and compared to control condition on Transwell inserts. After one month, the cell cultures were treated with FITC-labelled latex beads (Sigma) for 48 hours at 37°C. The beads were previously washed in 0.9% sterile NaCl and resuspended 1:100 in 15% KO-SR medium. The cells were then washed three times in PBS and fixed in 4% PFA at RT. Cells were then briefly permeabilized with 0.1% Triton X-100 in PBS and blocked with 3% bovine serum albumin (BSA; Sigma) in PBS. Phalloidin (1:1000; P1951, Sigma) was used for staining actin filaments. Nuclei were counterstained with Hoechst. The internalization of beads was visualized under Nikon Eclipse Ti-E fluorescent microscope. For quantification, the number of

beads ingested was counted using ImageJ. The uptake of beads was expressed as the percentage of cells containing the fluorescence beads.

3.2.2.7 Adult human RPE cell culture on dDM

Adult human retinal pigment epithelial (ahRPE) cells were obtained from The Eye Bank for Sight Restoration (New York, NY, USA). Primary RPE cells were isolated from one donor with written informed consent for research purpose signed by the next of kin. A cryovial of 5.0 x 10^5 cells was shipped to the Veneto Eye Bank Foundation in dry ice. After arrival, the cryovial was thawed in a 37°C water bath for 3 minutes. Thawed cell suspension was centrifuged at 259 x g for 5 minutes. The cell pellet was re-suspended in base medium for ahRPE cells containing DMEM/F12 and αMEM solution with 2% FBS plus additional supplements (Fernandes et al., 2018). For initial cell thawing and plating, base medium was supplemented with FBS to achieve a final concentration of 10% (v/v) FBS. The cells where then plated in SynthemaxTM II-SC Substrate (Corning) -coated 24-well culture plate at a density of ~ 1.0 x 10^5/1.9 cm^2 and maintained in a humidified incubator kept at 37°C in 5% CO^2. The media was changed every 4th day. Cells were cultured for a minimum of 4 weeks. For gene expression analysis, ahRPE cells were plated either on dDM unfolded over Transwell inserts 12-well format (2.75 x 10^5 cells/dDM) or SynthemaxTM II-coated Transwell inserts 24-well format (0.75 x 10^5 cells/insert). These cells were not further used in the comparison study.

3.2.2.8 Real Time PCR

Total RNA was extracted from H09-RPE cells after 30 days of culture on dDM using the RNeasy Plus Mini Kit (Qiagen). The extracted RNA was retrotranscribed into cDNA using the High Capacity cDNA Reverse Transcription kit (Thermo Fisher Scientific). The resulting cDNA was amplified in a quantitative RT-PCR and analyzed with the same protocol described in 3.1.3.2 of the Methods. The relative levels of gene expression of RPE markers, including RLBP1 (also known as CRALBP), RPE65 and MERTK were determined by the comparative Ct method using the $2^{-\Delta\Delta CT}$ and normalised to GAPDH housekeeping gene. Each amplification was run in triplicate and at least three independent experiments were

analysed. H09-RPE cells and primary human RPE cells cultivated on Transwell inserts were designated as reference samples.

3.2.3 Human Bruch's membrane

Aiming to investigate the contribution of different types of scaffold to hPSC-derived RPE cell cultures, samples of Bruch's complex (intended as Bruch's membrane plus choroid) were included in the comparison study. As the physiological membrane of the RPE cells, the BM has the potential to provide the best environment for these cells. This tissue was used only during the comparison study, since the inability of using it for transplantation purposes.

3.2.3.1 Preparation of human BM explants

The eye globes were received after the removal of the anterior chamber. They were placed in a custom-made silicon mold with the sclera pinned to it with 27-gauge needles to secure the eye during the dissection procedure. The mold has a 3 cm cavity in the center, that is enough to contain a human eye, and the silicon material was chosen for its ease of mold and to allow the insertion of needles. 1 X PBS was added to the chamber to keep the sclera hydrated during processing. Since the eye was delivered without the anterior chamber, it was nearly impossible to prevent the collapse and folding of the interior layers. The retina was already detached, except for the optic nerve and the peripheral ends, where the retina fuses with the ciliary body. The vitreous humour was removed as much as possible with the use of a vitreous cutter. At this point, double distilled water (ddH_2O) was added into the eye cup for 20 minutes at RT. This step allowed complete removal of the retina and promoted RPE cells detachment. No additional scraping was needed. Floating RPE cells appeared as brownish golden spots. The eyes were then transferred to a 100 mm Petri dish filled with 1x PBS for the separation of the BM/choroid from the sclera. A punch of 12 mm diameter was used to cut round pieces of BM/choroid and sclera. At this point, the complex BM and choroid was peel off by cutting the blood vessels and the connective tissue that anchor them and paying attention not to touch any inner spot of the explant. Once separated from the underlying sclera, the BM complex were positioned on a

12 mm diameter mesh with the BM facing up. The mesh provided support for the explant. The sample was then assembled between the upper and lower parts of a CellCrown™24NX (Scaffdex, Tampere, Finland) (Figure 12). Some explants were fixed in scanning electron microscope (SEM) fixative (Electron Microscopy Sciences, Hatfield, PA, USA) for further SEM analysis. The RPE/choroid cannot be separated further. The samples locked in the Cell Crown inserts were placed in a 24-well plate and incubated overnight at 4°C in 1 X Antibiotic-Antimycotic (Thermo Fisher Scientific).

***Figure 12**: Use of the CellCrown™24X model with explant of human BM.*

3.2.3.2 hPSC-RPE cell culture on BM explants

The Cell Crown allowed to flatten the BM complex by tightly sealing the membrane between the two parts of this particular insert. By doing this, tissues positioning and stretching were optimized for further cell culture and assays. The 24-well plate containing the Cell Crown inserts were transferred in a humidified incubator and filled with RPEMM. After thawing, hPSC-RPE cells were seeded in RPEMM added with rock inhibitor Y27632 (1:1000; R&D Systems) at a density of 2.0 x 10^5 cells/cm^2 on top of the BM complex. Additional medium was put on the basal side of the insert to create two distinct compartments. Particular attention was paid to avoid the formation of air bubbles on the basal side of the inserts.

3.3 GENERATION OF POLARIZED hPSC-RPE PATCHES

For the assays described in the next section, at least four 3D cultures were used per cell line for each investigated scaffold.

3.3.1 3D culture on PLGA scaffold

Considering the ongoing clinical trial conducted by Dr. Kapil Bharti and his lab, the PLGA scaffold was taken as “gold standard” of RPE transplantation. This scaffold was provided at -20°C by Stellenbosch Nanofiber Company (Montague Gardens, Cape Town, South Africa) as small sterile patches of 1.18 – 1.2 cm diameter. Each patch was positioned under sterile conditions on the basal part of a Snapwell. A silicone ring was used to fix and flatten the scaffold on the bottom of the Snapwell. The resulting surface of the scaffold available for the cell culture after the introduction of the silicone ring was ~ 0.79 cm^2. Once assembled, the upper and lower parts of the Snapwell were sealed by melting the plastic with a surgical cautery (Cardinal Health, Waukegan, IL, USA). Prior to cell cultivation, PLGA scaffold was coated with Vitronectin and left for 14 hours undisturbed in the incubator. H09-RPE and AMDCD-RPE were plated on to PLGA scaffold either after thawing or enrichment on day 42. 3.75 x 10^5 cells per scaffold were seeded in RPEMM with the addition of rock inhibitor 1:1000.

3.3.2 Comparison analysis

Second checkpoint aimed to evaluate all the different generated 3D cultures for maturity and functionality of the differentiated RPE cells. To highlight any differences the behaviour of derived-RPE when cultured on the selected scaffolds, a structural, molecular and functional comparison was made among all RPE-patches. RPE cultures on Transwell inserts were taken as control condition.

3.3.2.1 SEM and TEM analysis

Tissue engineered products were fixed in SEM fixative made of 2% glutaraldehyde in 0.1M Sodium Cacodylate Buffer, pH 7.4, for 1h at room temperature and washed in PBS. For transmission electron microscopy (TEM), the samples were brought to the National Eye Institute (NEI/NIH, Bethesda, MD, USA) Electron Microscopy core for further processing and imaging. For SEM, tissue engineered products were dehydrated in increasing concentrations of ethanol and then dried into the Critical Point Dryer (Leica, Wetzlar, Germany). Samples were mounted on

an aluminium stub with a carbon tape disc and sputter coated with gold. Images were taken with a Zeiss EVO 10 SEM (Zeiss, Oberkochen, Germany).

3.3.2.2 Cryosections and immunostaining

Cryosectioning was used for de-epithelialization and decellularization assessment of the hAM and the DM, respectively. Intact and treated biological tissues were fixed with 4% PFA in PBS and left overnight at 4°C, then rinsed three times in PBS. Fixed tissue samples were first placed in 7% sucrose, then in 15% sucrose in PBS for 4 hours followed by overnight storage in 30% sucrose in PBS. The day after the samples were embedded in Cryobloc compound (Diapath, Bergamo, Italy), taking care to avoid bubbles. Cryosections (10 µm thickness) were stained with hematoxylin and eosin (H&E) and visualised using an optical microscope (Zeiss).

For immunofluorescence assays, slices or cells were blocked with 4% PFA at RT for 20 minutes and permeabilized using 0.5% Triton X-100 solution for 30 minutes. Further blocking step was performed at RT in 3% BSA. Primary antibodies used in this study are listed in Table 4 and prepared in PBS 3% BSA. Sections or cells were incubated overnight at 4°C. Specific antibodies coupled to Alexa Fluor 488 or 594 were used as secondary antibodies. Sections were then counterstained with DAPI Fluoromont-G and imaged using the Nikon Eclipse Ti-E fluorescent microscope using 40x oil immersion objective.

In the comparison study, the RPE monolayers over the selected scaffolds were incubated for 1 hour at RT in a PBS buffer containing 1% BSA, 0.5% Tween 20 and 0.5 % Triton X to allow permeabilization and blocking of non-specific sites.

Subsequently, the samples were labelled with the tight junctions protein ZO1 (1:200; 1A12, Thermo Fisher Scientific), RPE65 (1:200; NBP2-95096, Novus Biological), PMEL (1:200; C392380, Lifespan Biosciences, Lynnwood, WA, USA), tipe IV collagen (1:200; ab6311, Abcam, Cambridge, UK), Phosphoezrin (1:100; 3141, Cell Signaling Technology, Danvers, MA, USA) and Phalloidin Alexa Fluor 647 (1:1000; A22287, Thermo Fisher Scientific). The secondary antibodies Alexa Fluor 488 anti-rabbit IgG (1:500; A32731), Alexa Fluor 555 anti-mouse IgG (1:500; A32727) and Alexa Fluor 555 anti-rabbit IgG (1:500; A32732), (all from Thermo Fisher Scientific) were added for 1 hour at room temperature in the dark at with a 1:500 dilution (Table 4). Both secondary antibody fluorophores were chosen to

have a similar emission spectrum in the far-red wavelength in order to increase the signal to noise ratio. Indeed, the extracellular matrix of the biological membranes contributes to autofluorescence due to the relatively high quantum yield of collagen and elastin. The RPE cell cultures were imaged using a Zeiss LSM 980 with Airyscan 2 (Zeiss) in Multiplex Mode, for enhancing signal-to-noise ratio at high acquisition speed and low laser power. For image editing and processing, either ImageJ (University of Wisconsin, WI, USA) or Zeiss ZEN Microscopy Software (blue edition) were used.

3.3.2.3 REShAPE

Machine Learning is a type of Artificial Intelligence which is based on the idea that systems can learn from data, identify patterns and make predictions with minimal human intervention. Among many categories of Machine Learning, one of these is artificial Neural Networks. These are set of algorithms that are modelled after human brains in terms of architecture. Compared to other kinds of Machine Learning systems, artificial Neural Network algorithms are capable of tweaking the learning algorithms and can determine their own adjustments and generate the best predictions (LeCun et al., 2015). Every artificial Neural Network has layers, whose function is to receive an input, transform it in some way and then output to a different layer. Convolutional Neural Networks (CNN) are special type of artificial Neural Networks that are popularly used to analyze images. Differently from other categories of neural networks, the CNN has hidden layers, called convolutional layers. In a convolutional layer, the process is convolutional, which means that the process is applied several times across the input (an image). The convolutional layers are the ones that are capable of detecting patterns on the image through the use of filters (or neurons). For instance, the patterns that a filter can detect can be edges, such as the borders of a cell. Geometric filters are usually at the beginning of the network, but the deeper the network goes, the more sophisticated the filters become. This happens because every layer aggregate and recombine features from the previous layer.

A CNN algorithm has been trained to recognize RPE cell borders from images of samples labelled by immunofluorescence. The algorithm would generate a binary mask of segmented RPE borders, and this output would be manually corrected to provide the “right answer” on which the algorithm would learn. Once trained, the

CNN algorithm is fed with images of fluorescently labelled RPE cells and the binary mask images that are generated become the input for the REShAPE (Retinal Epithelium Shape And Pigment Evaluator) software for cell shape analysis.

The binary segmentation produced by the CNN algorithm is transferred to REShAPE for cell shape analysis. REShAPE is an open-source Fiji plugin for image analysis developed in Dr. Kapil Bharti's laboratory. For every cell in a field of view that has been successfully segmented, REShAPE provides quantification of more than 25 different shape metrics. The raw data are stored in a spreadsheet to allow for statistical analysis. In addition, the software creates images of segmented cells for every metric analyzed, where every cell is color-coded according to the raw values. The shape metrics that can be analyzed with the software give measurements of cell dimensions, such as area and perimeter, measurements of elongation, such as length of major and minor axis, and measurements of cell regularity, such as hexagonality score and number of neighbours. The analysis of data and the graphs have been done using R software ("R Core Team (2018). R: A language and environment for statistical computing. R Foundation for Statistical Computing, Vienna, Austria). The R packages "plyr" and "ggplot2" have been use for data handling and plotting respectively (Wickham, 2011). The Dunnett's test, a method for post hoc pairwise multiple comparisons, was used to compute statistical analysis by comparing the scaffold-conditions to control groups. A 95% family-wise confidence level has been used. The assumption of normality was tested with Shapiro-Wilk's test. Since tests for normality are sensitive to sample size, the test was conducted on an unbiased subset of data of each condition. Moreover, Quantile-quantile (Q-Q) plots were drawn to assess normality on the whole dataset of each group. One-way ANOVA was used to evaluate between-group variance before performing Dunnett's test. Shapiro-Wilk's test and one-way ANOVA were carried out using the R package "dplyr" (Wickham et al., 2020), while Q-Q plots were drawn using the R package "ggpubr". Data are displayed as boxplots, where box limits represent the first and third quartile, the central line shows the median and the whiskers indicate the 5^{th} and 95^{th} percentile, so that the range specifies 90% of the data. For REShAPE morphometric analysis, single-cell measurements are considered as technical replicates, while each cell culture is considered as biological replicate.

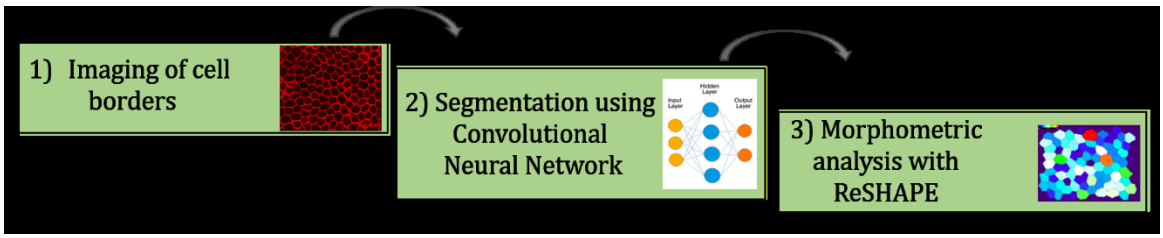

***Figure 13**: RPE cell borders segmentation and morphometric analysis. Images of RPE cell borders were segmented using a CNN algorithm, which was trained on mature iPSC-RPE. The algorithm produces a binary mask that is subsequently analyzed by REShAPE. In addition to the spreadsheet with the raw data, REShAPE generates color coded images for different shape metrics. Every RPE cell is color coded according to the value of each parameter.*

3.3.2.4 TER measurement

Transepithelial electrical resistance (TER) was initially measured for H09-RPE cells as well as for adult RPE cells cultured on Transwell inserts with the Millicell® ERS-2 meter and electrode system (Merck Millipore, Burlington, MA, USA) along the weeks. Later in the study, electric intactness was measured using EVOM2 and EndOhm chamber (World Precison Instruments, Sarasota, FL, USA). At least three biological replicates were measured for each scaffold-condition. To obtain true resistance value, resulting TER (Ωcm^2) values were multiplied for the corresponding surface area.

3.3.2.5 VEGF Elisa

In the case of H09-RPE cell on hAM and related control on Transwell inserts, cell culture supernatants from the upper and lower compartments either of the nitinol ring or the insert were collected after 48 hours of cell culture at 37°C. Enzyme-linked immunosorbent assay (ELISA) was performed to assess the amount of PEDF secreted in the RPE conditioned culture medium with the Human SERPIN F1 ELISA kit (Thermo Fisher Scientific) and analyzed at 1:2 dilution according to the manufacturer's instructions. Basal media were diluted 1:10 for VEGF quantification using Human VEGF ELISA kit (Thermo Fisher Scientific), following manufacturer's instructions. Media volume and insert growth area were used to calculate PEDF and VEGF levels.

First experiments with H09-RPE cells over acellular DM, the cells were incubated in serum free media for 48h after 28 and 56 days of culture, respectively.

Subsequently, conditioned media were collected and ELISA was carried out to assess the amount of VEGF secreted in the H09-RPE conditioned culture media.
The data on PEDF and VEGF secretion are expressed as mean ± SD (standard deviation). Two-way ANOVA followed by Bonferroni comparisons test was performed using GraphPad Prism version 5.0.0 (GraphPad Software, San Diego, CA, USA). Values were considered statistically significant at P values below < 0.05.
During the scaffold-comparison study, cell culture supernatants from the cell basal side, were collected every week. VEGF measurements were done in triplicate using the human VEGF Quantikine ELISA kit (R&D System), as per to manufacturer's protocol. The R package ggplot 2 was used for the graphic representation of the data.

3.4 IN VIVO STUDY

3.4.1 Rodents

Rowett nude (RNU) Crl:NIH-FOXn1^{mu} immunocompromised rats and Sprague Dawley (SD) albino rats not immunocompromised were used to test the delivery and integration of the hPSC-RPE patch. The rats were fed according to the body weight and maintained in an aseptic and temperature-controlled environment. All animals were handled in accordance with the Association for Research in Vision and Ophthalmology (ARVO) statement for the use of animals in Ophthalmic and Vision Research.

3.4.2 Transplantation

A total of 10 rats underwent surgery in one or both eyes. For *in vivo* experiments, H09-RPE cells cultured as monolayers on dDM or PLGA scaffold were implanted for direct comparison between the two selected substrates.

3.4.2.1 Surgical procedure

The rats were anesthetized with intraperitoneal injection of 100mg/kg of ketamine and 10 mg/kg of xylazine. Both eyes of each rat were used for transplantation surgeries (Figure 14). Two drops of a local anesthetic (0.5% proparacaine; Akorn, Inc., Lake Forest, IL, USA) were applied to the eye to be transplanted for eye numbing. 0.5%% tropicamide and 2.5% phenylephrine (Akorn) were given drop wise to dilate the eyes (mydriasis). The eyes were slightly proptosed with an in-house tool and an appropriate amount of GenTeal Tears (Alcon, Geneva, Switzerland) was squeezed on top of the cornea. A glass coverslip was placed on the eye to allow internal eye view. A small lateral sclerotomy posterior to the limbus was made using a slit knife (Alcon), followed by a vitreous displacement with Healon® Pro (Johnson & Johnson, New Brunswick, NJ, USA). Retinotomy was made using a 33 Ga curved tip Hamilton syringe and retinal detachment was performed with the injection of 0.25% Healon in the subretinal space. After surgery, B.N.P. Triple Antibiotic Ophthalmic Ointment (Bausch + Lomb, Laval, Canada) was applied topically on transplanted eyes and the rats were allowed to recover from anesthesia in a thermal care incubator. The whole surgery was performed under an operating microscope (Zeiss).

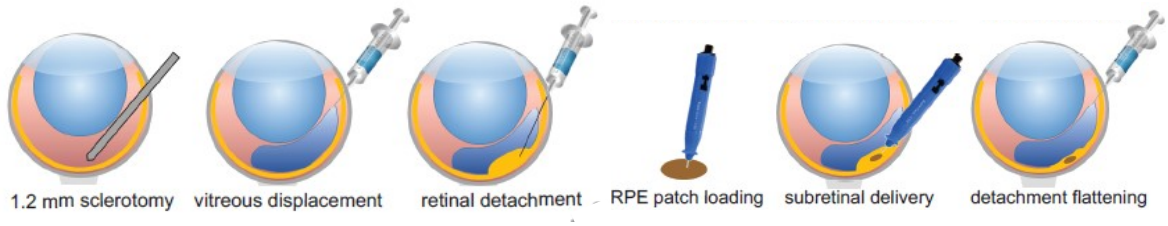

***Figure 14**: Schematic of the 0.5 mm diameter H09-RPE-patch transplantation in rat subretinal space.*

3.4.2.2 H09-RPE-patch

The H09-RPE patch cultured on the Snapwell was cut with a 0.5 mm Rapid-Core biopsy punch (Ted Pella Inc., Redding, CA, USA). The small patch sample embedded in Healon was initially released from the tool to allow the separation of the patch from the underlying Snapwell with the aid of some forceps. The patch of cells alone was then reloaded in the biopsy punch and introduced through the sub-scleral space into the subretinal bleb. At this point, the H09-RPE cell sheet was

ejected from the cutting tip into the subretinal space of the animal. Additional Healon was injected on top of the retina to flat the retinal detachment after implantation.

Table 3 shows the implanted rat eyes and the type of RPE-patch grafted for each eye, along with other readouts and information.

***Table 3**: List of the rats underwent implantation surgery. Each eye received the H09-RPE patch either on PLGA or on dDM. The best resulting implants in term of integration and visualization have been highlighted in green.*

Rat ID	Breed	Sex	Weight (gr)	Implant right eye	Implant left eye	Cells	Surgery date	Dimension of the implant Ø (mm)
c.65923	RNU	M	360	PLGA	**dDM**	H09 p31	5.1	1.5
c.65919	RNU	M	380	PLGA	**dDM**	H09 p31	4.18	1.5
c.65916	RNU	M	320	NA	**dDM**	H09 p31	6.2	0.5
c. 65918	RNU	M	420	**dDM**	PLGA	H09 p31	6.13	0.5
c.65917	RNU	M	350	PLGA	**dDM**	H09 p31	6.13	0.5
c. 65921	Albino	M	450	**dDM**	PLGA	on dDM: H09 p29 on PLGA: H09 p31	6.22	0.5
c. 65922	Albino	M	480	**dDM**	PLGA	on dDM: H09 p29 on PLGA: H09 p32	6.22	0.5
c. 65920	RNU	M	470	**dDM**	**dDM**	H09 p29	7.3	0.5
c. 65923	Albino	M	500	**dDM**	**dDM**	H09 p30	6.28	0.5
c. 65924	Albino	M	550	**dDM**	**dDM**	H09 p29	Left eye: 6.28 Right eye:7.3	0.5

Abbreviations and symbols: ø, diameter; dDM, decellularized Descemet's membrane; ID, identifier; NA, not applicable; PLGA, poly(lactic-co-glycolic acid); RNU, Rowett nude.

3.4.3 Live imaging

OCT analysis was carried out one or two months after surgery to morphologically assess the retina after the surgical manipulation of the eye and to locate implant placement in the subretinal space. The rats were adequately anesthetized prior to analysis. OCT was preformed using Spectralis (Heidelberg Engineering,

Heidelberg, Germany) with a 550 degree lens. The region of interest (ROI) was placed in the center and both averaged single B-scan across ROI and volume OCT scans covers entire ROI was performed. Follow-up function of the instrument was used to allow for OCT scans at the same retinal location for the second time point one week later. Spectralis was also used for capturing fluorescein angiogram with intravenous injection of Sodium Fluorescein (Akorn). Early (first minute) and late phase (5 minutes) angiograms were recorded.

3.4.4 Histology

After OCT analysis, the rats were euthanized by intracardiac injection of pentobarbital (Akorn). The eyes were enucleated using ocular forceps and placed straight in Davidson's fixative. Anterior chamber, along with lens and vitreous were removed under a stereomicroscope and incubated in PBS. The surgery area was dissected out and replaced in Davidson's. Some of the samples were sent to Histoserv Inc. (Germantown, MD, USA) for further sectioning. The remaining samples were prepared for cryosectioning following the protocol described in 3.3.2.2. After the treatment of the tissue with sucrose, the samples were placed in the -80 °C freezer until sectioning on the cryostat could be performed. Serial cryosections of 10 – 15 µm were collected around the grafted areas and histological stained with H&E. The slides were then imaged on Nikon Eclipse Ti-E fluorescent microscope.

***Table 4**: List of the antibodies used in the study.*

Primary antibodies	Origin	Source	Dilution	Catalog #
α-SMA	Mouse	R&D Systems	1:400	MAB1420
Bestrophin 1	Rabbit	Thermo Fisher	1.100	PA589606
Claudin 19	Mouse	R&D Systems	1:200	MAB6970
Claudin 3	Rabbit	Thermo Fisher	1:100	34-1700
CRALBP	Mouse	Abcam	1:200	Ab15051
CRALBP	Mouse	Thermo Fisher	1:500	MA1-813
Ezrin	Goat	Abnova	1:100	PAB7060
LIN-28	Mouse	Thermo Fisher	1:400	MA1 - 016
Na^+K^+-ATPase	Mouse	Abcam	1:200	ab7671
NANOG	Goat	R&D Systems	1:200	AF1997
Occludin	Mouse	Thermo Fisher	1:100	33-1500
OCT-3/4	Goat	R&D Systems	1:200	AF1759
OTX2	Goat	R&D Systems	1:200	AF1979
Phalloidin	Synthetic	Sigma	1:1000	P1951
Phalloidin Alexa Fluor 647	Synthetic	Thermo Fisher Scientific	1:1000	A22287
Phosphoezrin	Rabbit	Cell Signaling	1:200	3141
PMEL	Mouse	LS Bio	1:200	LS-C392380
RPE65	Rabbit	Novus Biologicals	1:200	NBP2-95096
SOX17	Goat	R&D Systems	1:200	AF1924
TRA-1-60	Mouse	Merck Millipore	1:200	Mab4360
Type IV collagen	Mouse	Abcam	1:200	ab6311
TYRP1	Mouse	Novus Biologicals	1:500	NBP2-32901
ZO1	Rabbit	Thermo Fisher	1:200	61-7300
ZO1 Alexa Fluor 488	Mouse	Thermo Fisher	1:200	1A12

Secondary antibodies	Origin	Source	Dilution	Catalog #
Alexa Fluor 488 anti-goat IgG	Donkey	Thermo Fisher	1:800	A11055
Alexa Fluor 594 anti-goat IgM	Goat	Thermo Fisher	1:800	A21044
Alexa Fluor 488 anti-mouse IgG	Donkey	Thermo Fisher	1:800	A21202
Alexa Fluor 555 anti-mouse IgG	Goat	Thermo Fisher Scientific	1:500	A32727
Alexa Fluor 594 anti-mouse IgG	Donkey	Thermo Fisher Scientific	1:800	A21203
Alexa Fluor 488 anti-rabbit IgG	Goat	Thermo Fisher Scientific	1:500	A32731
Alexa Fluor 555 anti-rabbit IgG	Goat	Thermo Fisher Scientific	1:500	A32732

4. RESULTS

4.1 EFFICIENT IN VITRO DIFFERENTIATION OF RPE CELLS FROM A hESC LINE

H09 hESCs grew as colonies with typical morphology and expression of pluripotency markers, as shown in Figure 15A, i-v. Furthermore, feeder-free H09 hESCs were capable of spontaneous differentiation to all three embryonic germ lineages (Figure 15B, ii-iv). The spontaneous differentiation approach yielded smaller and either dark or lightly pigmented RPE cells with a smoother epithelial morphology. TER measurements indicated tight junction integrity and an intact epithelial barrier function (Figure 15H). Protein of the cellular junctions (occludin, claudin 3, ZO1, claudin 19) localized at junctional complexes and indicated therefore mature tight junctions. Confocal stacks of tight junction protein labelling confirmed monolayer structures (Figure 15E, ii, iv). Cells expressed the RPE-specific proteins CRALBP and ezrin, as well as the transporter proteins bestrophin 1 (Best1) and apically localized sodium-potassium pump (Na^+K^+-ATPase) (Figure 15E, i, iii). Furthermore, the cells showed correct RPE functionality by phagocytosis of porcine POS (Figure 15D), and PEDF and VEGF secretion from the apical and basal side of the monolayer, respectively (Figure 15I,J). RT-PCR showed lack of expression of the pluripotency markers OCT-3/4 and NANOG (Figure 15F, G).

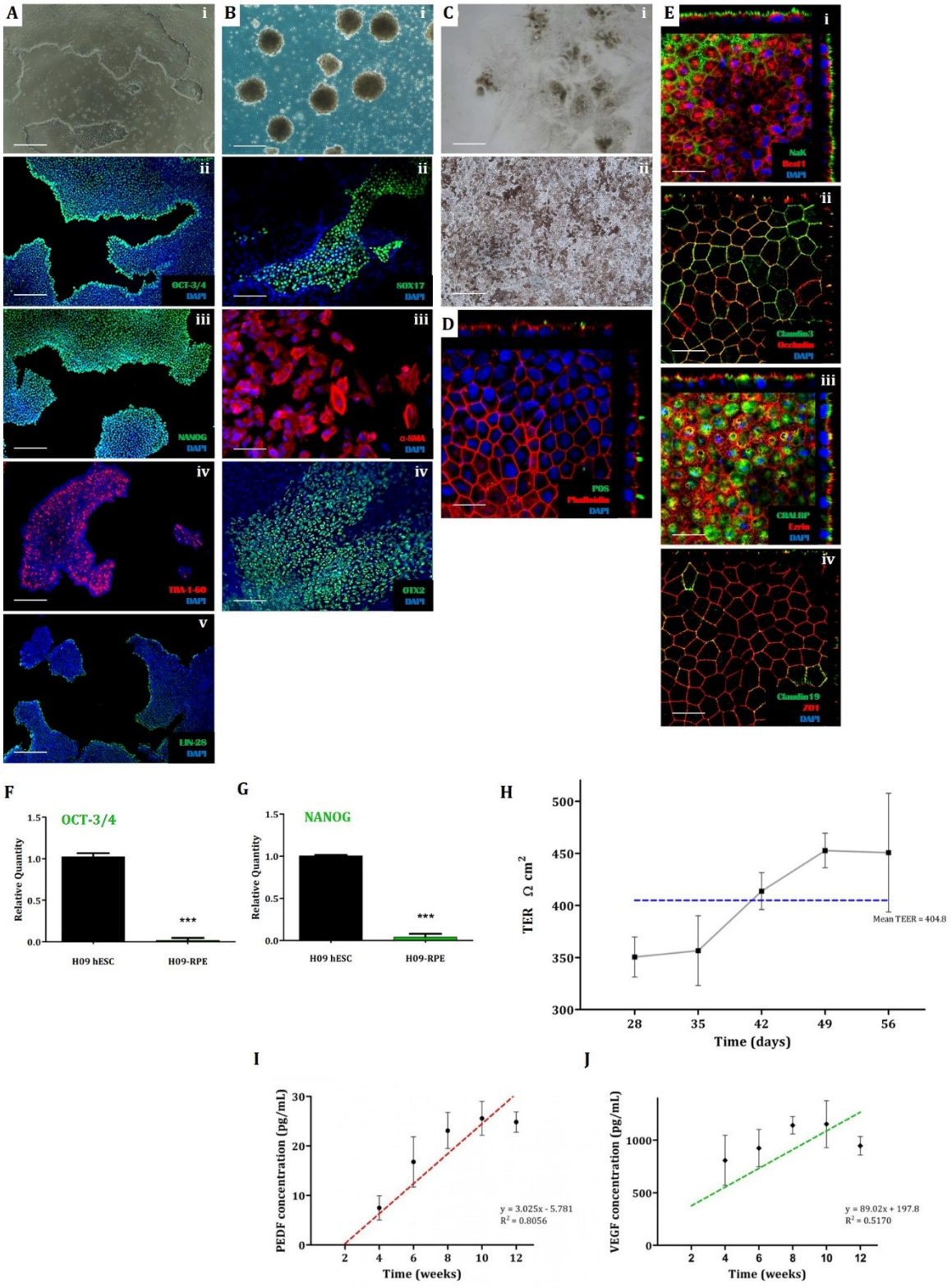

Figure 15*: Characterization of H09 hESC-derived RPE. (**A**) Feeder free culture of H09 hESCs and confirmation of their pluripotency (**i**) H09 hESC colonies, (**ii-v**) expression of pluripotency markers OCT-3/4, NANOG, TRA-1-60 and LIN-28. (**B**) EBs formation and generation of the three embryonic germ lineages (**i**) EBs in suspension culture, (**ii-iv**) once replated the EBs showed expression of proteins of the three germ lineages. (**C**) Bright-field images depicting (**i**) H09-hESC differentiation with pigmented colonies arising, (**ii**) cobblestone morphology of derived RPE. (**D**) Internalization of POS by H09-RPE cells. (**E**) Confocal immunofluorescent micrographs depicting staining for typical*

*RPE markers as part of the characterization of the RPE monolayer (**i**) confirmation of RPE polarity by apical expression of Na+K+-ATPase, (**ii**, **iv**) evidence of mature tight junctions. (**F**, **G**) Purity of H09-RPE cells confirmed by RT-PCR. (**H**) Assessment of H09-RPE barrier function using transepithelial volt/ohm meter. (**I**) Quantification of PEDF and (**J**) VEGF secretion in spent culture medium along the weeks on Transwell insert using an ELISA assay. Scale bars = 100 µm. Best1, bestrophin 1; EBs, embryoid bodies; hESC, human embryonic stem cells; NaK, Na+K+-ATPase; PEDF, pigment epithelium-derived factor; POS, photoreceptor outer segments; RPE, retinal pigment epithelium; TER, transepithelial electrical resistance; VEGF, vascular endothelial growth factor.*

4.2 DECELLULARIZATION ASSESSMENT OF BIOLOGICAL MEMBRANES

4.2.1 Thermolysin effectively de-epithelialized hAM (dhAM) whilst maintaining structural and molecular integrity

Histological examination of the hAM samples showed that all three enzymatic methods (thermolysin, trypsin-EDTA and Dispase II) were comparable in terms of hAM de-epithelialization efficiency, while maintaining the tissue structure. Only a few epithelial cells occasionally remained on dhAM with no differences in trypsin-EDTA and thermolysin treatments. Overall, tissue structure was maintained in both de-epithelialization methods. On the other hand, we observed severe damage to the hAM architecture and some fragmentation of the stromal matrix following Dispase II processing.

Intact and thermolysin-treated hAM cryosections showed positive staining for laminin α5 and CIV in the basement membrane, thus indicating a uniform and well-preserved basement membrane in hAM devoid of epithelium. Partial damage to the basement membrane was observed after trypsin-EDTA treatment, with frequent laminin α5 and CIV unlabelled regions interspersed among the basement membrane. Positive staining for laminin α5 and CIV was present in Dispase II-treated hAM cryosections, but with more diffuse and faint signals than in the iAM, demonstrating a loss of tissue integrity (Figure 16).

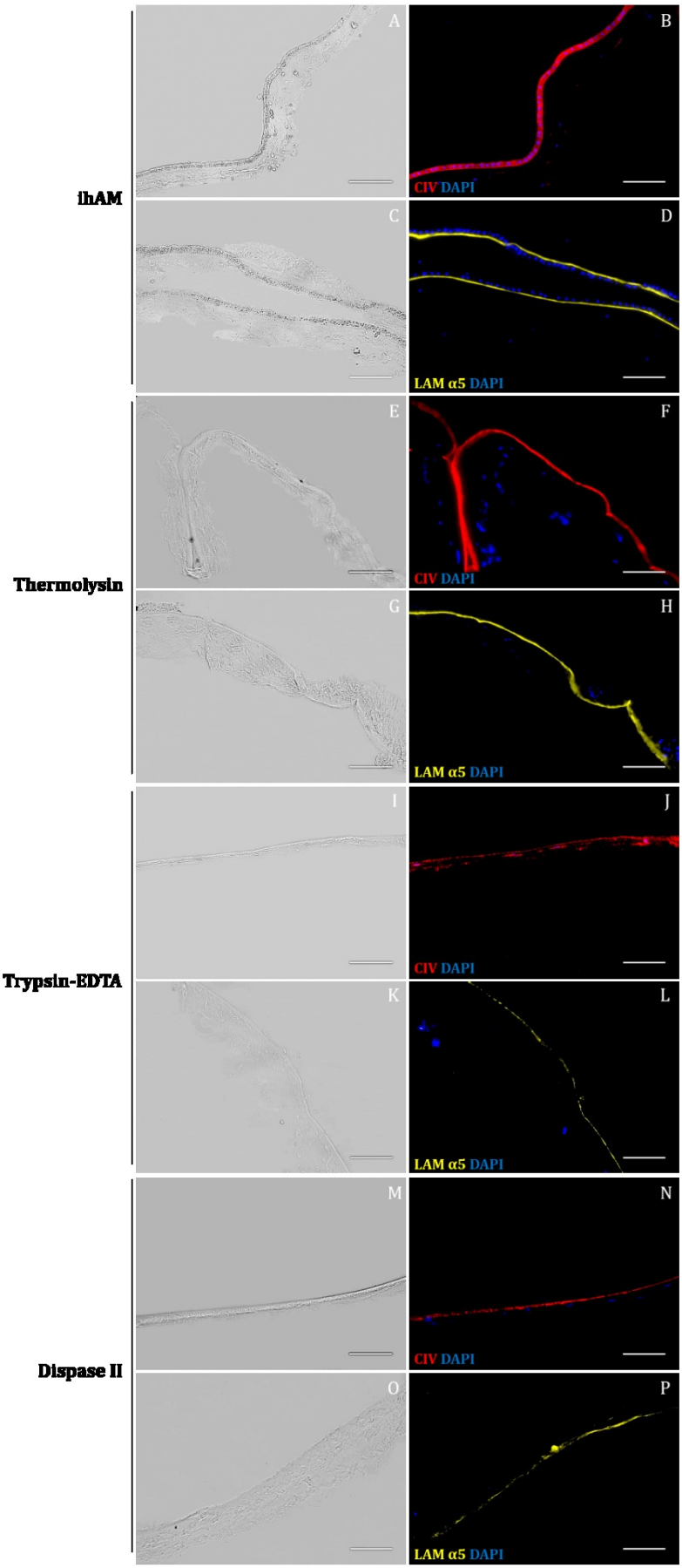

***Figure 16**: Evaluation of hAM de-epithelialization techniques. Immunostaining for basement membrane markers, CIV (B, F, J, N; red) and laminin α5 (D, H, L, P; yellow) in cryopreserved intact*

hAM (B, D) and following denuding using thermolysin (F, H), trypsin-EDTA (J, L) and Dispase II (N, P). Human amniotic epithelial cell and stromal cell nuclei were stained with DAPI (blue). Scale bars = 100 µm. hAM, human amniotic membrane; ihAM, intact hAM.

4.2.2 DM decellularization provides an allogenic risk-free biomembrane

Samples of corneal endothelium were analyzed before and after the decellularization treatment with a stereoscopic microscope (Figure 17A, left panels). Corneal endothelial cells removal was investigated by immunostaining. No endothelial cells were found on thermolysin-treated DM, according to the lack of ZO1 and Na^+/K^+-ATPase on en face immunofluorescence staining of the tissue (Figure 17A, right panels). Laminin α5 and CIV showed positive staining in control and dDM. The expression of these two ECM markers on dDM indicate that the integrity of the membrane was preserved after treatment. Furthermore, the enzymatic treatment did not affect the polarized pattern expression pattern of these markers, since laminin α5 was restricted to the endothelial rim of the DM, while CIV was scattered along the stromal side (Figure 17B).

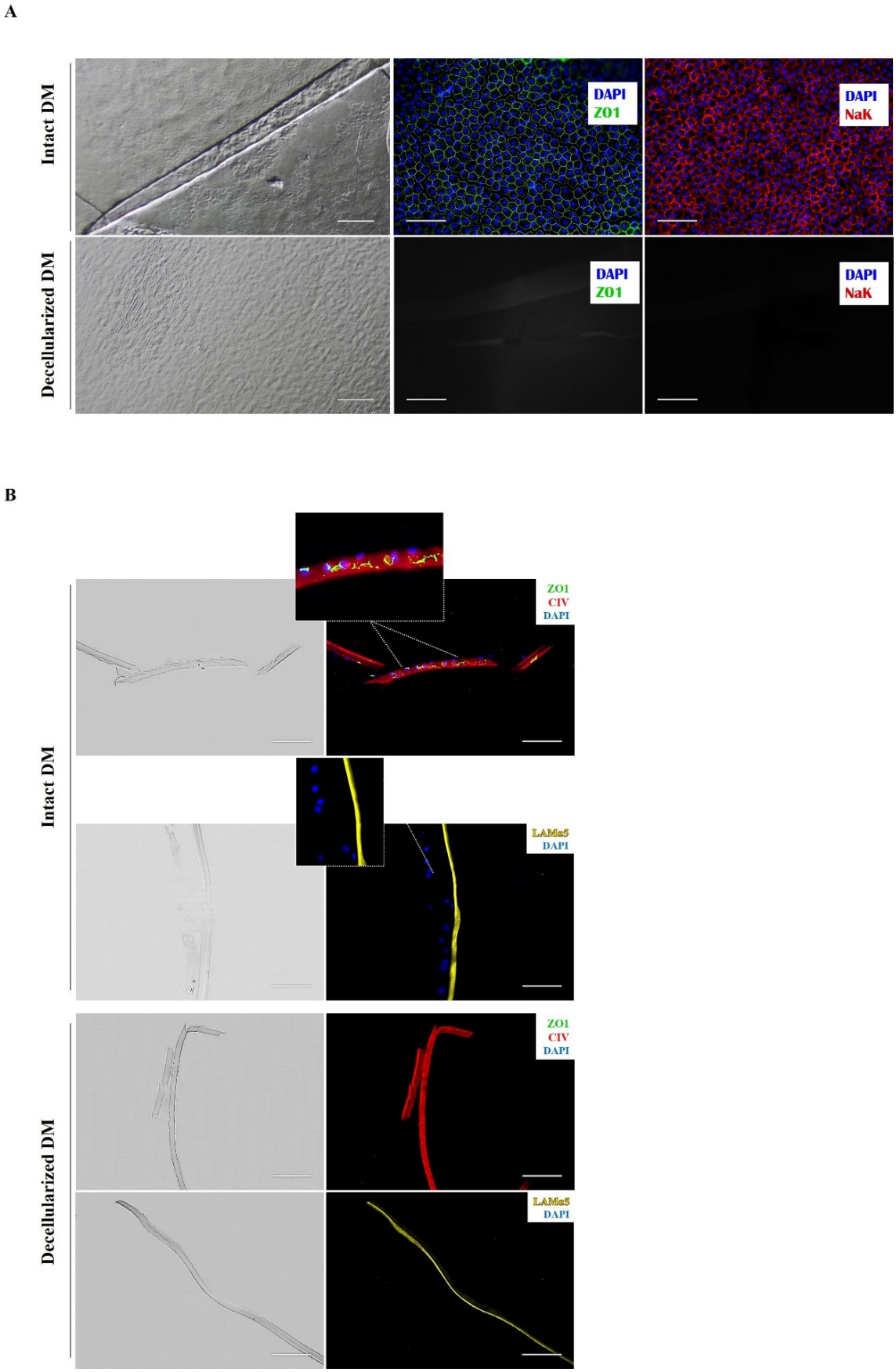

***Figure 17**: Assessment of DM denudation technique. (**A**) Representative stereoscopic microscope and immunofluorescence images of the DM before (upper panels) and after (lower panels) the decellularization process. The staining shows the expression of tight junction protein ZO1 (green)*

*and sodium-potassium pump Na+/K+-ATPase (red) on DM before (upper panels) and after (lower panels) the decellularization process. (**B**) Immunostaining of ZO1 (green), CIV (red) and laminin α5 (yellow) on DM cryosections before (upper panels) and after (lower panels) the decellularization process. The bright-field images show the entire intact (upper panels) and denuded (lower panels) tissues. Dotted rectangles indicate the regions that are magnified in the adjacent panels. All nuclei were stained with DAPI (blue). Scale bars = 100 µm. CIV, type IV collagen; DM, Descemet's membrane; LAMα5, laminin α5; NaK, Na+/K+-ATPase.*

4.2.3 Architecture of aged human BM explants

Explants of human BM were prepared from either the macular or peripheral areas of eyes of elderly donors (> 65 years). Tezel et al. reported that the initial reattachment of native human RPE seeded onto human BM depends on the layer of BM available for cell reattachment (Tezel and Priore, 1999). Unfortunately, the condition on which the explants were isolated prevent to carry out additional assays based on the choice of the best layer of the BM to be exposed for further cell plating. Previous researches have included in their studies donor eyes having specific acceptance criteria. Among these, death-to-enucleation time was no more than 7 hours and death-to-receipt time was no more than 48 hours (Sugino et al., 2011a, 2011b). The tissues used in the current study were collected primarily for corneas donation. In this field, the death-to-enucleation time does not affect the quality of the cornea, and the latter can be stored in appropriate medium for more than 24 hours before further processing. In addition, the circumstances of delivery of the intended tissues were extreme and the consequent death-to-receipt time was far beyond the 48 hours. These reasons posed several challenges to the quality of the tissues included in the study, most of whom had different degree of degeneration, with collapsed internal structures at the time of explants preparation (due to previous removal of the anterior segment). These conditions hindered a proper isolation of BM explants and they might have affected cell cultures outcome. Assuming that the native RPE cells were already dead at the time of isolation, enzymatic and chemical treatments were avoided to prevent further tissue damage. The anatomy of the BM layer exposed varied depending on the degree of tissue degeneration and manipulation. In general, the explants did not show a uniform morphology throughout the dissection bed. Most of the tissues had an uneven surface characterized by interspersed cross-linked collagen fibers

arranged in fused bundles. Some leftovers patches of RPE basement membrane were scattered throughout the explants (Figure 18A). Figure 18 shows samples of Bruch's membrane and choroid explant that were collected during the study. Untreated explants exposed inner collagen layer mainly consisting of collagen fibers that run unidirectionally. Large clusters of interfibrillar spaces were filled with extracellular debris. Globular ECM proteins formed aggregates in some areas and were attached along the course of the fibers.

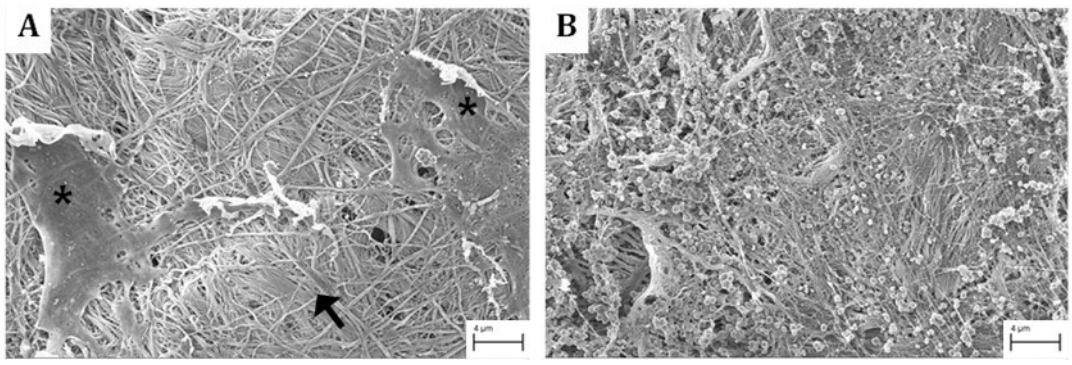

***Figure 18**: SEM of BM and choroid explants from a > 65-year old donor. Untreated explants show several crosslinked collagen fibers (A, black arrow). Smooth patches of RPE basal lamina could be easily identified throughout the samples (A, black asterisks). ECM proteins aggregate on the collagen matrix (B, black stars). Scale bars = 4 µm.*

4.3 hPSC-RPE CELL CULTURE ON BIOLOGICAL SCAFFOLDS

The three biological membranes used in the research have not been evaluated simultaneously, except for the DM and the Bruch's complex. Initially, the use of each membrane followed the need to find a physical support able to support the RPE cells and that could be used in transplantation studies, rather than a direct comparison between different scaffolds.

4.3.1 Inconsistency of hESC-RPE cells culture on thermolysin dhAM

For the study on cell culture using the hAM, H09 hESC line was subjected to spontaneous differentiation method. To achieve a homogeneous monolayer of RPE cells, visible pigmented foci were mechanically isolated and plated in 15% KO-DMEM medium. H09-derived RPE cells were expanded to passage 2 and then tested for either characterization on pre-coated Transwell inserts or generation of

viable culture over the dhAM. In order to push cell attachment, RPE cells were plated at high density (2.0 X 10^5 cells/cm^2) in KO-DMEM supplemented with 10% FBS on thermolysin pretreated hAM locked into the Amnio Ring (Harkin et al., 2017). After four weeks of H09-RPE cultured over dhAM, patches of pigmented cobblestone-like cells were visible throughout the membrane (Figure 19A). These cells showed a positive staining for putative RPE marker MITF, while tight junction formation was demonstrated by ZO1 staining (Figure 19B). Immunofluorescence on cryosections was carried out to assess the basement membrane integrity and generation of a H09-RPE cells monolayer onto the dhAM. Basement membrane markers were found to be strongly expressed in all the samples, forming a bright line, thus showing that laminin α5 and CIV can be clearly detected on the basement membrane. Having evaluated the presence of an undamaged basement membrane, we proceeded by identifying H09-RPE cells using the RPE differentiation markers PMEL and RPE65. Samples of intact hAM were taken as controls (Figure 20). The consistent expression of PMEL and a faint RPE65 staining further testified the H09-RPE differentiation on top of the dhAM. PMEL and RPE65 revealed an irregular staining pattern. Indeed, there were areas of tissue where the two markers were not detected. These areas were interspersed between areas of intense or faint expression. These data indicated the lack of a uniform monolayer of cells on top of the dhAM, despite the presence of an intact basement membrane (Figure 20).

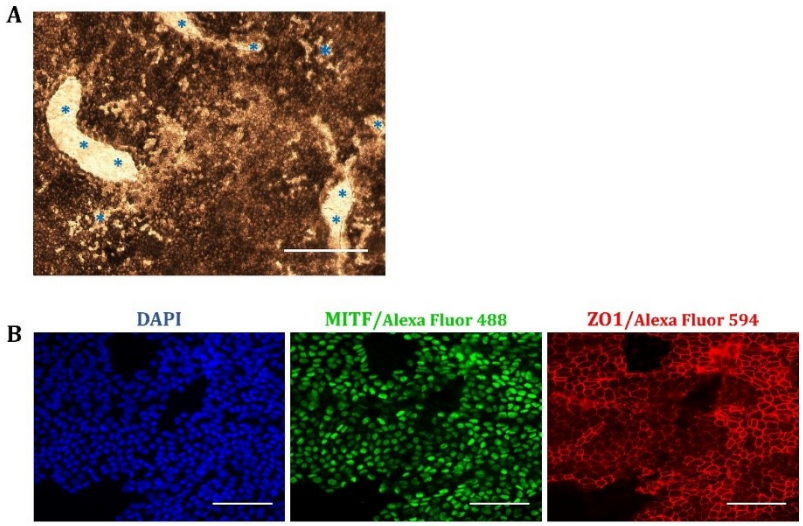

Figure 19: H09-RPE cells culture on thermolysin dhAM. *(**A**) Optical microscope image of H09-RPE cells on dhAM locked into the amnion ring, 4 weeks post-seeding. Groups of pigmented cobblestone-like RPE cells are scattered across the tissue, among areas of empty dhAM (blue asterisks). Scale bar = 100 µm. (**B**) Marker analysis of H09-RPE cells grown on top of thermolysin-*

dhAM showed positive staining for MITF (green) and ZO1 (red). The nuclei were counterstained with DAPI (blue). All scale bars = 100 µm. dhAM, denuded human amniotic membrane; RPE, retinal pigment epithelium.

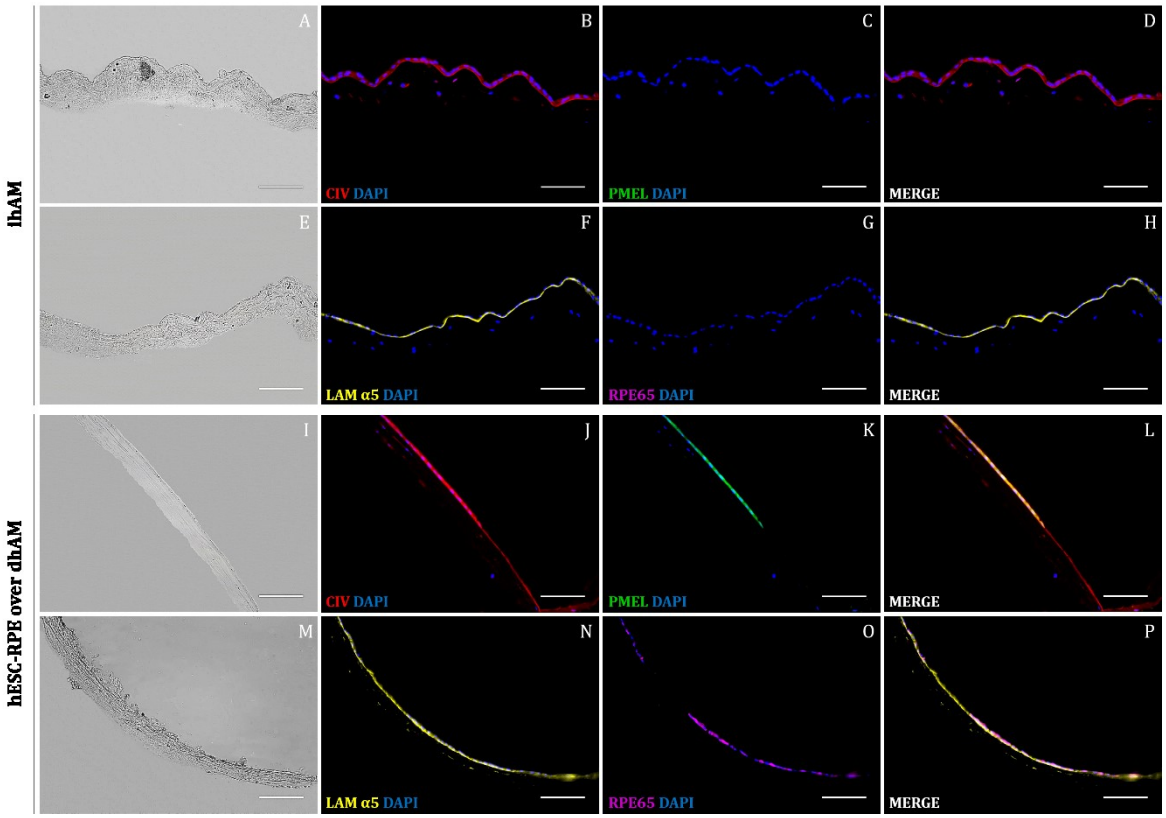

***Figure 20**: H09-RPE monolayer on thermolysin dhAM. Immunofluorescent staining of RPE differentiation markers, PMEL (C, K; green) and RPE65 (G, O; magenta) and basement membrane markers, CIV (B, J; red) and laminin α5 (F, N; yellow) in cryopreserved intact hAM (A–H) and H09-RPE cells culture on dhAM following thermolysin treatment (I–P). RPE markers identified differentiated H09-RPE cells over dhAM (K, O), while basement membrane markers demonstrated the preservation of the basement membrane following thermolysin treatment (J, N). Merged images showed areas of membrane where RPE markers were not detected, despite a proper distribution of the basement membrane markers (L, P). intact hAM was used as control. hAECs, RPE cells and stromal cells nuclei were stained with DAPI (blue). Scale bars = 100 µm. CIV, type IV collagen; dhAM, denuded hAM; hAM, human amniotic membrane; hESC, human embryonic stem cell; ihAM, intact hAM; LAMα5, laminin α5; RPE, retinal pigment epithelium.*

4.3.2 hESC-RPE cells successfully repopulate decellularized DM

To confirm the ability of the denuded DM to support RPE cell culture, hESC-derived RPE cells were seeded over the endothelial-side surface of the dDM and

cultured for one month. At 24 hours, calcein-AM staining (Figure 21A) was used to calculate the number of adherent cells expressed in relation to the initial cell seeding density. Compared to control condition on Transwell, higher attachment efficiency was observed for cells on dDM (Figure 21B). BrdU assay was carried out to assess the growth rate of RPE cells along the weeks. The incorporation of the BrdU represented by the percentage of BrdU positive cells was quantified for RPE cells cultured over dDM and compared with the percentage found in control on Transwell (Figure 21C). The percentage of proliferative cells at 24 hours was greater for cells over dDM, demonstrating the affinity of the RPE cells for the new substrate.

Confluence was reached after 1 week in both cultures and no substantial difference was observed in morphology. RPE cells developed their characteristic hexagonal shape and they started to acquire a rich pigmentation from the second week of culture. The staining pattern of ZO1 revealed consistent morphology and a uniform organization of intercellular junctions of RPE cells after 4 weeks of culture over dDM. In addition, MITF, Best1 and OTX2 proteins were investigated by immunostaining to display the *in vitro* expression of typical mature RPE markers (Figure 22A). The cryosections shown in Figure 22B enabled the visualisation of the H09-RPE monolayer on top of the denuded DM through PMEL labelling. The tissue was stained with laminin α5 and CIV. Properties and functionality of H09-RPE cells on the new substrate were further investigated through TER measurements and VEGF secretion (data not shown). Phagocytosis assay showed the ability of H09-RPE cells to internalized latex beads when cultured over the dDM, confirming the functionality of these cells over the new matrix (Figure 23).

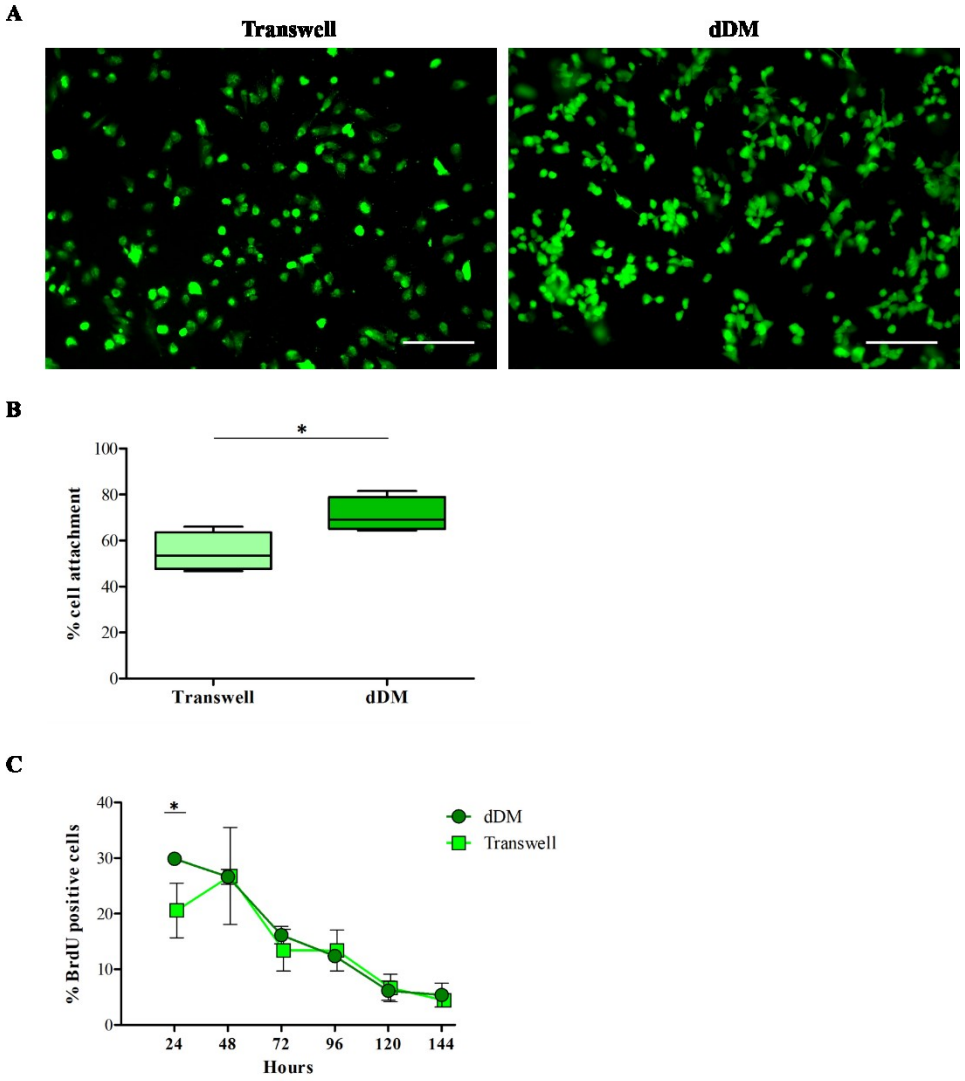

***Figure 21**: The DM provides optimal cues for H09-RPE cells initial attachment and proliferation. (**A**) Immunofluorescence for Calcein AM (green) allows the visualisation of viable H09-RPE cells 24 hours post-seeding on dDM and on Transwell insert. Scale bars = 100 µm. (**B**) Percentage of initial cell attachment on dDM compared to control on Transwell insert. Each box represents mean ± s.d. for fourfold experiments. *p=0.028. (**C**) The graph shows the percentage of proliferative BrdU-positive cells on dDM and on Transwell inserts at different time points during the first week of culture. Each time point represents mean ± s.d. for triplicate experiments. *p=0.032. BrdU, bromodeoxyuridine; dDM, decellularized Descemet's membrane.*

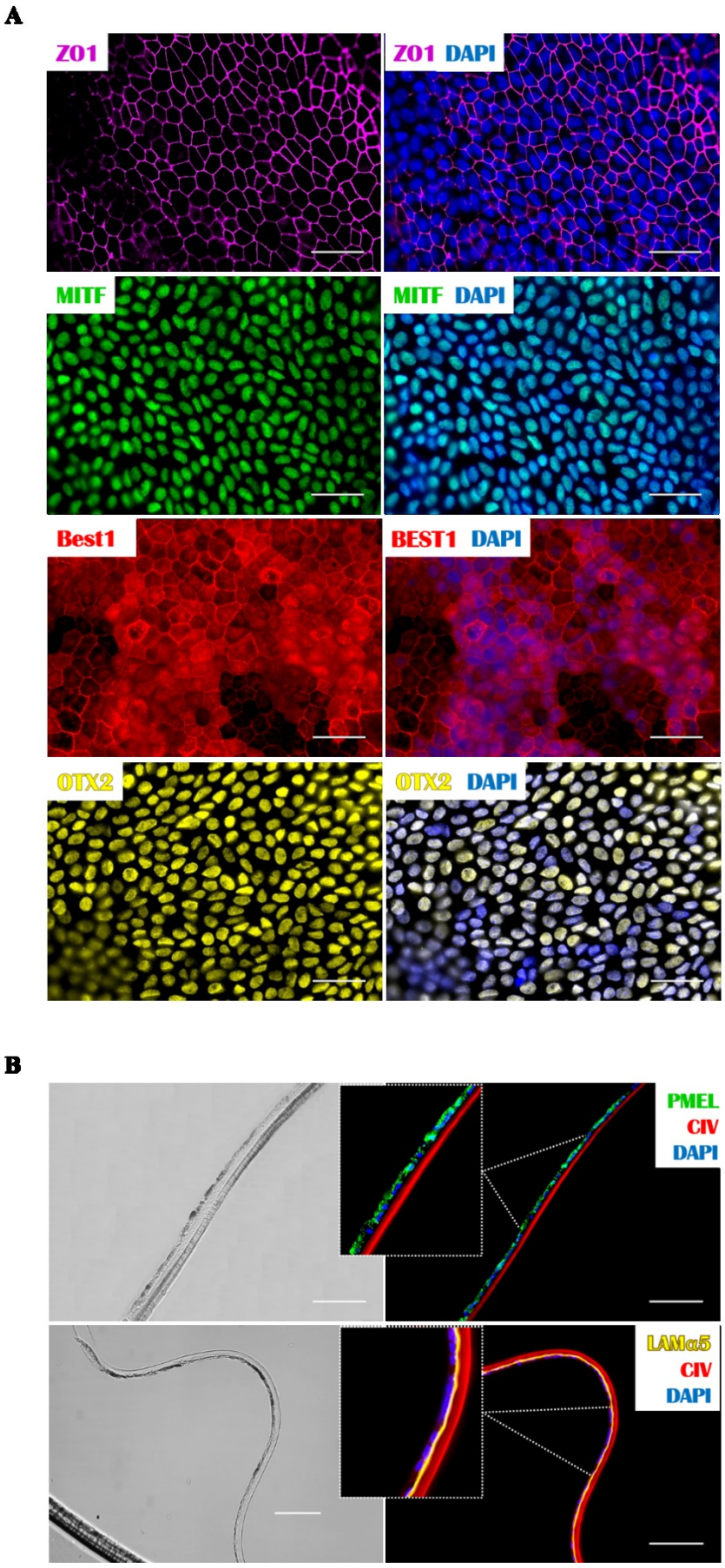

***Figure 22**: H09-RPE cell culture over the dDM. (**A**) Immunostaining for typical RPE markers ZO1 (magenta), MITF (green), Best1 (red) and OTX2 (yellow) in H09-RPE cells cultured on dDM after 1*

*month of culture. Dotted rectangles indicate the regions that are magnified in the adjacent panels. Scale bars = 100 µm. (**B**) Immunofluorescence of H09-RPE cells cryosections cultured on dDM after 1 month of culture, demonstrating the development of a confluent monolayer of H09-RPE cells over the denuded ocular membrane. H09-RPE cells express premelanosome protein PMEL (green). Denuded DM shows positive expression for CIV (red) and LAMα5 (yellow). Dotted rectangles indicate the regions that are magnified in the adjacent panels. All nuclei shown in blue were counterstained using DAPI. Scale bars = 100 µm. Best1, bestrophin1; CIV, type IV collagen; LAMα5, laminin α5.*

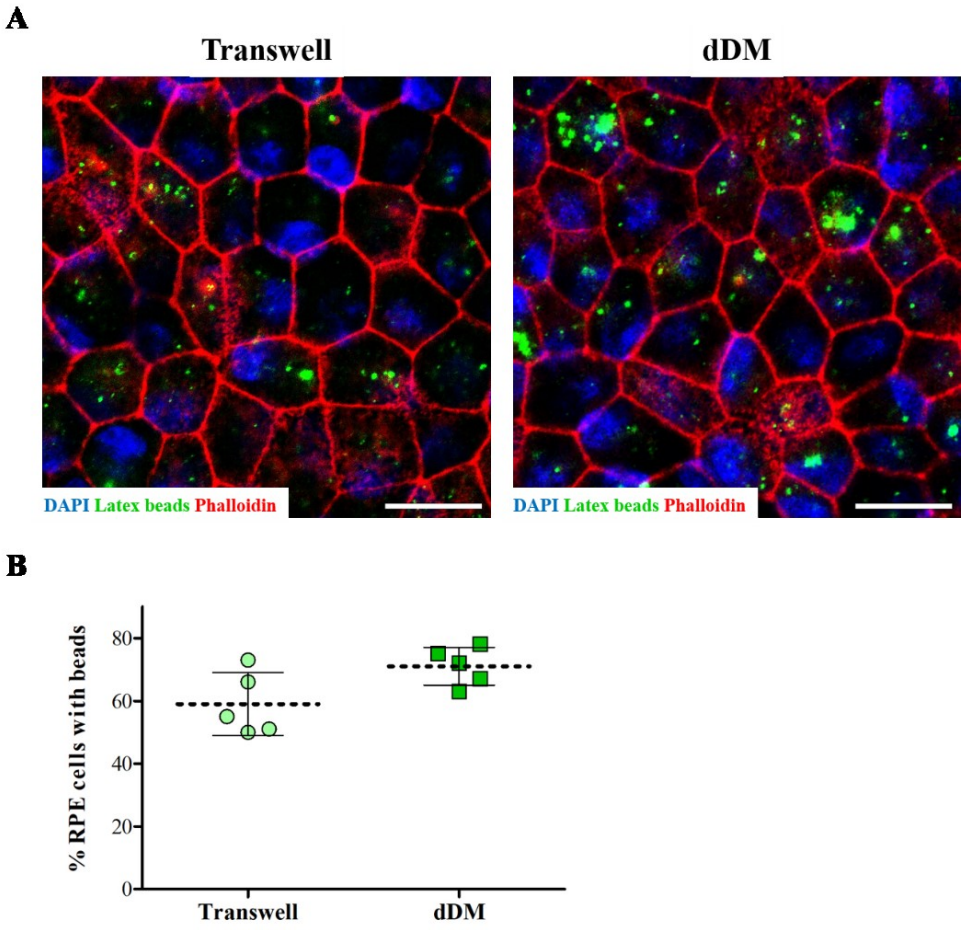

***Figure 23**: Phagocytic function of H09-RPE cells on dDM. (**A**) Latex beads uptake (green) in H09-RPE cells over dDM. Actin filaments were stained with phalloidin (red). Scale bar = 50 µm. (**B**) Percentage of H09-RPE cells internalizing the fluorescent beads when cultured on the dDM and under control condition on Transwell, respectively. Latex beads counts were obtained from five individual field if views, with each field containing ≥ 80 cells. Data represent mean ± s.d. *p=0.062. dDM, decellularized Descemet's membrane; RPE, retinal pigment epithelium.*

4.3.2.1 DM enhances hESC-RPE cell maturation

The differentiation of the H09-RPE when cultured on dDM or pre-coated multiwells was assessed by measuring the expression levels of early and late RPE related genes. RNA was collected from differentiated H09-RPE cells after 4 weeks of culture on dDM. The levels of RLBP1 and MERTK were slightly increased in derived RPE cells cultivated over the Descemet tissue, even if the differential expression pattern did not show statistically significant differences. On the other hand, a significant variation was found in the expression levels of RPE65 (Figure 24A). This result suggests the presence of cues on the dDM that could speed up the maturation of RPE cells derived from pluripotent stem cells. To corroborate these findings, ahRPE cells from donor were tested for gene expression analysis. These cells showed also a significant boost in RPE65 expression level when plated over the dDM compared with the same cell lineage cultured on SynthemaxTM II-coated multiwells (Figure 24B). A decrease in the expression of genes involved in the visual cycle is expected in ahRPE cells. In this regard, the significant increase in RPE65 expression during the culture of ahRPE cells on dDM could indicate that the membrane is able to retain or restore RPE cell function, probably due to its molecular composition, thus providing an ideal microenvironment for H09-RPE cell culture.

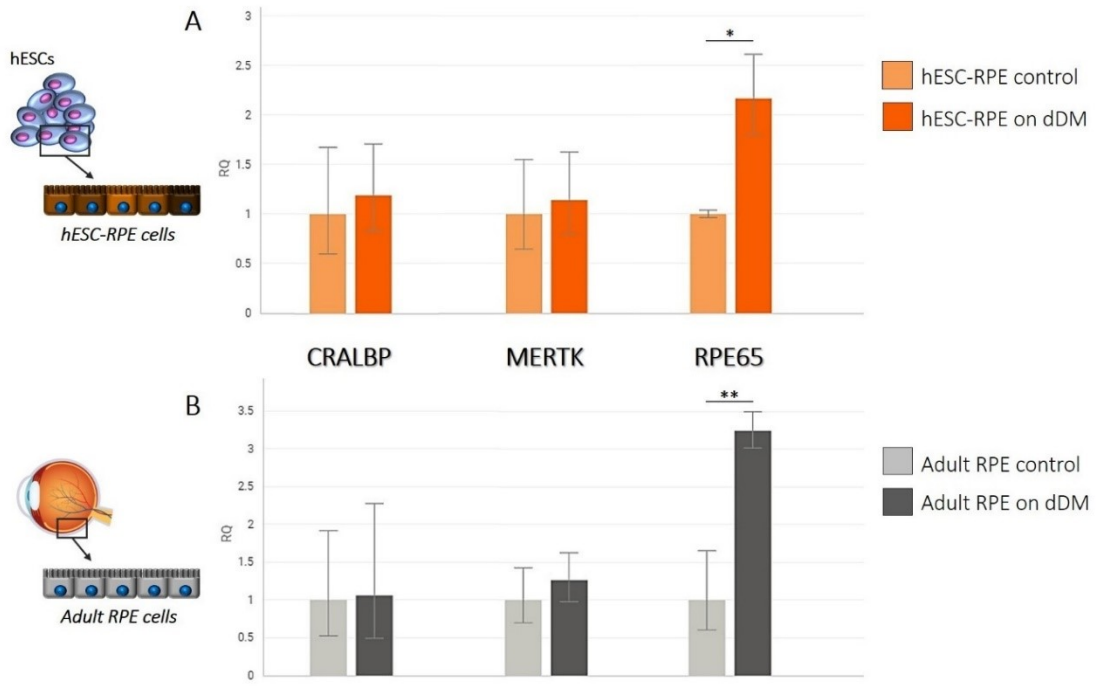

***Figure 24**: Quantitative analysis of gene expression of CRALBP, MERTK and RPE65 by RT-PCR. The bar graph in **A** shows the gene expression comparison between H09-RPE cells cultured on*

*dDM and H09-RPE cells cultured on pre-coated Transwell inserts used as control. In **B**, the same comparison is carried out between adult RPE cells cultured on dDM and adult RPE cells cultured on Synthemax™ II-coated multiwells. Measurements in each graph were normalized to the expression level of related control condition. Values are given as the mean ± s.d. for triplicate experiments. *p = 0.027 and **p = 0.020. dDM, decellularized Descemet's membrane; hESC, human embryonic stem cells; RPE, retinal pigment epithelium.*

4.3.3 Ability of hPSC-RPE cells to resurface aged BM

hPSC-RPE cells plated onto explants of BM reached confluence within 7 ± 4 days. hPSC-RPE cells did not reach confluence on severely degenerated tissues in which deep layers of the BM were exposed. Cell resurfaced BM as a monolayer and had highly variable morphology. In particular, cell shape and size were highly variable with many explants covered by large, thin, flattened or elongated cells. Cellular morphology ranged from round, to flattened or extremely flattened, to spindle-shaped, or rectangular. In H09-RPE cell cultures, BM was totally or almost totally resurfaced except for few small defects in coverage by these cells. Furthermore, H09-RPE showed dark pigmentation on this membrane. SEM revealed a monolayer of small, hexagonal-shaped H09-RPE cells on the BM, which appeared healthy up to 5 weeks in culture (Figure 25A).

Defects in BM resurfacing could be seen in explants with AMDCD-RPE. In the tissues showing almost complete coverage, AMDCD-RPE defects were of variable size, and often larger than the control condition on Transwell inserts. The morphology of these cells was variable: flat, extremely flat, or spindle-shaped to varying degrees. On the explants showing the worst resurfacing, the cells were large and ballooned. Cell morphology ranged from flat or elongated cells with smooth surfaces to small, compact cells. SEM imaging showed areas of explants covered by degenerating cells. Compact cells were located next to areas of defects (Figure 25B). Cell bordering the AMDCD-RPE defects were either elongated, forming a distinct border around the defect, or extended processes into the defect. In these areas, filamentous pseudopodia were extended from the RPE to basal lamina leftovers. No footplates were seen from the cell to an area of exposed inner collagenous layer.

After five weeks of culture, BM and the underlying choroid were intact. The choriocapillaris endothelial cells were lost in all explants, but intact pigmented choroidal cells were still present.

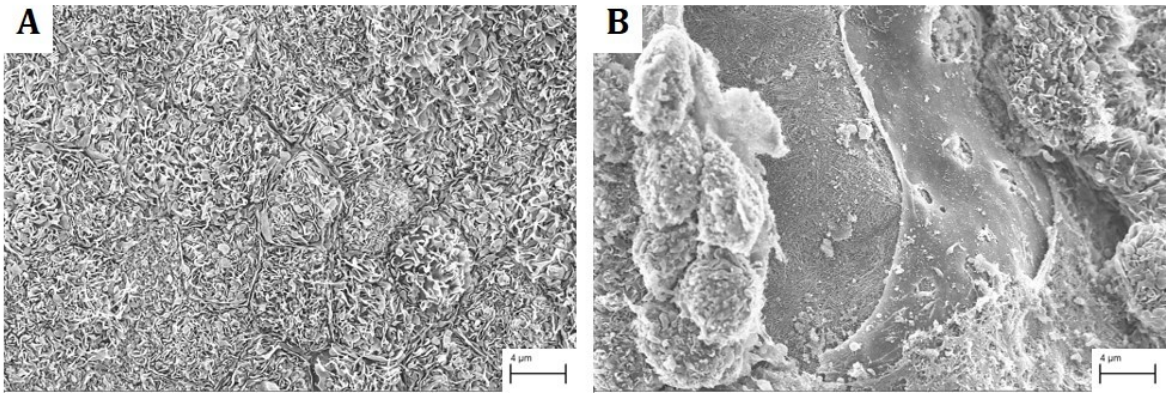

***Figure 25**: hPSC-RPE seeded onto explants of BM and choroid. (**A**) H09-RPE cells are able to resurface the membrane despite the nature of the BM's layer exposed after isolation. The monolayer consists of tightly packed cells with hexagonal appearance. (**B**) The morphology of the AMDCD-RPE cells is altered in areas of the explants with defects revealing the RPE basement membrane and/or the inner collagenous layer. Occasional cell extensions can be found on the defects. Scale bars = 4 µm.*

4.4 BIOMECHANICAL CHARACTERIZATION OF DM

AFM was used to emphasize any morphological changes occurring after enzymatic treatment. A pre-stripped whole corneal endothelium was chosen as positive control. This tissue had areas free of endothelial cells that allowed DM exposure for the AFM assay. We compared the topography and the surface roughness of these areas with DM which underwent decellularization. Controls and thermolysin-treated samples revealed a complex topography made of interspersed twisted fibers forming a densely packed structure. Several bumps and randomly oriented small diameter collagen fibrils were visible across the surface. The basement membrane-like matrix forms a close-knit and uniform design with small pores scattered along the surface. Compared to thermolysin-treated DM, the endothelial-side surface of the control membrane exhibited larger and more evident collagen fibrils (Figure 26). According to literature, ECM composition and properties have a major impact on cell behaviour (Fiejdasz et al., 2018; Vahle et al., 2014). Among others, surface roughness was estimated to underline a possible correlation with cell attachment. Roughness parameters were

calculated as mean Sq values for intact and denuded DM samples in four different spots along the endothelial-side of the tissues (Table 5). Surface analysis indicated a decrease in roughness of the decellularized membranes by ~ 50%, which was likely due to a smoothening of the surface following the enzymatic treatment. To provide evidence of the relation between surface roughness and cell adhesion, we calculated the Sq value of the stromal-side of the DM, where H09-RPE cells were unable to grow. We found a further reduction in roughness values compared to control condition, as a mirror of the different composition of the DM face in front of the corneal stroma.

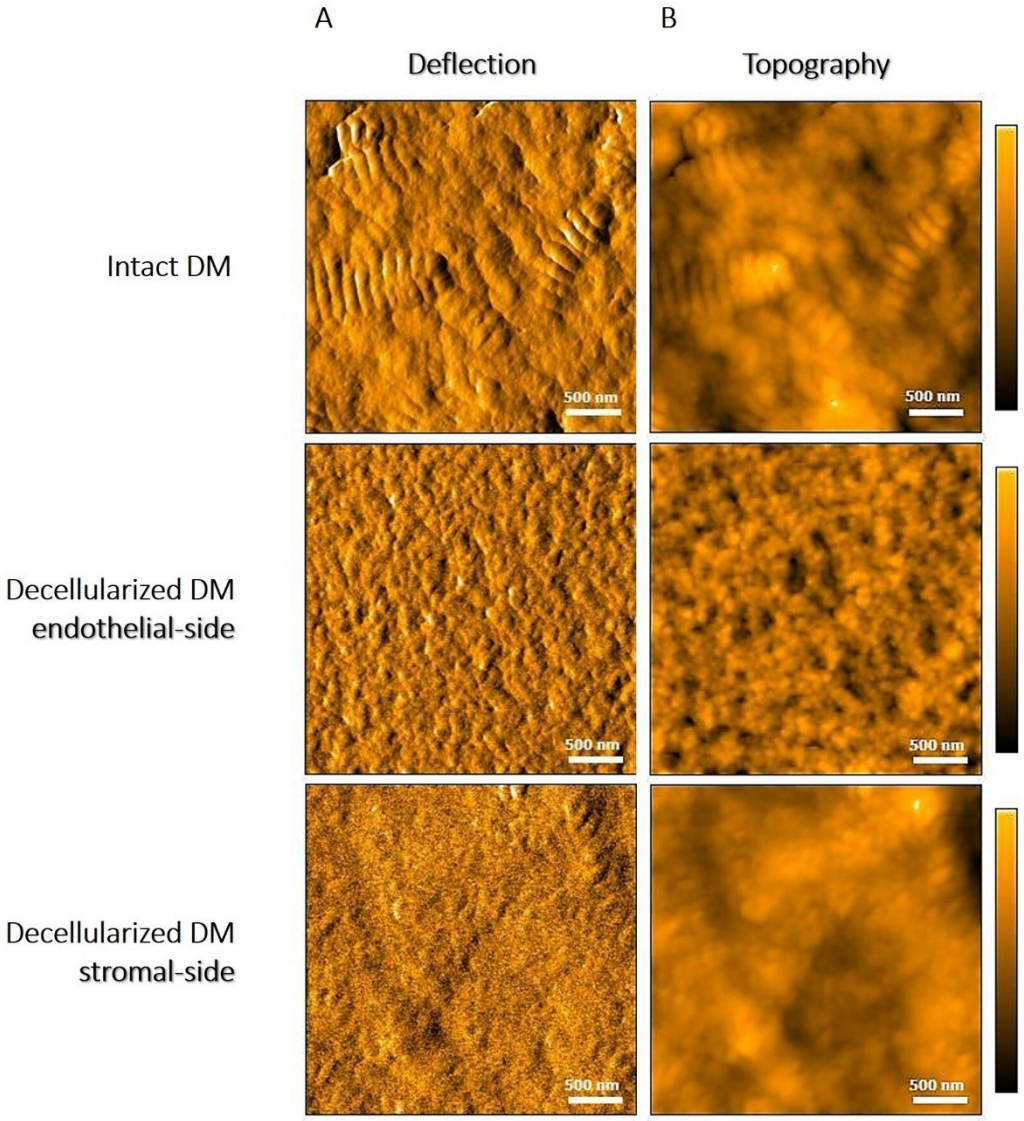

***Figure 26**: AFM analysis of DM's surface before and after decellularization. AFM images representing (**A**) deflection and (**B**) topography of intact and denuded tissue. Image scale: 3 x 3 µm. The coloured bars depict the height. Scale bars = 500 nm. DM, Descemet's membrane.*

***Table 5**: Calculation of roughness; ± s.d.*

Sample	Roughness [nm]
DM	10.29 ± 3.31
dDM endothelial-side surface	5.09 ± 0.72
dDM stromal-side surface	3.14 ± 0.57

Abbreviations: dDM, decellularized Descemet's membrane; DM, Descemet's membrane.

4.5 DIRECT DIFFERENTIATION BOOSTS RPE GENERATION

In the first part of the study, the generation of the RPE cells relied on the ability of the H09-hESCs to spontaneously differentiate into RPE cells. The distinctive cobblestone morphology and pigmentation of the RPE cells allowed to collect pigmented areas that appear upon differentiation of H09-hESCs. This method was often inefficient in obtaining a pure population of H09-RPE cells. Furthermore, there was a strong need to reduce the timing of differentiation and make it compatible with large-scale production to treat millions of patients. Using the direct differentiation protocol yielded RPE in half the time of the spontaneous method, together with increasing the differentiation efficiency and allowing to obtain a pure population of RPE cells without manual enrichment. Aiming at recapitulating the developmental origin of the RPE, the addition of cytokines and small molecules promoted the exit of the H09-hESCs from their pluripotent state toward the eye field lineage with a stronger efficiency than the spontaneous differentiation. Since the goal of the switch to a direct differentiation method was shortening the timeline of the protocol, a direct comparison of the two differentiation strategies was not carried out. Even if both directed- and spontaneously-derived H09-RPE cells yielded pigmented cells with the expected morphology, morphological variations were found between derivation methods within the same H09-RPE line once RPE was successfully derived. Overall, H09-RPE cells undergoing direct differentiation showed increased pigmentation compared to spontaneously-derived H09-RPE cells. In addition to reduced pigmentation, these latter RPE yielded patches of cells lacking phase-bright tight junctions and cobblestone morphology, suggesting the presence of other than RPE cells.

During direct differentiation, RPE derivation efficiency was quantified by flow cytometry at days 25 (RPE progenitors) and 40 (mature RPE) of differentiation. At day 40, RPE cells were fixed and analyzed for positive CRALBP and TYRP1 expression. For H09-RPE, the derivation efficiency was 98.8%, based on TYRP1 positive cells. At day 25, RPE progenitors are then replated and grown for an additional 2 weeks in 5% RPE media without enrichment, to allow pigment granules to mature. During this time, H09-RPE showed a monolayer of darker pigmented cells and improved cuboidal RPE morphology. Fluid-filled domes also appeared in these wells.

In general, the manual processing of the cell cultures could prevent consistency of the two methods to be established. Operator variability could impact on the proliferation and differentiation of the H09 hESC line, especially during the spontaneous protocol where the manual picking of the pigmented foci is highly dependent on technical skills. If the quality of a differentiation run was poor, culture wells showed minimal pigmentation and contained non-RPE contaminating cell types that extended neural tracks throughout the cell culture. In the case of direct differentiation method, the checkpoint of differentiation quality at Day 25 could prevent a poor differentiation run to continue, thus avoiding the waste of time and materials/reagents.

4.6 COMPARISON STUDY

As part of the research project, a comparison study was proposed. The study aimed to compare RPE cells differentiated from either the H09 hESC line or an iPSC line named AMDCD when cultured on the different selected scaffolds include in this work: denuded DM, the PLGA scaffold taken as “gold standard” of RPE transplantation and explants of human Bruch’s complex. Cell cultures on Transwell inserts were taken as reference condition. This study was conducted at the National Eye Institute/NIH in Dr. Kapil Bharti’s laboratory. The different 3D cultures were evaluated for maturity and functionality of the differentiated RPE cells.

4.6.1 hESC-RPE cells develop a tight monolayer on PLGA scaffold

Trans-epithelial electrical resistance was used as a reliable and rapid method to confirm the quality of differentiation and examine tight junction integrity along with monolayer permeability of the different scaffold-condition cultures. Among the great advantages in the use of the TER method there are monitoring of living cells and absence of any risk for the viability of the cell cultures. The technique is based on measuring ohmic resistance. For these measurements, the positioning and stretching of each scaffold during cell culture was mandatory to ensure correct resistance readings. Furthermore, the estimation of the TER over time to study the development of barrier function has been used as a sign of readiness for further functional testing and implantation studies. The minimum threshold of 400 Ωcm^2 for epithelial resistance per unit area was used to determine the quality of the RPE monolayer on top of each scaffold (Figure 27). Based on this assumption, the batch of AMDCD-RPE cells investigated in this study resulted poorly differentiated, because the TER values were slightly below or just around the threshold for the control condition. Considering this, we relied on H09-RPE TER values for comparing the different scaffold-conditions. According to these data, the H09-RPE cells formed proper tight junctions when cultivated on top of the PLGA scaffold. The inability of the H09-RPE cultivated on dDM to reach the threshold of TER along the weeks could represent a deficit in barrier integrity of these cells during their stage of growth on top of this membrane. H09-RPE on the Bruch's membrane demonstrated a similar outcome. Only few of the examined samples showed electrical properties similar to the H09-RPE patch on PLGA scaffold. This inconsistency in TER values among the two biological membranes could be addressed either to intrinsic tissue variability or the loosening of the membrane during cell culture. In addition, the natural concave shape of the DM *in vivo* prevented a complete flattening of this membrane on a flat surface, likely leading to uneven cell growth and proliferation, with slower or incomplete maturation of cells on a wrinkled, wavy structure.

H09-RPE cells cultured on Transwell inserts showed the highest TER values, with measurements going far beyond the threshold.

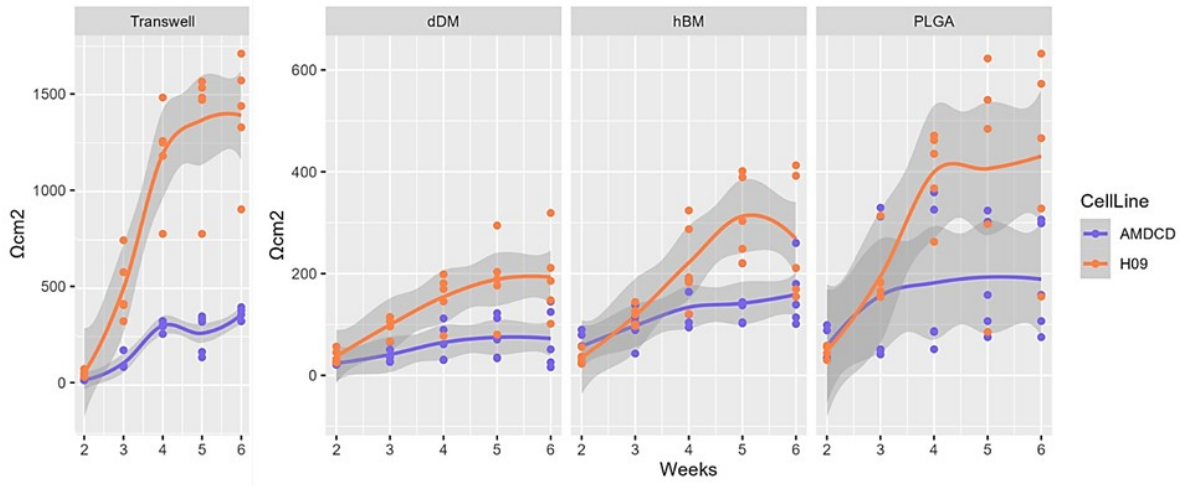

***Figure 27**: Trans-epithelial electrical resistance measurements of hPSC-RPE cells culture on the different selected scaffolds. dDM, decellularized Descemet's membrane; hBM, human Bruch's membrane; PLGA, poly lactic-co-glycolic acid.*

4.6.2 Phenotypic characterization of hPSC-RPE cell cultures on selected scaffolds

One of the aims of the comparison study was to investigate whether the selected scaffolds affect hPSC-RPE phenotype. Different techniques were used to study RPE morphologic features. In addition to TER, immunofluorescence was useful to locate the expression of typical RPE markers, TEM was valuable to inspect fine morphological alterations, while SEM analysis revealed modifications in apical processes structures.

At Day 40 immature RPE cells were enriched by negative selection, as per differentiation protocol, and seeded on different scaffolds for maturation. hPSC-RPE cells were fed for 5 weeks until full maturation.

TEM confirmed the poor quality of the AMDCD-RPE batch in term of differentiation efficiency: large vacuoles were visible in all the tested scaffold-conditions and the aberration of the tight junctions was in line with the low TER values measured for these cultures. On the other hand, H09-RPE tight junctions appeared intact in TEM images in all the scaffold-culture conditions. Several pigment granules were present on the apical side of RPE cells. In mature RPE, mitochondria appear to be short and restricted to the basal side of cells, all around the nuclei. While H09-RPE cells showed correctly localized mitochondria, AMDCD-RPE had these organelles spread laterally of nuclei. Interestingly, while no fine intracellular structure defects

were identified, the RPE monolayer seemed to have different height among each scaffold (Figure 28).

SEM confirmed the presence of apical processes on all the scaffold-RPE patches. Compared with the control condition, RPE cell cultures showed slight modifications in their apical structures among the selected scaffolds. A major difference was evident between the two cell lines: H09-RPE cells presented finger-like structures that have long and thin cylindrical shape, also referred to as microvilli or apical processes, while AMDCD-RPE cells had petal-like apical processes that are constituted by flat sheets of membrane (Fisher and Steinberg, 1982; Steinberg and Wood, 1974).

The heterogeneity of RPE in the neural retina in human eyes has been demonstrated previously. Several morphometric features distinguish these different phenotypic populations of RPE cells. Among the differences, the phenotype of RPE apical processes is considered a discriminatory feature among RPE subpopulations, and these projections reflect the physical interaction of RPE with rod and cone photoreceptors. The distribution and density of the finger-like apical processes indicate that they are associated with rods. Instead, petal-like structures wrap around cone outer segments. Therefore, it cannot be ruled out that the different hPSC lines used in this study might differentiate toward a certain phenotype of RPE cell.

A

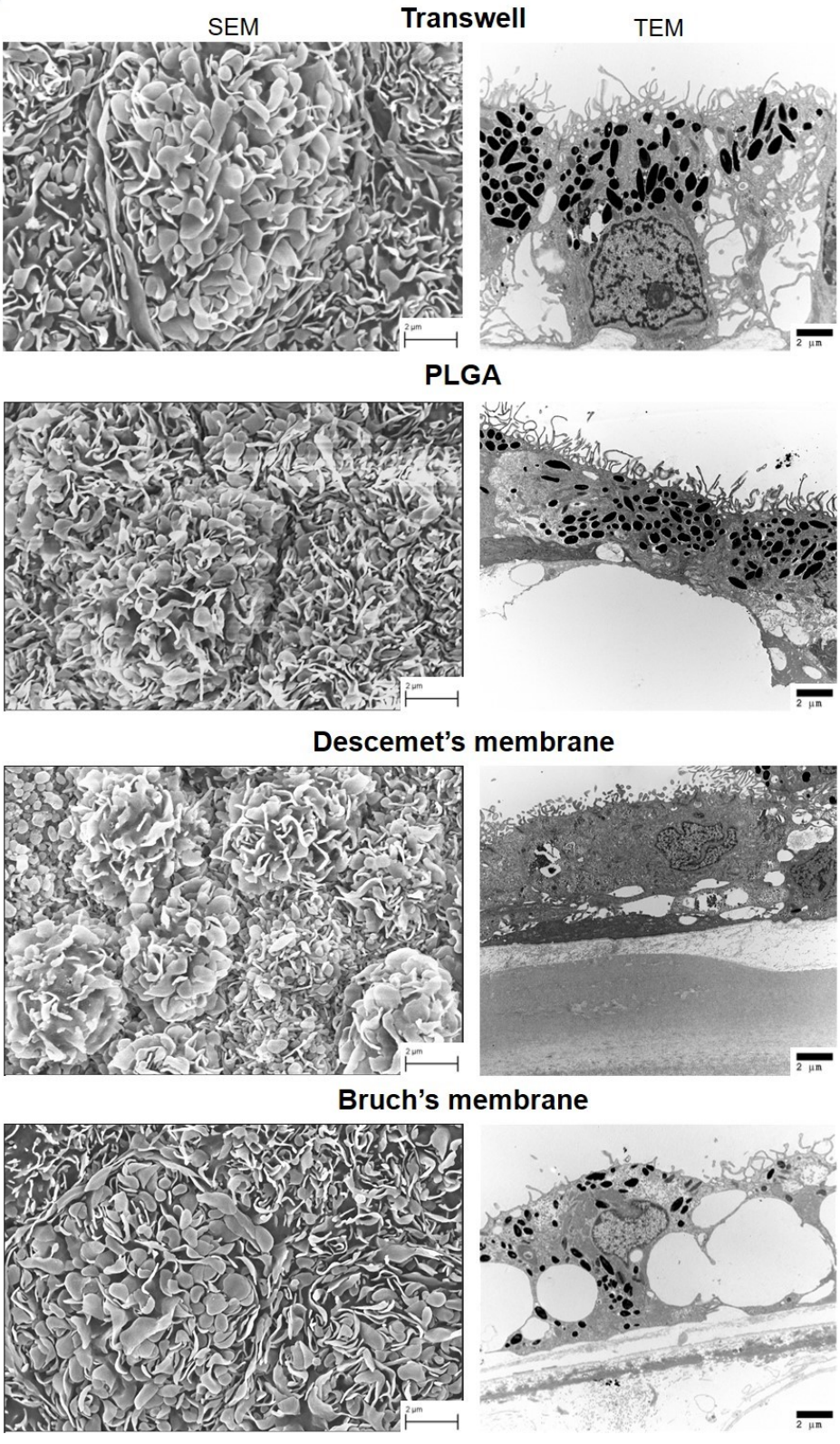
SEM
Transwell
TEM
2 µm
PLGA
Descemet's membrane
Bruch's membrane

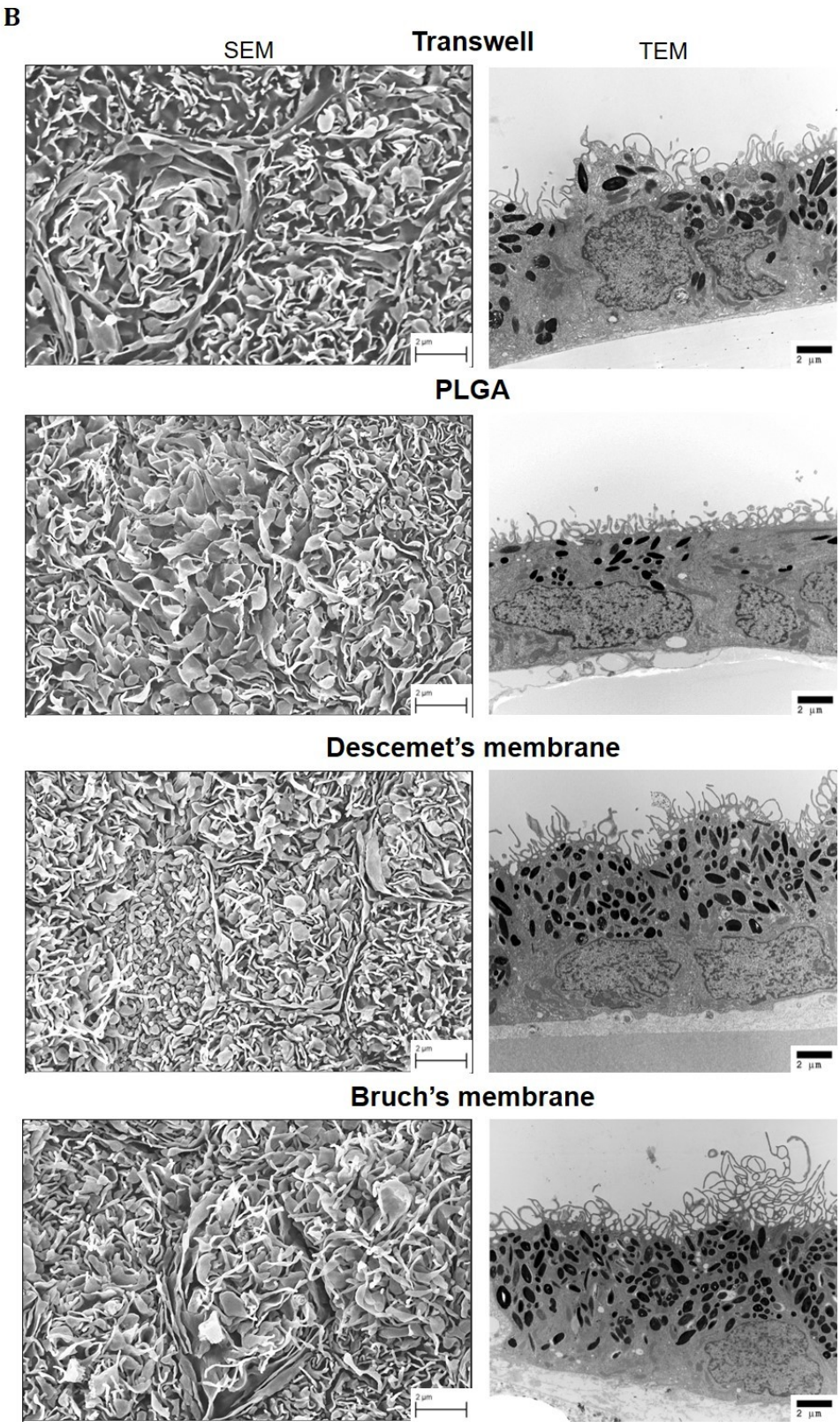

***Figure 28**: SEM and TEM images of AMDCD-RPE (**A**) and H09-RPE cells (**B**) cultured on each of the scaffold included in the study. Severe fine morphological alterations were detected with TEM imaging in AMDCD-RPE cells (**A**). Scale bar = 2 µm. PLGA, poly lactic-co-glycolic acid; SEM, scanning electron microscope; TEM, transmission electron microscope.*

RPE is a highly polarized monolayer of cells, and only by achieving this polarization RPE can perform its functions, by allowing compartmentalized localization of organelles and proteins and differential secretion of molecules on the apical or basal side of the monolayer. Immunostaining was used to study the polarization of the hPSC-RPE cells on top of the different scaffolds, along with inspecting gross morphological alterations and differences between the RPE monolayers. After staining for mature RPE markers, the imaging was performed with Airyscan, a technique based on confocal laser scanning microscopy (Figure 29). A critical issue during imaging was the autofluorescence coming from the structural elements such as collagen and elastin of the two biological membranes, in particular of the Bruch's membrane. Stack images of Bruch's membrane protein CIV and phosphoezrin staining enabled the visualization of cell polarization. Expression of phosphoezrin was not very consistent in all the cultures. For the AMDCD-RPE cells, the staining appeared particularly faint, especially for phosphoezrin. Since ezrin is a major determinant in the maturation of surface differentiations of RPE and that the phosphorylation of ezrin on T567 turns ezrin into the active conformation which is often accompanied by enhanced cellular activity, the low expression of this enzyme in AMDCD-RPE cells could be another major result of the poor differentiation quality of these cells. For H09-RPE, CIV was nicely expressed on the basal side in all the scaffold-conditions. On the dDM, H09-RPE showed a strong expression of CIV, according with the collagen nature of this membrane (Figure 29A).

PMEL staining highlighted melanosomes or melanin (a transmembrane glycoprotein present in melanosomes). According with the high level of pigmentation of the RPE cells, PMEL was highly expressed throughout the cell cultures.

Phalloidin, by enhancing actin filaments, aided to detect areas of undifferentiated cells among the cultures. Stress actin filaments are normally present in hPSC-RPE after seeding, but disappear when cells assume the characteristic cobblestone pattern. These filaments were visible at later stages of maturation in AMDCD-RPE cultures among areas of undifferentiated cells (Figure 29B).

RPE65 is a component of the vertebrate visual system, playing a critical role for the regeneration of rhodopsin in the visual cycle by regenerating visual chromophore, 11-cis-retinal, for rod and cone visual pigments (Kiser, 2022). RPE65 localizes in the cytoplasmic space and it is expressed in RPE cells at full

maturation. Considering the involvement of this protein in the visual cycle, it is not expected to be highly expressed in RPE cell cultured *in vitro* that has never come across photoreceptors. However, RPE65 expression occurred among the scaffold-conditions. For AMDCD-RPE on the BM complex, it appeared dim compare to control condition (Figure 29C). To better understand the level of this protein on each culture, a relative protein quantification is needed.

By forming strong cellular junctions, RPE cells act also as a barrier. Among different types of junctions, tight junctions are located toward the apical side of RPE and are the major players in the formation of the barrier. The staining for ZO1 enhanced different patterns of RPE cells and these were in line with the morphometric findings. With maturation on top of the selected scaffolds, H09-RPE cells become compact and hexagonal. AMDCD-RPE appeared larger and elongated when cultured on PLGA and BM complex, a sign that polarization and maturation are affected (Figure 29C). This staining justified the TER values measured for these cell cultures and it can be assumed the formation of loose tight junctions.

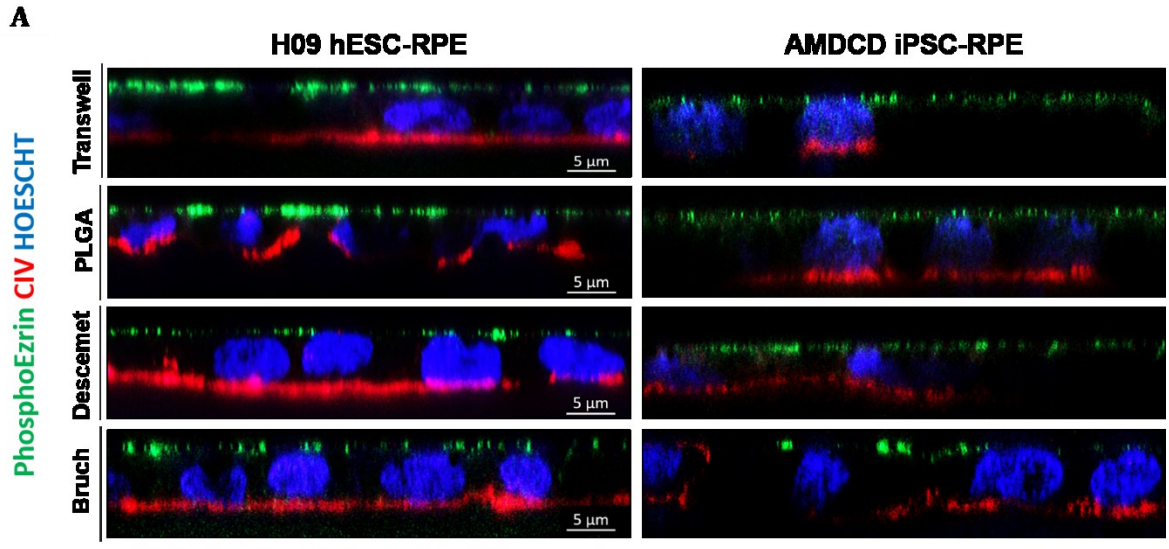

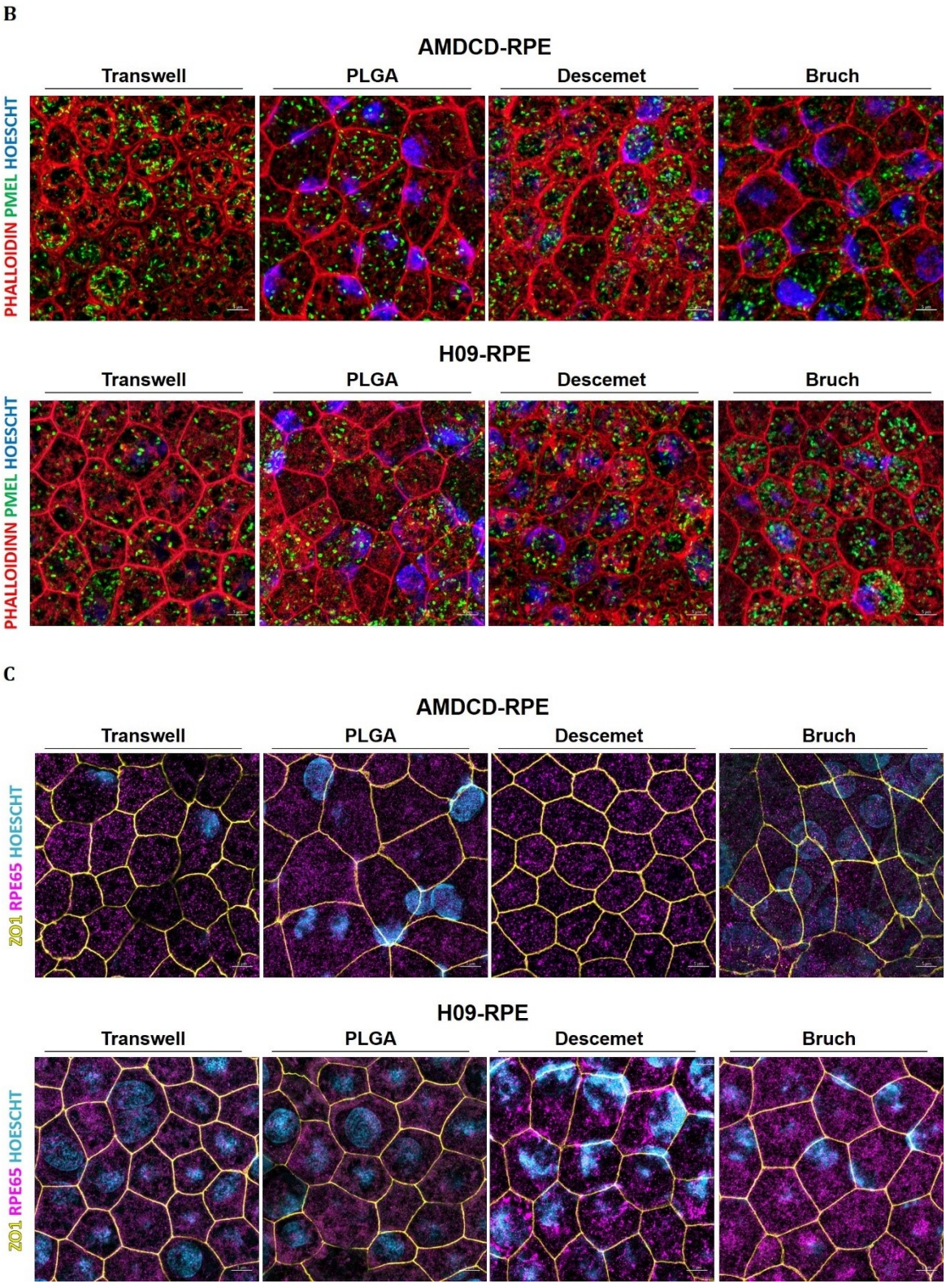

***Figure 29**: Expression of mature-RPE markers by AMDCD-RPE and H09-RPE. Immunofluorescence staining of AMDCD-RPE and H09-RPE cell monolayers on the different scaffolds for Phosphoezrin and type IV collagen (green and red, respectively) (**A**); PMEL and Phalloidin (green and red, respectively) (**B**); RPE65 and ZO-1 (magenta and yellow, respectively) (**C**). At least 3 different samples were analyzed. In A, images correspond to maximal projections of z stacks. Scale bar = 50 µm. Bruch, Bruch's membrane; CIV, type IV collagen; Descemet,*

Descemet's membrane; hESC, human embryonic stem cell; iPSC, induced pluripotent stem cell; PLGA, poly lactic-co-glycolic acid; RPE, retinal pigment epithelium.

4.6.3 Increased variability in hPSC-RPE shape metrics when cultured over BM explants

ReShAPE allowed a comparison of the RPE cell cultures on the different selected scaffolds based on morphometric features of the cells. The software was run separately for both cell lines. For every scaffold-condition, RPE cell borders were immunolabelled with ZO1, recognizing tight junctions. Since in RPE cells actin filaments form a polygonal ring that connects tight junctions along cell borders, a fluorophore conjugated phalloidin was also used to enhance cell border staining. The resulting cell culture was imaged and cell shapes were analyzed. Color-coded images are representative images that display the quantification of cell shapes for every metric analyzed. REShAPE enhances several differences between the cultures, and in some cases also a clear heterogeneity across the same sample.
In the case of AMDCD cell line, the derived RPE cells show distinct metrics when cultivated on BM compared to other scaffolds. For instance, AMDCD-RPE cells presented smaller area on Transwell inserts compared to the same cells when cultivated on PLGA and BM. The cells on the BM appeared to be irregular in shape compared with the other scaffold-conditions. As a result, in the color-coded images of aspect ratio and hexagonality score, the color gradients are more pronounced than on the other scaffold-cultures. The graph shows a direct comparison of AMDCD-RPE cell dimensions across the different cell cultures on the selected scaffolds. The cell area for the AMDCD-RPE on the BM increases drastically, suggesting that when cultivated on BM, RPE cell areas tend to remain bigger (Figure 30A).
For H09 RPE, the differences in metrics between RPE cultures on different scaffolds are not very prominent, except for the cells on the BM, which resulted very elongated and irregular (Figure 30B).

As a remark, the optimization of the cell cultures layout played a major role in the outcome of the ReShAPE analysis. Indeed, when the tissues were not properly flattened and stretched, the resulting cell cultures appeared very heterogeneous. By visual inspection, it was noticed that the presence of several folds and waves

all over the scaffold-culture conditions affected cell proliferation and growing. In these areas, the cells become much larger and irregular, probably in response of an uneven surface. Because of this pleomorphism occurring to cells around the wavy areas, there is a high variability of cell size, elongation and regularity among the samples. This was especially true for the H09-RPE and it is reflected in the increase in standard deviation (Figure 30B).

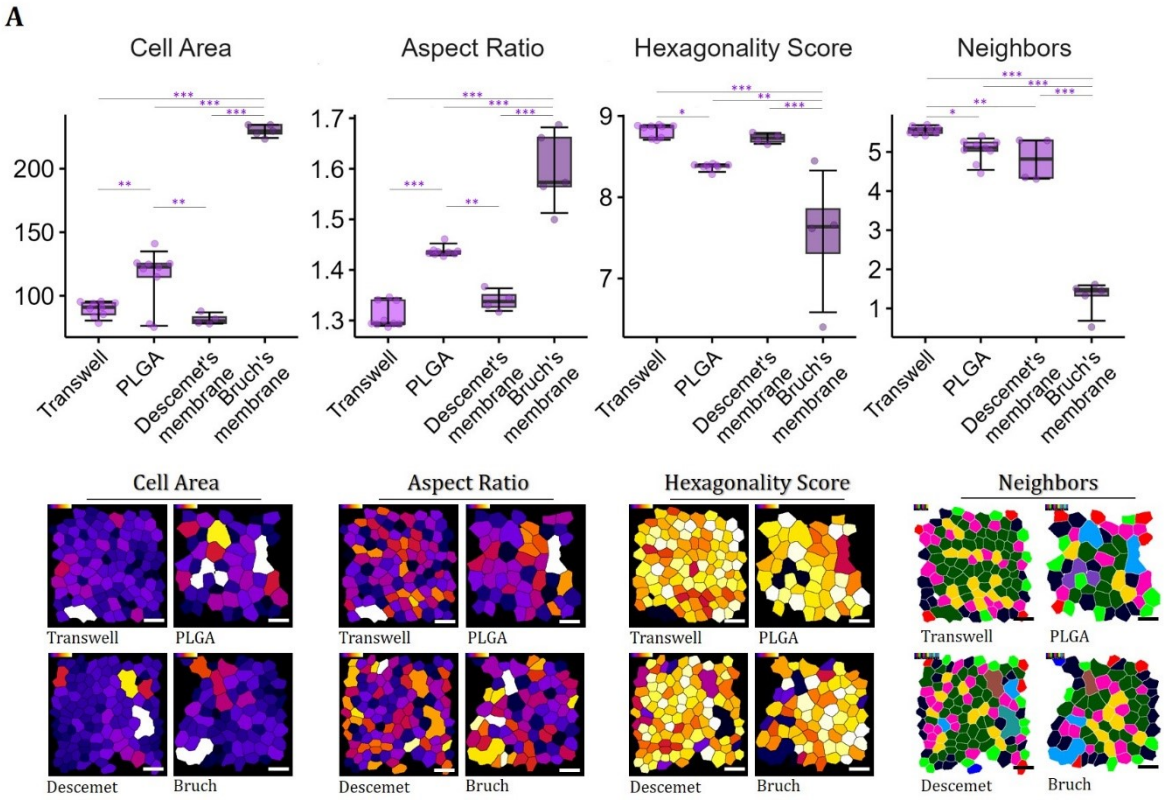

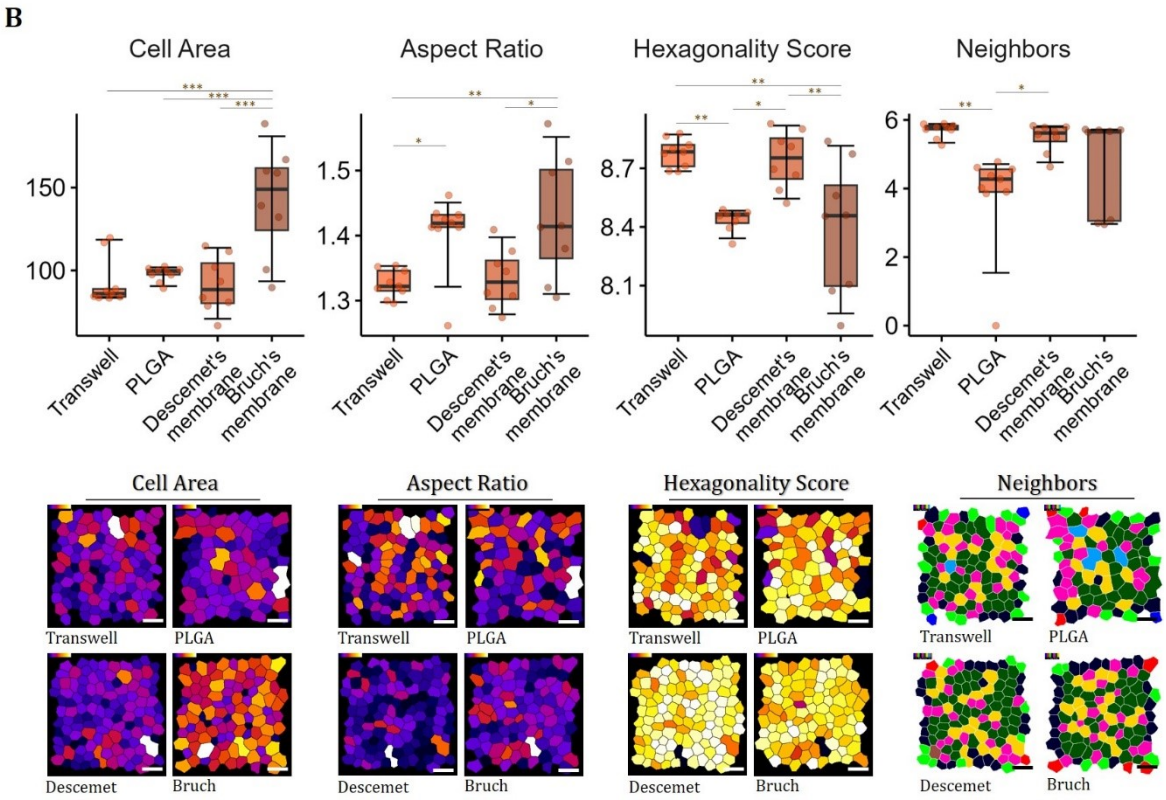

Figure 30: *Morphometric comparison of AMDCD-RPE (**A**) and H09-RPE (**B**) cells when cultured for five weeks on different selected scaffolds. The boxplots show the comparison of a shape metric between the different scaffold-conditions for each hPSC line. The shape metrics analyzed are cell area, aspect ratio, hexagonality score and neighbors. The panels below each graph show color-coded images for every metric analyzed, where every cell is color-coded according to the raw values. Bruch, Bruch's membrane; Descemet, Descemet's membrane; PLGA, poly lactic-co-glycolic acid.*

***Table 6**: Dunnett's test to compare differences in cell area, aspect ratio, hexagonality score and neighbors between the hPSC-RPE cell cultures grown on different scaffolds (* p < 0.05, ** p < 0.01, *** p < 0.001).*

AMDC RPE

Cell Area		
Comparison	**P value**	**Stars**
Transwell-PLGA	0.055	**
DM-Transwell	0.7658	
BM-Transwell	4.20E-14	***
DM-PLGA	0.0037	**
BM-PLGA	1.69E-12	***
BM-DM	4.51E-13	***
Aspect ratio		
Comparison	**P value**	**Stars**
Transwell-PLGA	8.85E-07	***
DM-Transwell	0.5273	
BM-Transwell	4.32E-12	***
DM-PLGA	0.0010	**
BM-PLGA	2.99E-07	***
BM-DM	1.59E-09	***
Hexagonality Score		
Comparison	**P value**	**Stars**
Transwell-PLGA	3.19E-02	*
DM-Transwell	0.9555	
BM-Transwell	4.64E-06	***
DM-PLGA	0.2854	
BM-PLGA	1.11E-03	**
BM-DM	1.32E-04	***
Neighbors		
Comparison	**P value**	**Stars**
Transwell-PLGA	1.63E-02	*
DM-Transwell	0.0055	**
BM-Transwell	1.31E-14	***
DM-PLGA	0.6509	
BM-PLGA	1.44E-14	***
BM-DM	3.91E-13	***

H9 RPE

Cell Area		
Comparison	**P value**	**Stars**
Transwell-PLGA	0.9474	
DM-Transwell	0.9991	
BM-Transwell	9.85E-05	***
DM-PLGA	0-9101	
BM-PLGA	4.00E-04	***
BM-DM	1.00E-04	***
Aspect ratio		
Comparison	**P value**	**Stars**
Transwell-PLGA	3.21E-02	*
DM-Transwell	0.9933	
BM-Transwell	7.90E-03	**
DM-PLGA	0.0706	
BM-PLGA	9.11E-01	
BM-DM	1.92E-02	*
Hexagonality Score		
Comparison	**P value**	**Stars**
Transwell-PLGA	4.40E-03	**
DM-Transwell	0.9815	
BM-Transwell	1.30E-03	**
DM-PLGA	0.0143	*
BM-PLGA	9.72E-01	
BM-DM	4.80E-03	**
Neighbors		
Comparison	**P value**	**Stars**
Transwell-PLGA	3.10E-03	**
DM-Transwell	0.9679	
BM-Transwell	2.04E-01	
DM-PLGA	0.0135	*
BM-PLGA	3.35E-01	
BM-DM	4.40E-01	

Abbreviations: BM, Bruch's membrane; DM, Descemet's membrane; PLGA, poly lactic-co-glycolic acid; RPE, retinal pigment epithelium.

4.6.4 Unexpected pattern of VEGF secretion within the different scaffold-conditions

ELISA was used to assess the levels of VEGF in basal spent culture media, since VEGF has physiologically a trend towards directional basolateral secretion.

VEGF did not increase in a time-dependent manner in all the cell cultures. Again, this assay enhances significant differences between the two hPSC derived-RPE cells used in the study rather than among the different scaffold-conditions investigated for each cell line. In the control condition (Transwell inserts), the levels of VEGF for both cell lines appeared to be consistent with the data on VEGF secretion found in the literature (Figure 31). By contrast, basolateral secretion is differentially impacted throughout the scaffold-conditions. Overall, the resulting data might be due to factors that might alter RPE polarized secretion of VEGF. Considering the inadequate differentiation quality of the AMDCD-RPE cells, the increased secretion of the pro-angiogenic factor among the scaffold-conditions compared to control could be related to impairment of cellular processes that modulate the concentration of VEGF in a polarized fashion. To validate this hypothesis, next step would be to assess the levels of VEGF in the apical media. In the case of H09-RPE cells, VEGF secretion showed a different pattern compared to the same cells on Transwell inserts (Figure 31). The relative low amount of VEGF in dDM and BM complex cell culture conditions could be related to the possibility that the thickness of these membranes impeded the release of VEGF into the basolateral media and artefactually reduced VEGF in the basal conditioned media. This applies particularly to H09-RPE cells on BM complex, where the presence of the choroid with a thickness up to 350 µm can lead to an underestimation of VEGF secretion.

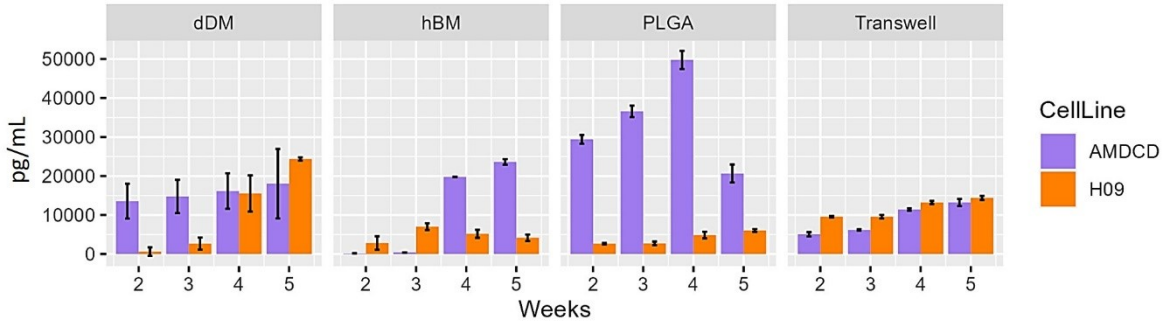

***Figure 31**: Graph showing the basal VEGF secretion for the hPSC-RPE cell cultures on the different investigated scaffolds. Values are given as the mean ± s.d. for triplicate experiments. dDM, decellularized Descemet's membrane; hBM, human Bruch's membrane; PLGA, poly lactic-co-glycolic acid.*

4.7 H09-RPE PATCH ON THE DM FAILS TO INTEGRATE IN THE SUBRETINAL SPACE OF RATS

To investigate potential delivery methods and short-term integration of H09-RPE patch either on dDM or PLGA scaffold, 0.5 mm diameter patches were transplanted in the sub-retinal space of six immunocompromised and five normal albino rat eyes. Normal albino rats were used as “training” rats for the optimization of the surgical procedure and the investigation of the best patch delivery tool. The lack of pigmentation in the rat eyes aided in the identification of the pigmented H09-RPE during surgery, thus having an optimal inside eye view during the whole procedure. Since immunocompromised rats barely show any form of rejection or inflammation, they were more suitable for studying the localization and integration of the cell patch in the retina.

The damage of the recipient retina can occur at any time during the surgery, yielding technically challenging the introduction of the potential cell therapy product in the sub-retinal space. The grafting strategy adopted was previously established in Dr. Bharti’s lab and it mainly relies on the use of an in-house patch loader tool for the delivery of the cell sheet. The injection tool has a plunger able to retrieve the patch of cells and release it in the preferred location.

Five weeks post-surgery OCT, fluorescein angiography and fundus infrared imaging enabled the visualisation of the different cell patches under the rat retina by showing their location and integration. Out of these eleven eyes, six eyes retained an intact RPE monolayer structure. *In vivo* imaging techniques confirmed successful integration of H09-RPE on PLGA by showing a flatten sheet of cells fitting under the host retina. On the contrary, H09-RPE on dDM was not able to unfold under the retina, and the integration into the rat RPE does not occur. Moreover, the failure of the DM to flatten would result in an increased thickness of the photoreceptor layer, leading to abnormal retinal architecture in the transplanted area.

Histological analysis should have confirmed the OCT data. Unfortunately, we were unable to spot the H09-RPE patch either on PLGA or dDM on histological cryosections of the eyes of rats. Indeed, the small size of the implant compared to that of the rat eye (6 – 7 mm) prevented us to identify the cell sheet within the subretinal space (Choi et al., 2021). We opted for an implant size of 0.5 mm to prevent potential surgical complications such as suprachoroidal haemorrhage and

failure of the retinal tissue to heal and reattach to the underlying layers after the surgery. Furthermore, the physiological pigmentation of the RNU rat retinas put additional challenges in the histological identification of the cell patches. We hope that further histological sections on the albino rats will facilitate this analysis thanks to the complete lack of subretinal and choroidal pigmentation of these rats' eyes.
Some fibrosis was noticed for the albino rat eyes. No sign of systemic toxicity of the transplant were noted in rats, as suggested by maintained their food consumption and body weight gain by all animals throughout the 8-week period, suggesting the safety of human H09-RPE cells as a transplantable patch. No teratoma formation appeared during this period.

These data suggested that the PLGA scaffold can provide effective support for the hPSC-RPE cells. On the other hand, the DM holds significant challenges due to its natural features. Above all, the tendency to roll upon itself when is peeled off from its biological location.
Overall, these rat experiments indicate that H09-RPE patch on PLGA scaffold maintains its monolayer architecture after transplantation in the sub-retinal space of rodent eye as opposed to H09-RPE on dDM that shows limited ability to form a monolayer in the same environment.

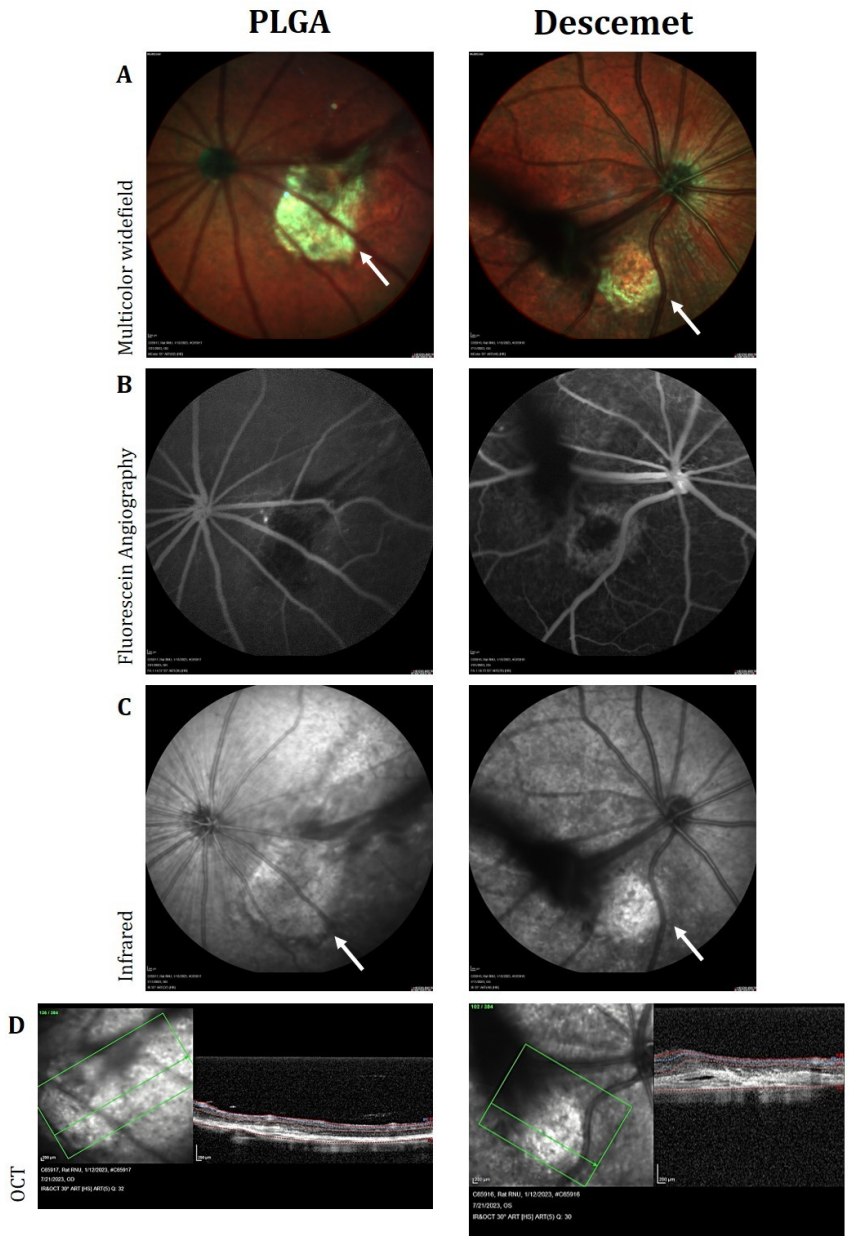

***Figure 32**: Visualization of transplanted H09-RPE patches in the subretinal space of rat eyes. (**A**) Eye fundus images aid in the localization of the transplanted H09-RPE on top of the two different scaffolds: PLGA (left) and Descemet's membrane (right). (**B**) Fluorescein angiography assesses the anatomy and physiology or retinal and choroidal circulation. Some damage to the blood vessels is visible in the areas of retinal detachment. (**C**) Representative En face infrared images. White arrows mark the location of the grafted H09-RPE-patches at four weeks post-surgery (A, C). (**D**) OCT shows sub-retinal location of the 0.5 mm diameter H09-RPE sheets. H09-RPE-patch on PLGA integrates into the rat retina, while H09-RPE-patch on DM is not able to flatten in the transplanted area. The position of each section is indicated on the left image with a bold green arrow. Descemet, Descemet's membrane; OCT, optical coherence tomography; PLGA, Poly(lactic-co-glycolic acid).*

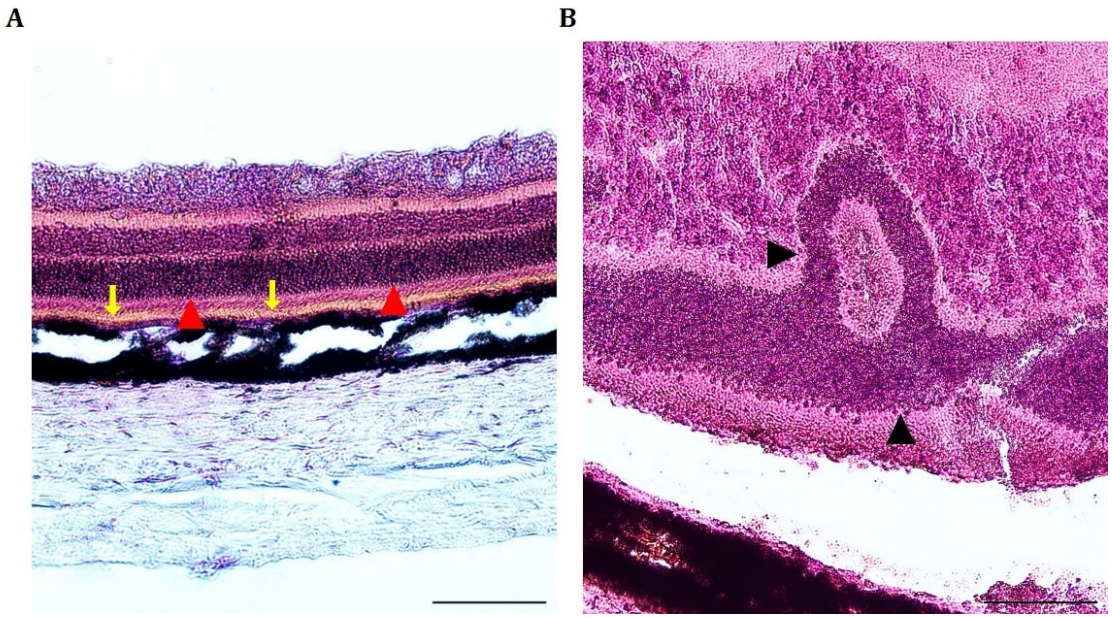

***Figure 33**: Representative H&E images of RNU rat retinas two months after transplantation. (**A**) Histology shows the presence of an intact outer nuclear layer (ONL, red arrowheads) with un underlying layer of retinal pigment epithelium (RPE, yellow arrows). (**B**) A degenerated ONL (black arrowheads) with characteristic waves, whorls, and rosettes is visible throughout the retina of a second RNU rat that received the H09-RPE-patch on DM. Spontaneous retinal alterations such as rosettes occur frequently in laboratory animals like rats, but we firmly believe that these adverse effects arose as a consequence of the surgery. In both images, the choroidal layer that appears to be detached from the retina is believed a histological artifact. Scale bars = 100 µm.*

5. DISCUSSION

Physical disruption and functional impairment of the RPE are common features of human degenerative diseases such as AMD. Current treatments have high rate of recurrence, therefore no effective therapies exist for these conditions. Several groups are testing stem-cell based approaches to replace degenerated RPE cells in the submacular space, although a common striking strategy is yet to be found.
This work aimed to formulate a construct capable of entering the field of RPE transplantation for the dry form of AMD, and potentially competing with current studies that have already entered a clinical trial.

The discovery that hESCs undergo spontaneous differentiation toward the anterior neuroectoderm and eye field lineages encouraged several research groups to establish a range of directed and nondirected derivation methods to promote the differentiation of these cells toward the RPE fate (Rowland et al., 2012). These findings have extensive implications for the treatment of retinal degenerative disorders, leading in recent years to the development of cell therapy products moving toward the clinic. Owing to their distinct pigmentation, RPE cells were one of the first cell types to be identified during hPSC differentiation. The use of PSCs to generate RPE overcame many disadvantages experienced with primary or immortalized RPE cell cultures, such as insufficient supply and defects in recapitulating *in vivo* RPE hallmarks. PSC-derived RPE can therefore represent a valuable source to obtain large quantities of high-quality RPE cells for the use in human (Hazim et al., 2017a).
In our study, the successful derivation of RPE-like cells was performed from a commercially available hESC line. Since the clinical and industrial applications of hPSCs require standardized and preferably nonxenogeneic culture conditions, we initially used a previously validated spontaneous differentiation protocol characterized by xeno-free and defined differentiation conditions for hPSC-RPE cell production. By maintaining a xeno-free environment with a focus on both media and substrate constituents, we sought to facilitate the translation of these research products to ATMPs to be used *in vivo* in clinical applications. Animal-derived products represent a great concern in the field of regenerative therapies for the potential hazard of product-induced immunogenicity or contamination from animal pathogens (Bharti et al., 2011; Mallon et al., 2006; Vaajasaari et al., 2011).

Besides, the inherent variability associated with different lots of xenogeneic components could shield narrow phenotypes that raise between patient-derived cell lines or differentiation methods. Normalizing culture conditions through the removal or replace of animal origin products with suitable alternatives aids in the differentiation toward the RPE fate more close resemblance to the *in vivo* environment (Sridhar et al., 2013). Furthermore, the devoid of additional exogenous growth factors using this method simplify the set-up of more reproducible culture system.

The approach described by Hongisto et al. (Hongisto et al., 2017) and reproduced in this study relied on the use of a xeno-free serum replacement together with a combination matrix made of LN-521 and type IV collagen. These two proteins are major constituents of the RPE basal lamina and promote single-cell attachment and survival. LN-521 was also used for coating H09-hESCs in a feeder-free platform. This system, even if simple and flexible, was based on single-cell passaging. Since these prolonged culture conditions could lead to karyotype changes associated to growth and differentiation advantages, a short safe window of H09-hESCs passaging was used to begin differentiation.

To help the differentiation towards retinal phenotypes, a brief period of suspension culture by way of EBs improved cell survival. Once replated as 2D culture, H09-hESCs showed the first pigmented colonies at day 14. These dark islands exhibited cobblestone morphology with cuboidal shape similar to typical RPE. Manual enrichment followed by long-term cultures led to RPE cells of variable degrees of pigmentation. Purity and successful cryopreservation were achieved by controlled passaging of H09-RPE no more than twice. Additional single-cell passaging could result in abnormal proliferation of the differentiated RPE cells and EMT due to the loss of RPE cell-cell contacts (Vaajasaari et al., 2011). Morphological changes typical of EMT could also be initiated by initial low cell seeding density. At the end of the differentiation period, H09-RPE cells were highly organized and pigmented. Characterization assays to examine RPE maturity and functionality confirmed that the derived RPE cells met general requirements in terms of quality. Immunostaining for typical RPE proteins were properly expressed and localized, indicating correct cellular polarization. Tight junction proteins including ZO1, occludin and claudin 19 showed normal expression and localization. The presence of these junctions was reflected functionally by the elevated TER of the cell cultures. After 42 days of differentiation, the TER had

reached 400 Ωcm^2. A good end point for matured RPE cells is 200 Ωcm^2, meaning that there is a tight epithelium. A range of TER values around this number have been assessed from primary and immortalized RPE cell lines (Hornof et al., 2005; Mannermaa et al., 2010). The PSC-RPE cells have shown superior ability to other RPE cell cultures in forming a highly polarized monolayer. Considering this, the TER value of 400 Ωcm^2 was taken as threshold. Surface localization of MERTK which participates in the ingestion of POS suggested *in vitro* phagocytosis capability of the H09-RPE cells. POS phagocytosis represents one of the most important functions of the RPE cells. *In vivo*, the RPE takes part in the visual cycle by recycling non-functional POS. The derived H09-RPE cells revealed *in vitro* functionality by binding and internalizing bovine POS. Growth factors secretion further corroborated the functionality of the H09-RPE cells. Indeed, our data demonstrated that the derived RPE cells were able to secrete PEDF and VEGF from the apical and basal side, respectively.

The so-called spontaneous RPE derivation method used in the first part of the study allowed us to obtain RPE cells with sufficient yield and purity. However, we believe that the time- and labour-consuming manual steps required within this protocol prevented us to gain a pure population of putative RPE cells.

Recently, more specific differentiation approaches and more efficient purification and selection methods have been developed for these cells (Cho et al., 2012; Hazim et al., 2017b; Idelson et al., 2009; Osakada et al., 2009). These strategies rely on mimicking whole eye development by using specific signalling molecules. By recapitulating the events that occur during retinogenesis, we aimed to improve RPE derivation using the direct differentiation method described by Sharma et al. (Sharma et al., 2022). Moreover, this approach has been used in a current clinical trial for AMD (Sharma et al., 2019). From a cell therapy manufacturing perspective, it was the perfect compromise to generate eligible RPE cells for transplantation. This protocol has been used to produce RPE cells from over 65 iPSC lines. One of this line (the AMDCD-iPSC) was used during the comparison study. For the first time, this derivation method was tested on a hESC line (H09-hESCs). A pure population of RPE cells expressing mature RPE markers and forming strong tight junctions was successfully derived from the H09 hESC line. Analysis by flow cytometry showed that the RPE cells obtained after Day 40 purification step had a purity of 98.8%, depending on the RPE marker chosen. Compared to H09-RPE cells obtained with the spontaneous method, the same

cells derived through direct differentiation revealed a strong dark pigmentation. Even though pigmentation level is used as a marker of hPSC-RPE maturity, previous studies reported that there is not a straight correlation between them (Bennis et al., 2017). In addition, Sorkio et al. (Sorkio et al., 2014) demonstrated an opposite association of pigmentation with TER. Nevertheless, the TER values measured for our direct-derived H09-RPE cells after five weeks on Transwell inserts were the highest we found compared to previous measurements. The role of pigmentation remains controversial. The pigment in melanosomes acts as Ca^{2+} storage and excess light binder, but also as antioxidant by eliciting cytoprotective functions (Rózanowski et al., 2008). Pigmentation may alter aspects of physiology and functionality of the intact RPE monolayer, but further studies are in need to understand how the degree and timing of pigmentation influence RPE derivation efficiency and maturation.

The generation of cells with potential therapeutic impact from stem cells is mandatory, but not sufficient for the development of a cell therapy for clinical application. The formulation and the delivery of the final product have major consequences for the success of this type of treatment. Considering the advantage of using a supportive substrate for improving the integration and functionality of the putative RPE cells once transplanted *in vivo*, we started looking for a promising scaffold that could reproduce as close as possible the natural environment in which RPE grows. This biomaterial should act as analogue of the ECM, in order to help restoring the cellular microenvironment.

At the beginning of this study, we opted for a biological scaffold that is closer to the RPE native environment, the hAM. Alongside its biocompatibility attributes, the hAM has been well tolerated during experimental surgery in rat retina and shown to stimulate the proliferation of RPE cells in a pig model of choroidal neovascularisation (Kiilgaard et al., 2012). First, we aimed to identify the most effective process to denude the hAM without damaging the underlying basement membrane. Additional rationales of the de-epithelialization process were to minimize the immunogenic potential of the hAM in future transplantation experiments (Keane et al., 2015, 2012; Wilshaw et al., 2006), reducing inter- and intra-donor variability among different batches of amniotic membrane (Hopkinson et al., 2006; López-Valladares et al., 2010), and increasing transparency by lessening the thickness of the tissue. We precluded a whole decellularization of

the hAM samples, in order to preserve important stromal factors critical for cell expansion and wound healing (Riau et al., 2010; Schulze et al., 2012). Enzyme-based methods were employed to avoid the long treatment time necessary with the use of chemical reagents such as EDTA or sodium dodecyl sulfate (SDS) (de Melo et al., 2007; Roy et al., 2016; Shortt et al., 2008; Wilshaw et al., 2006). The great variability in specimen thickness was determined by the progressive thinning of the hAM the farther the sample was taken from the umbilical cord (Connon et al., 2010).

Laminin α5 and CIV were used to assess the integrity of the hAM's basement membrane. Immunofluorescence staining of the de-epithelialized hAM revealed that all of the three tested de-epithelialization approaches successfully removed the epithelial cells from hAM surface, but that there was a significant difference between the methods as regards the damage to the basement membrane. In our study, Dispase II turned out to be the less safe method for the basement membrane, with a tendency to dissolve several ECM molecules (Lim et al., 2009). It also had a wrecking effect on the stroma, in line with what had been observed previously by others. In the field of *in vivo* ocular surface reconstruction, the maintenance of hAM's stromal growth factors seems to be crucial in wound healing and inflammation reduction after hAM transplantation (Zhang et al., 2013). We speculated that these factors could also be beneficial after the introduction of the hAM into the subretinal space of patients with retinal dystrophy. Incubation with 0.25% trypsin-EDTA preserved the basement membrane and maintained stromal integrity. Similar results were obtained with thermolysin, which is a zinc neutral heat-stable metalloproteinase (Miyoshi et al., 1998). After thermolysin treatment, we generated a fully de-epithelialized hAM with intact basement membrane and stroma. We established H09-derived RPE cell cultures on different pretreated hAMs to highlight any dissimilarities between the cultures. Previous reports on the use of hAM as a biological matrix to sustain RPE growth and differentiation involved primary native RPE cells derived from animal sources or human donors (Akrami et al., 2011; Capeáns et al., 2003; Ohno-Matsui et al., 2005; Singhal and Vemuganti, 2005; Stanzel et al., 2005). To our knowledge, there is only one research group working with hESC-RPE cells cultured over a de-epithelialized hAM (Ben M'Barek et al., 2020, 2018b, 2017).

H09-RPE cells seeded over de-epithelialized hAM revealed different experimental outcomes. We achieved an uneven monolayer of H09-RPE cells, mainly made of

patches of cells scattered along the membrane and interspersed between empty areas of basal membrane. These clusters of cells resembled the typical morphology and pigmentation of RPE cells. The same pattern was observed on cryosections of RPE cells cultured over hAM and stained for RPE65 and PMEL. The expression of the two markers confirmed the formation of a patchy layer of cells on top of the de-epithelialized hAM, with areas devoid of cells. These results showed that in the case the cells adhered and they were able to differentiate properly, they did not form a confluent monolayer. In the aforementioned papers regarding the potential of the hAM to sustain native RPE cells culture (Akrami et al., 2011; Capeáns et al., 2003; Ohno-Matsui et al., 2005; Singhal and Vemuganti, 2005; Stanzel et al., 2005), the fetal tissue was mostly denuded by enzymatic method, such as 0.25% trypsin and Dispase II, whereas our study, consistent with more recent findings (Hopkinson et al., 2008; Lim et al., 2009; Zhang et al., 2013), underlined the risk of compromising the basement membrane after the use of such enzymes. Considering the results of the research groups who experimented the culture of native RPE cells over de-epithelialized hAM, we dealt with queer outcomes and incomplete information. Capeáns et al. showed patches of RPE cells surrounded by areas of bare membrane, demonstrating the attachment of the cells and their organization in tight colonies of large cuboidal to round cells, but no evidence of a confluent monolayer (Capeáns et al., 2003). In the cases where a monolayer of RPE cells was achieved (Akrami et al., 2011; Ohno-Matsui et al., 2005; Singhal and Vemuganti, 2005), the morphology appeared to be seriously jeopardized. Furthermore, the use of native RPE cells could have a significant difference in cell adhesion and proliferation on the de-epithelialized hAM compared to hESC-derived RPE cells. The full *in vitro* derivation may explain the hardship of these cells to efficiently proliferate over a whole new biological environment, while the isolated primary RPE cells would better recover in a substrate resembling the natural *milieu* of the Bruch's membrane (Stanzel et al., 2005). Based on the assumption that the interaction between ECM proteins and integrins assures cell adhesion and migration over a substrate (Mi et al., 2012), we hypothesized a mismatch between the surface molecules and the corresponding cell receptors (Norde and Lyklema, 1991). Further tests are needed to establish if this may be linked to a cell deficiency or a partial damage of the de-epithelialized hAM basement membrane. The hAM preservation process could also have a negative influence on the culture of hESC-RPE cells over the tissue. Indeed,

cryopreservation has been reported to cause severe changes on hAM morphology and biochemical composition (Hopkinson et al., 2006). Cultures on de-epithelialized hAM were carried out for a maximum of 4 weeks. After this time, a severe loss of tissue integrity could be appreciated following histological examination.

The biological characteristics of hAM in terms of donor variations have been proven to have a major impact on their physical and chemical properties (Mi et al., 2010). The lack of transparency due to the wide variation in the thickness of the supplied membranes hindered a proper evaluation of the cell culture along the weeks. As reported elsewhere, membrane thickness has been correlated with the location in relation to the placenta. The age of the donor, as well as gestational age have been shown to affect tissue composition (López-Valladares et al., 2010), which may lead to different cell culture outcomes. An early characterization of the tissue would be preferred prior to any research or clinical use, to select the best tissue to be used as biological substitute to support the host cells.

Karim Ben M'Barek and colleagues demonstrated in their work that the hAM efficiently supports the culture of human pluripotent stem cell-derived RPE cells (Ben M'Barek et al., 2017). However, stressing on the reproducibility limit of the hAM application for the RPE cells, in their results they suggest to check the adhesion of the RPE cells few days after cell seeding. This remark raises the hypothesis of a possible failure in cell attachment as evidence of the variability of the experimental procedure.

To summarize our data, the experience in the use of the hAM as scaffold for the H09-RPE cells led us to rule out this membrane as potential candidate to sustain the putative RPE cell culture.

Considering these findings, we attempted to look for new potential substrates for the derived-RPE cells. Within the Veneto Eye Bank Foundation, the endothelial cell density is the eligibility criterion for corneal tissues. If this cell density is below a defined value, the cornea is not suitable for transplantation and it can be used for other-than clinic purposes. From these discarded tissues we were able to retrieve corneal endothelium and the underlying DM. After the isolation of the whole corneal endothelium, the removal of the endothelial cells was performed prior to H09-RPE culture. Corneal endothelium presents as a monolayer of fully differentiated and static cells (Last et al., 2009). Considering the inability of these cells to proliferate, we found that the proposed enzymatic treatment leads to

complete and easy removal of endothelial cells, ensuring a reliable protocol to standardise decellularized DM.

AFM analysis revealed that the DM possesses a rich topography, forming a dense structure of hardly visible small pores. This organisation reflects its function within the context of the corneal endothelium. By regulating the corneal water content, the DM acts as a filter, allowing the introduction of small molecules into the aqueous humour (Abrams et al., 2000). Despite the acceptable biocompatibility of the DM as a natural scaffold, we investigated whether surface properties following decellularization of the membrane could impact on cell adhesion. Surface roughness has been positively correlated with cell adhesion and proliferation. It has been proven that rough surfaces, as well as improving surface texture, can facilitate cell attachment (Zareidoost et al., 2012). Our results showed a decrease in surface roughness after the treatment of the DM. The enzymatic digestion of thermolysin could be responsible for smoothing the surface of the DM, probably due to removal of some remaining ECM ligands (Tezel et al., 2004) within the posterior non-banded layer of the DM, mainly produced by corneal endothelial cells. Nevertheless, our results encourage the use of the DM for hESC-RPE cell culture, even in the presence of some loss into the ECM framework of the DM endothelial-side after the enzymatic treatment, the latter being undeniable mandatory to ensure a scaffold free of any previous cellular component. On the other hand, the analysis of the stromal side of the DM exhibited differences in roughness compared to the endothelial-side, suggesting individual properties of the two sides of the same tissue. The different deposition of biomolecules during DM development and the formation of distinct layers in close contact with separate environments elucidate these differences (Ali et al., 2016). According to this, the additional decrease in roughness of the stromal-side of the DM accounts for adhesion deficiency of the H09-RPE cells when seeded on this surface. Correct DM labelling is therefore imperative to distinguish the endothelial-side of the DM on which developing a functional monolayer of hESC-RPE cells is possible.

We demonstrated that H09-RPE cell adhesion to dDM occured in about 24 hours. H09-RPE cells deposited on the new matrix as cell patches and then proliferate, ultimately organising in a tight monolayer of epithelial-like cells after 7 days of culture. After this time, cells stopped proliferating, consistent with the *in vivo* situation where RPE cells are quiescent and division appears only as a result of disease condition (Abu Khamidakh et al., 2018). Additional coating on the top of

the dDM was unnecessary, since the only dDM was capable of supporting the growth of the cells. Conversely, H09-RPE cells spread on pre-coated plastic surface by maintaining a single cell-phenotype. The number of adherent cells on the dDM after 24 hours resulted to be significantly higher than that in the control group, thus revealing not only a viable structural support for the H09-RPE cell culture, but also a beneficial effect of the DM proteins for the H90-RPE cell attachment. This justified the prominent cell proliferation activity during the first 24 hours of culture, leading to an increase of the overall cell proliferation rate over the dDM in relation to control condition at 24 hours.

H09-RPE cells on dDM revealed excellent cobblestone-like morphology, showing evidence of tight junctions at 2-3 weeks after seeding. In addition, maturation markers appear more rapidly on cells cultured over the DM than those on controls.

Transwell inserts cultures of RPE over dDM were established to provide further evidence of the positive influence of the membrane on RPE physiological functions such as phagocytosis. The phagocytic activity of H09-RPE cells was enhanced when the cells where cultured over the dDM compared to the control condition, even though not significantly.

We also examined the gene expression patterns of RPE marker genes CRALBP, MERTK and RPE65. No significant differences were observed at the end of the 4-weeks culture period, when the cells appeared to be mature enough, suggesting the absence of adverse effects on normal H09-RPE cells biology. Only the expression of RPE65, which is typically involved in visual pigment recycling and maintenance of photoreceptors, was significantly increased when the cells were cultured over the dDM. These results indicated that dDM could contain cues that promoted H09-RPE cell maturation. To further verify these data, ahRPE cells were tested for culture over dDM and gene expression analysis. It is well documented that ahRPE cells in culture lose their pigmentation and acquire a more fibroblastic shape, leading to partial dedifferentiation (McLenachan et al., 2017). In our model, primary RPE cells on dDM regained typical and uniform RPE phenotype by assembling in a closely packed monolayer of hexagonal cells. Moreover, the new substrate significantly boosted RPE65 gene expression compared to cells grown on SynthemaxTM II-coated multiwells. This underlined likely inhibition of RPE dedifferentiation, along with providing an ideal microenvironment for the H09-RPE cell culture (McLenachan et al., 2017).

In this part of the study, we highlighted the feasibility of the DM to support the attachment, proliferation and viability of H09-RPE cells over a 4-week period, potentially acting as a biological dressing in the context of the subretinal space. DM represents a perfect substitute of a whole ECM by owning all the features of a native tissue's basement membrane. Molecular composition could resemble basement membrane characteristics, with prominent content in CIV, laminin and fibronectin. Especially for CIV, its abundant presence in all layers of adult DM can explain H09-RPE cells' strong affinity for the membrane. As recently reported, RPE cells preferentially interact with this type of collagen, which is found abundantly in the RPE basal lamina (Eamegdool et al., 2020). Besides its biocompatibility and its flexible, but robust nature, DM holds the advantage of being already accepted for intraocular use at a regulatory level. Furthermore, DM could represent an exclusive scaffold for the xeno-free culture of H09-RPE cells by avoiding the need of any animal component for initial adhesion and culture maintenance.

In light of these initial findings, we initially proposed the DM as a tissue engineering tool to support hPSC-RPE cells, hence representing a potential therapeutic strategy in the field of regenerative medicine for retinal degeneration.

Choosing the appropriate scaffold to ensure the success of the tissue engineering product is critical and the optimal construct remains a challenge. Furthermore, if the RPE cell graft is intended to be implanted in areas of atrophy, changes in Bruch's membrane due to degenerative conditions and/or aging are also to be taken into account. Modifications at the BM level that decrease the bioavailability of ECM proteins and limiting cell-matrix interactions could have an adverse effect on the transplanted cells. Even in the presence of a supportive matrix underlying the healthy RPE cells, these latter might be affected by abnormal environmental cues that could alter the survival of the RPE patch in the long term (Gullapalli et al., 2005; Sorkio et al., 2015). With this in mind, we pursued to assess the effect of aged BM on hPSC-RPE cell attachment and morphology. Previous works demonstrated that the layer of the BM available for cell reattachment affects the morphology and behaviour of native human RPE cells (Tezel et al., 1999; Tezel and Priore, 1999). The BM explants included in this research were harshly damaged, thus the anatomic layer for cell attachment was not uniform throughout the tissue surface. We also observed lots of variability in cell culture outcome depending on the extent of tissue degeneration. We found that despite the status

of the explant, the morphology and level of cell confluence depended on the quality of the differentiated RPE cells. AMDCD-RPE cells showed impaired resurfacing compared to H09-RPE, which instead grew robustly over the BM, showing homogeneous appearance of the cells and reaching confluence in most of the samples. Later experiments demonstrated that AMDCD-RPE were poorly differentiated, and the resulting cultures presented areas of contaminating cells. There are few differences between the explant system used in the current study versus previous findings, including: the different source of RPE cells, the type of explant treatment for native RPE cells removal, the use of serum-containing medium vs our serum-free medium, and the presence of live choroidal and vascular endothelial. We cannot exclude indeed, that the survival of the pluripotent-derived RPE cells could be even related to the degree of underlying choroidal tissue degeneration (da Cruz et al., 2007). Moreover, the results from past experiments revealed that submacular and peripheral BM differ in the ability to support RPE survival following initial attachment, while we did not select the explant based on their retinal location.

In a second part of this research, we sought to compare different scaffolds under identical experimental conditions, in order to enhance inherent differences in the resulting hPSC-RPE cell cultures. Besides, the simultaneous investigation of biological and synthetic scaffolds intended to determine the superiority of one over the other, which could lead to higher cell culture outcome and, consequently, successful implantation.

We included in this part of the study the DM, the BM and the PLGA scaffold, taken as benchmark for cell therapy. In addition, we considered cultures on Transwell inserts as reference *in vitro* condition. We conducted the experiments on the H09-RPE and on the abovementioned iPSC line AMDCD. This line is commonly used in Dr. Bharti's laboratory and the putative RPE generated using direct differentiation process are generally used as control cells. After five weeks of culture on pre-selected scaffolds, H09-RPE and AMDCD-RPE cells were tested for maturity and functionality.

A substantial issue we faced prior to cell culture was to establish a way of mounting these biomaterials in preparation for cell culture. This step aimed to optimize the properties of each scaffold by providing appropriate tension to ensure substrate flattening and stretching for optimal cell attachment and growth. Other prerequisites of the mounted cultures were to create two different compartments

with independent feeding and being able to visualize cell culture using non-invasive techniques. The tissue culture plastics used for mounting these scaffolds were our best available options, but further improvements will be necessary to overcome specific limitations. First of all, the inability to directly monitor cultures by phase-contrast microscopy due to the lack of transparency of the Snapwells.

As well as other epithelia, the RPE has to fulfil a range of barrier and transport functions. To confirm the integrity and permeability of the monolayer, we measured TER across the monolayers. According to the resulting TER values of the AMDCD-RPE along the weeks, it was evident that the integrity of their tight junctions was severely impaired. On Transwell condition, hPSC-RPE cells usually develop strong junctions due to the formation of a snugly packed monolayer of cells, and the *in vitro* TER values are expected to raise higher (> 400 Ωcm^2) than *in vivo*. H09-RPE cells seemed to validate this observation, while the AMDCD-RPE did not show this trend. These data suggested that some issues could have arisen during AMDCD cell differentiation and the AMDCD-RPE did not fully matured. As per H09-RPE, only the PLGA-culture condition was able to reach the threshold, while the cultures on the two biological membranes failed this goal. It is important to bear in mind the presence of factors that could have affected the TER measurements. Among these, the accuracy of the measurement techniques based on the selection and usage of electrodes could alter TER reading. The electrodes known as STX2/“chopstick” electrode pair can introduce variability between measurements when the positioning is not consistent (Srinivasan et al., 2015). To overcome this problem, we used the EVOM2 and EndOhm chamber to secure mechanical stability and reproducibility, avoiding the need for manual holding of the electrodes. The instrument allowed to measure the TER on Transwell inserts, PLGA scaffold and DM-culture conditions. Unfortunately, the Cell Crown insert design made difficult the use of the EVOM2, and the TER of the BM cultures were calculated using the chopsticks.

TER values have shown to be temperature dependent (Matter and Balda, 2003). To avoid temperature fluctuation which could alter TER measurement, we equilibrated the cell cultures at room temperature for 10 minutes. Alternatively, a temperature-corrected TER (Blume et al., 2010) would eliminate temperature bias and permit comparison of TER values measured at different temperatures (Srinivasan et al., 2015). Controlling all these factors for each experimental

condition during TER quantification can be challenging, thus we do not exclude the likely over- or underestimation of some values in our experiments.

We attempted to replicate the culturing conditions as closely as possible between the investigated scaffolding material groups, hoping to see any alteration in morphology according to the scaffold-condition in which the cells were grown over. To evaluate cell morphology across the samples we employed SEM, TEM and confocal microscopy analysis. All techniques were performed after culturing cells for 5 weeks. This period is currently the optimal culture time ascertain in Dr. Bharti's laboratory for the complete maturation of iPSC-RPE-patch prior to transplantation. H09-RPE grown on the selected biomembranes formed a monolayer and acquired typical and homogenous RPE phenotype (pigmented, hexagonal, cobblestone like, closely packed cells). Furthermore, H09-RPE cells exhibited high degree of polarity with apical localization of Phosphoezrin and CIV. Confluent H09-RPE monolayers developed differentiated properties as evident by the expression pattern of RPE-specific marker proteins and, once confluence was reached, cells stopped dividing. The inhibition of cell growth is essential, because differentiated RPE cells normally remain dormant throughout life and proliferation only occurs in disease. In contrast with the homogenous appearance of the H09-RPE on all the tested scaffold-conditions, AMDCD-RPE manifested in general an odd morphology, depending on the area of the culture analyzed. Interestingly, the appearance of the cell surface by SEM did not correlate with the actual condition of the cells. Extensive apical processes were visible on SEM images suggesting proper culture development, although TEM images revealed severe RPE defects on all the scaffold-conditions, as well on Transwell inserts. The poor quality of AMDCD-RPE on the reference condition indicated that these defects were directly related to the cells themselves, rather than to RPE-matrix interactions. If junctions are important in maintaining the RPE monolayer which is essential for its functionality, the abnormal and scattered ZO1 visualized on these cultures might be an indicator of losing polarity and undergoing EMT. This could explain the flattening and elongation of the AMDCD-RPE, especially on the Bruch's complex-condition. A major limitation during cell culture was the inability to estimate how long the cells took to reach full confluency on each scaffold. The lack of transparency of the Snapwells allowed to visualize the cells only when they regained pigmentation and formed tight junctions. Labelling the cells with a non-toxic cell tracking dye that allow for localization of living cells may be useful to

overcome this shortage and follow cell grow and proliferation over time. Given that H09-RPE looked uniform across the different scaffold-conditions, it would intrigue to study the expression profiles of these cells to research potential dissimilarities at a molecular level.

A total of four shape metrics was assessed to highlight differences in specific morphometric features among the cell cultures. To this aim, we used a CNN algorithm that allowed the recognition of cell borders from fluorescent signals and produced segmented images of RPE cells. These images were the inputs for REShAPE, which outputs the following morphological characteristics: cell area, aspect ratio, hexagonality and neighbors. Although the shape analysis showed us that the average cell size of BM-culture for either AMDCD-RPE or H09-RPE was bigger than on the other scaffold-conditions (including Transwell inserts), the color-coded images clearly revealed that the cultures with the most heterogenous shade of colors were the ones on PLGA scaffold. This could be due to a limitation of the method. The PLGA scaffold becomes rippled along the weeks, and after staining for ZO1, it is difficult to detect cell borders on the same focal plane. As consequence, ZO1 can appear faint or even absent in some areas of the same image. If this image is input in the algorithm, the latter fails in recognizing cell borders in such areas and the output data would miss some segmentation. To avoid this issue, it would be appropriate to exclude these areas from the analysis, as well as damaged areas due to sample manipulation. For both cell lines, the smallest RPE cells were present on DM and Transwell inserts, while bigger RPE cells grew over the BM. It would be interesting to identify the type of ECM molecule that links RPE cell size. We observed that the shift in cell size between H09-RPE cultures were not that prominent, except for H09-RPE on BM, which showed a high variability. In this regard, fascinating would be to correlate the variability in metrics observed in the BM-condition of H09-RPE with the layer of BM exposed for initial cell attachment. It is unlikely that seeding concentration induces a smaller cell size, because cells were seeded in different plate formats and concentration was adjusted accordingly, but the average cell area did not substantially change. It might be reasonable to think that cells of large size were the result of spaces left by dying cells and replenished by the expansion of neighboring cells (Ortolan et al., 2022). In the case of AMDCD-RPE on BM for example, this hypothesis seemed to overlap with the morphology data. We found a similar trend of increased elongation and decreased hexagonality and number of

neighbors within cell cultures on BM for both cell lines. On PLGA scaffold, H09-RPE cells showed a similar direction. Further connections could be made between shape metrics and function. For instance, few studies have shown that there is a decline in metabolic activity with increasing cell size (Miettinen and Björklund, 2017; Savage et al., 2007). The presence of RPE of different cell size suggested that the investigated scaffolds might foster changes at physiological level.

Cellular polarization is a crucial aspect of RPE biology. Without it, RPE cannot successfully perform its function. To maintain the integrity of the outer blood/retina barrier, RPE secretes certain molecules on the apical side, such as PEDF, and other molecules on the basal side, such as VEGF (Becerra et al., 2004; Blaauwgeers et al., 1999). The evidence of AMDCD-RPE poor differentiation observed in previous experiments was controversial with our VEGF data. In our results, VEGF secretion in AMDCD-RPE cells increased abruptly across the scaffold-conditions, especially when cultured on PLGA scaffold. Ohno-Matsui et al. demonstrated that VEGF secretion by RPE depends on the degree of differentiation (Ohno-Matsui et al., 2001). According to this statement, further investigations are in need to verify the consistency of these data. It is worthy to remind that appropriate levels of VEGF are vital for ocular homeostasis and integrity, but reaching a threshold level can induce neovascularisation (Peng et al., 2010). It might be useful to detect the VEGF mRNA levels of AMDCD-RPE before seeding, to see whether these high levels of VEGF are related to cell health or to cells-scaffold interactions. On the contrary, low levels of VEGF were measured for H09-RPE cells compared to control condition on Transwell inserts. The reason behind these values could be the inability of the support to fully model the *in vivo* basolateral secretion to the choroid. For the BM-condition, the presence of the whole Bruch's complex might impede the release of VEGF in the basal compartment (Chen et al., 2022). Surprisingly, we noticed an increase in the basal VEGF secretion of H09-RPE over the DM from week four compared to control on Transwell insert, hoping that it could be a consequence of pronounced maturation of H09-RPE cells over the DM. Future assays will be carried out to determine PEDF secretion levels from the apical side of the RPE cells, which might lead to more reliable data.

To our knowledge, there is a lack of data in the literature regarding DM transplantation into the subretinal space, thus we had no evidence on DM tolerability in the new environment. For this reason, we sought to investigate the

safety and integration of H09-RPE sheet on DM in rats. The FDA approved PLGA scaffold was used for comparison, since the formulation strategy of RPE cell therapy adopting this biodegradable material had already been demonstrated in an ongoing phase I clinical trial. Based on our experience, we witnessed that delivering the RPE cells as an organized monolayer had the advantage of better controlling the implant position in the subretinal space. Moreover, we were able to follow the overlying retinal structure for prolonged periods after grafting by the use of the OCT.

Based upon OCT data, the DM appeared folded in the subretinal space. This result was quite expected, considering that we were unsure of the DM folding status at the time of transplantation. The use of gas or silicon oil might represent a valid solution to bypass this issue. We are currently missing valuable and reliable histological information about the integration of the implants in the subretinal space. We believe that these data will corroborate the findings of the live imaging. We speculate that the formation of cell clumps in patch areas where the RPE was not able to integrate as monolayer was likely due to the unflattening of the DM during surgery. Cell clumps development could have drastic consequences on both cell survival and functionality (Algvere et al., 1999; Sheridan et al., 2009), and it might be related to cell migration after transplantation. The phenomenon of cell migration can be linked to tight junctions loosening (Carlsson et al., 2020), which in turn leads to cell-to-cell contact and anchorage dependence deficiency (White et al., 2017). On the other hand, we assume the preservation of the monolayer on the PLGA scaffold in transplanted areas. We did not assess DM orientation in the subretinal space in this study, but we are aware that it needs further evaluation.

The surgical technique used in this study is considered to be superior to transscleral approaches usually employ for rat transplantation surgery. The vitrectomy followed by retinotomy is therefore more appropriate and overcome the risk of damaging the blood-retina barrier with consequent immune cell infiltration occurring through transscleral route (Thomas et al., 2016).

For transplantation studies, we used immunodeficient RNU rats to reduce immunological problems. The H09-RPE sheets demonstrated to be safe in RNU, without neither inducing teratoma nor biodistribution concerns. In fact, during the follow up period (1 to 2 months) both patches could be safely delivered in the eyes of the rats without adverse events, suggesting that transplanted RPE have no adverse effect on the retina. Major signs of immune rejection such as inflammatory

cell infiltration and disruption of the transplant did not occur within our endpoint. Albino rats were also used to test the two H09-RPE sheets. Despite the lack of any immunosuppression regimen, no acute inflammation and large peri-membrane fibrosis were visible around the implants on these rats. Longer follow up will need to address immune reaction issues, which might not be observed during short periods (Khristov et al., 2018; Rajendran Nair et al., 2021).

Immune rejection is the major cause attempting transplanted cell survival. Adverse effects can be tolerated or reduced in humans with the application of adequate immune suppressants. Herein, future trials aim to generate hPSC banks of known human leukocyte antigen (HLA) to ensure HLA matching between hPSC-RPE sheet and the recipient, thus preventing graft rejection (Andrews et al., 2015; Ben M'Barek et al., 2020; Taylor et al., 2005; Wilmut et al., 2015).

Our results on transplantation demonstrated that the DM is not a suitable candidate for RPE transplantation, since it proved to be tough to handle during surgery. The PLGA scaffold on the contrary allowed a successful delivery of the RPE monolayer in the subretinal space.

Implantation studies on preclinical models carrying RPE dysfunction serve to assess the functionality of the transplanted cells and are currently missing in this work. Assuming that the hPSC-RPE cells are capable of rescuing native RPE degeneration in diseased models, the host retina should exhibit a trend toward recovery.

STUDY HIGHLIGHTS:

- We successfully derived fully mature and functional RPE cells from a hESC line (H09) using both spontaneous and direct differentiation methods.
- The intrinsic variability of the hAM prevented us from finding an optimal standardisation of the method. In our hands, H09-RPE cells failed to form a regular monolayer of cells when cultured over the biological tissue.
- Decellularized DM provided a suitable microenvironment for H09-RPE cells, potentially increasing their functionality in tissue engineering applications.
- The comparison study aimed to compare H09-RPE and AMDCD (iPSC)-RPE cell cultures on different scaffolding conditions.
- AMDCD-RPE cells revealed poor differentiation quality.
- H09-RPE formed a highly polarized monolayer over the PLGA scaffold.
- Barrier integrity was defective in H09-RPE cells when cultured over the DM.
- hPSC-RPE cultures on the BM showed the highest morphometric variability between the different scaffold conditions.
- Each investigated scaffold affected the hPSC-RPE cell monolayers to a different degree.
- H09-RPE on the DM failed to flatten in the subretinal space of rats. On the contrary, H09-RPE-patch on PLGA scaffold demonstrated proper integration in the transplanted area.

The microenvironment where the cells reside plays a vital role in the regulation of cell phenotype including cell morphology, polarity and function.

Researching and optimizing scaffolds for regenerative medicine applications in the field of retinopathies such as AMD has progressed in the formulation of novel cell therapy products aiming to replace the degenerating cells and restore the compromised *in vivo* environment.

Besides facilitating the delivery of the cell patch during implantation, the preferred scaffold should own attractive ECM components for the successful attachment and

growth of the overlying RPE cells. As a response to these features, the cultured cells might be able to accelerate the matrix secretion of ECM.

In the first part of this study, we focused on hPSC-RRPE derivation and characterization, and we tested the growth of these cells on two intended-to-use biological matrices. The lack of standardization encountered with the use of the hAM led us to disqualify this membrane as potential hPSC-RPE cell carrier. Although we provided data on the ability of the DM to support hESC-RPE cell culture, the natural folding of this tissue prevented ideal cell culture to be established and proper positioning of the cell patch when grafted into the subretinal space of rats.

This result enhanced the need for consistently manufactured and easy to handle scaffolds. In this sense, multiple biomechanical properties should be considered and correlated with cell viability, growth, functionality and transplantation. The possibility to create a predicting model of the best-fitting value for each of these properties that could lead to successfully handling, culturing and surgery of the selected scaffold would be highly desired.

A possible solution in attempting to use the DM as cell carrier could be to associate this tissue with a structure that could enhance its mechanical strength and support, without affecting its permeability. For instance, it would be intriguing to combine the DM with the PLGA scaffold, to see whether the two scaffolds could provide a synergistic effect for the survival of the grafted cells in the hostile milieu. Still, the DM could represent a suitable template for future scaffold for ocular tissue engineering.

On the other hand, the PLGA scaffold showed great potentials in the delivery of the RPE cell sheet, among which biodegradability. This property ensures the transplanted RPE to directly contact the native BM, without preventing choroidal circulation.

In the last part of this research, we witnessed the need for highly differentiated cells to be used during scaffold-comparison studies. Indeed, cell culture outcome relies upon differentiation efficiency even in the presence of a perfect suitable substrate. If the differentiation quality of a cell batch or a cell line is poor, we cannot demonstrate that the differences in morphology and/or functionality between cultures of the same cells are due to the influence of an underlying scaffold. We therefore believe that primary cells might be more appropriate for investigating cell cultures over different substrates.

Moreover, the choice of technique for mounting biomaterial prior to cell culture can impact the quality and the characteristics of the cell culture itself. Based on how biomaterials are mounted, it may be valuable to improve the mounting step to provide cell culture with additional support.

A major limitation within the study comparison of different scaffolds was the absence of an underlying choroidal circulation and overlying photoreceptors that normally

influence the RPE behaviour in the subretinal space. Similarly, culture conditions did not recapitulate the conditions in the subretinal space. Ongoing efforts are addressing the development of systems capable of mimicking retinal physiological aspects.

Understanding the complexity of *in vivo* retinal functioning and degenerative disease environment will likely aid in the creation of new therapeutic products relying on stem cell technology.

REFERENCES

Abrams, G.A., Schaus, S.S., Goodman, S.L., Nealey, P.F., Murphy, C.J., 2000. Nanoscale topography of the corneal epithelial basement membrane and Descemet's membrane of the human. Cornea 19, 57–64. https://doi.org/10.1097/00003226-200001000-00012

Abu Khamidakh, A.E., Rodriguez-Martinez, A., Kaarniranta, K., Kallioniemi, A., Skottman, H., Hyttinen, J., Juuti-Uusitalo, K., 2018. Wound healing of human embryonic stem cell-derived retinal pigment epithelial cells is affected by maturation stage. Biomed Eng Online 17, 102. https://doi.org/10.1186/s12938-018-0535-z

Adamis, A.P., Shima, D.T., Yeo, K.T., Yeo, T.K., Brown, L.F., Berse, B., D'Amore, P.A., Folkman, J., 1993. Synthesis and secretion of vascular permeability factor/vascular endothelial growth factor by human retinal pigment epithelial cells. Biochem Biophys Res Commun 193, 631–638. https://doi.org/10.1006/bbrc.1993.1671

Adorante, J.S., Miller, S.S., 1990. Potassium-dependent volume regulation in retinal pigment epithelium is mediated by Na,K,Cl cotransport. J Gen Physiol 96, 1153–1176. https://doi.org/10.1085/jgp.96.6.1153

Ahuja, P., Caffé, A.R., Holmqvist, I., Söderpalm, A.K., Singh, D.P., Shinohara, T., van Veen, T., 2001. Lens epithelium-derived growth factor (LEDGF) delays photoreceptor degeneration in explants of rd/rd mouse retina. Neuroreport 12, 2951–2955. https://doi.org/10.1097/00001756-200109170-00039

Akrami, H., Soheili, Z.-S., Sadeghizadeh, M., Khalooghi, K., Ahmadieh, H., Kanavi, M.R., Samiei, S., Pakravesh, J., 2011. Evaluation of RPE65, CRALBP, VEGF, CD68, and Tyrosinase Gene Expression in Human Retinal Pigment Epithelial Cells Cultured on Amniotic Membrane. Biochem Genet 49, 313–322. https://doi.org/10.1007/s10528-010-9409-1

Algvere, P.V., Berglin, L., Gouras, P., Sheng, Y., 1994. Transplantation of fetal retinal pigment epithelium in age-related macular degeneration with subfoveal neovascularization. Graefes Arch Clin Exp Ophthalmol 232, 707–716. https://doi.org/10.1007/BF00184273

Algvere, P.V., Berglin, L., Gouras, P., Sheng, Y., Kopp, E.D., 1997. Transplantation of RPE in age-related macular degeneration: observations in disciform lesions and dry RPE atrophy. Graefes Arch Clin Exp Ophthalmol 235, 149–158. https://doi.org/10.1007/BF00941722

Algvere, P.V., Gouras, P., Dafgård Kopp, E., 1999. Long-term outcome of RPE allografts in non-immunosuppressed patients with AMD. Eur J Ophthalmol 9, 217–230. https://doi.org/10.1177/112067219900900310

Ali, M., Raghunathan, V., Li, J.Y., Murphy, C.J., Thomasy, S.M., 2016. Biomechanical relationships between the corneal endothelium and Descemet's membrane. Exp Eye Res 152, 57–70. https://doi.org/10.1016/j.exer.2016.09.004

Alvarez Palomo, A.B., McLenachan, S., Chen, F.K., Da Cruz, L., Dilley, R.J., Requena, J., Lucas, M., Lucas, A., Drukker, M., Edel, M.J., 2015. Prospects for clinical use of reprogrammed cells for autologous treatment of macular degeneration. Fibrogenesis Tissue Repair 8, 9. https://doi.org/10.1186/s13069-015-0026-9

Andrews, P.W., Baker, D., Benvinisty, N., Miranda, B., Bruce, K., Brüstle, O., Choi, M., Choi, Y.-M., Crook, J.M., de Sousa, P.A., Dvorak, P., Freund, C., Firpo, M., Furue, M.K., Gokhale, P., Ha, H.-Y., Han, E., Haupt, S., Healy, L., Hei, D.J., Hovatta, O., Hunt, C., Hwang, S.-M., Inamdar, M.S., Isasi, R.M., Jaconi, M., Jekerle, V., Kamthorn, P., Kibbey, M.C., Knezevic, I., Knowles, B.B., Koo, S.-K., Laabi, Y., Leopoldo, L., Liu, P., Lomax, G.P., Loring, J.F., Ludwig, T.E., Montgomery, K., Mummery, C., Nagy, A., Nakamura, Y., Nakatsuji, N., Oh, S., Oh, S.-K., Otonkoski, T., Pera, M., Peschanski, M., Pranke, P., Rajala, K.M., Rao, M., Ruttachuk, R., Reubinoff, B., Ricco, L., Rooke, H., Sipp, D., Stacey, G.N., Suemori, H., Takahashi, T.A., Takada, K., Talib, S., Tannenbaum, S., Yuan, B.-Z., Zeng, F., Zhou, Q., 2015. Points to consider in the development of seed stocks of pluripotent stem cells for clinical applications: International Stem Cell Banking Initiative (ISCBI). Regen Med 10, 1–44. https://doi.org/10.2217/rme.14.93

Augustyniak, J., Zychowicz, M., Podobinska, M., Barta, T., Buzanska, L., 2014. Reprogramming of somatic cells: possible methods to derive safe, clinical-grade human induced pluripotent stem cells. Acta Neurobiol Exp (Wars) 74, 373–382.

Avery, S., Hirst, A.J., Baker, D., Lim, C.Y., Alagaratnam, S., Skotheim, R.I., Lothe, R.A., Pera, M.F., Colman, A., Robson, P., Andrews, P.W., Knowles, B.B., 2013. BCL-XL mediates the strong selective advantage of a 20q11.21 amplification commonly found in human embryonic stem cell cultures. Stem Cell Reports 1, 379–386. https://doi.org/10.1016/j.stemcr.2013.10.005

Ban, Y., Rizzolo, L.J., 2000. Differential regulation of tight junction permeability during development of the retinal pigment epithelium. Am J Physiol Cell Physiol 279, C744-750. https://doi.org/10.1152/ajpcell.2000.279.3.C744

Beatty, S., Koh, H., Phil, M., Henson, D., Boulton, M., 2000. The role of oxidative stress in the pathogenesis of age-related macular degeneration. Surv Ophthalmol 45, 115–134. https://doi.org/10.1016/s0039-6257(00)00140-5

Becerra, S.P., Fariss, R.N., Wu, Y.Q., Montuenga, L.M., Wong, P., Pfeffer, B.A., 2004. Pigment epithelium-derived factor in the monkey retinal pigment epithelium and interphotoreceptor matrix: apical secretion and distribution. Exp Eye Res 78, 223–234. https://doi.org/10.1016/j.exer.2003.10.013

Ben M'Barek, K., Bertin, S., Brazhnikova, E., Jaillard, C., Habeler, W., Plancheron, A., Fovet, C.-M., Demilly, J., Jarraya, M., Bejanariu, A., Sahel, J.-A., Peschanski, M., Goureau, O., Monville, C., 2020. Clinical-grade production and safe delivery of human ESC derived RPE sheets in primates and rodents. Biomaterials 230, 119603. https://doi.org/10.1016/j.biomaterials.2019.119603

Ben M'Barek, K., Habeler, W., Monville, C., 2018a. Stem Cell-Based RPE Therapy for Retinal Diseases: Engineering 3D Tissues Amenable for Regenerative Medicine. Adv Exp Med Biol 1074, 625–632. https://doi.org/10.1007/978-3-319-75402-4_76

Ben M'Barek, K., Habeler, W., Plancheron, A., Jarraya, M., Goureau, O., Monville, C., 2018b. Engineering Transplantation-suitable Retinal Pigment Epithelium Tissue Derived from Human Embryonic Stem Cells. J Vis Exp. https://doi.org/10.3791/58216

Ben M'Barek, K., Habeler, W., Plancheron, A., Jarraya, M., Regent, F., Terray, A., Yang, Y., Chatrousse, L., Domingues, S., Masson, Y., Sahel, J.-A., Peschanski, M., Goureau, O., Monville, C., 2017. Human ESC-derived retinal epithelial cell sheets potentiate rescue of photoreceptor cell loss in rats with retinal degeneration. Sci Transl Med 9, eaai7471. https://doi.org/10.1126/scitranslmed.aai7471

Ben M'Barek, K., Monville, C., 2019. Cell Therapy for Retinal Dystrophies: From Cell Suspension Formulation to Complex Retinal Tissue Bioengineering. Stem Cells Int 2019, 4568979. https://doi.org/10.1155/2019/4568979

Bennis, A., Jacobs, J.G., Catsburg, L. a. E., Ten Brink, J.B., Koster, C., Schlingemann, R.O., van Meurs, J., Gorgels, T.G.M.F., Moerland, P.D., Heine, V.M., Bergen, A.A., 2017. Stem Cell Derived Retinal Pigment Epithelium: The Role of Pigmentation as Maturation Marker and Gene Expression Profile Comparison with Human Endogenous Retinal Pigment Epithelium. Stem Cell Rev Rep 13, 659–669. https://doi.org/10.1007/s12015-017-9754-0

Bergersen, L., Jóhannsson, E., Veruki, M.L., Nagelhus, E.A., Halestrap, A., Sejersted, O.M., Ottersen, O.P., 1999. Cellular and subcellular expression of monocarboxylate transporters in the pigment epithelium and retina of the rat. Neuroscience 90, 319–331. https://doi.org/10.1016/s0306-4522(98)00427-8

Bharti, K., Gasper, M., Ou, J., Brucato, M., Clore-Gronenborn, K., Pickel, J., Arnheiter, H., 2012. A regulatory loop involving PAX6, MITF, and WNT signaling controls retinal pigment epithelium development. PLoS Genet 8, e1002757. https://doi.org/10.1371/journal.pgen.1002757

Bharti, K., Miller, S.S., Arnheiter, H., 2011. The new paradigm: retinal pigment epithelium cells generated from embryonic or induced pluripotent stem cells: Retinal pigment epithelium cells generated from stem cells. Pigment Cell & Melanoma Research 24, 21–34. https://doi.org/10.1111/j.1755-148X.2010.00772.x

Bharti, K., Rao, M., Hull, S.C., Stroncek, D., Brooks, B.P., Feigal, E., van Meurs, J.C., Huang, C.A., Miller, S.S., 2014. Developing cellular therapies for retinal degenerative diseases. Invest Ophthalmol Vis Sci 55, 1191–1202. https://doi.org/10.1167/iovs.13-13481

Bialek, S., Joseph, D.P., Miller, S.S., 1995. The delayed basolateral membrane hyperpolarization of the bovine retinal pigment epithelium: mechanism of generation. J Physiol 484 (Pt 1), 53–67. https://doi.org/10.1113/jphysiol.1995.sp020647

Bialek, S., Miller, S.S., 1994. K+ and Cl- transport mechanisms in bovine pigment epithelium that could modulate subretinal space volume and composition. J Physiol 475, 401–417. https://doi.org/10.1113/jphysiol.1994.sp020081

Bibb, C., Young, R.W., 1974. Renewal of fatty acids in the membranes of visual cell outer segments. J Cell Biol 61, 327–343. https://doi.org/10.1083/jcb.61.2.327

Binder, S., Krebs, I., Hilgers, R.-D., Abri, A., Stolba, U., Assadoulina, A., Kellner, L., Stanzel, B.V., Jahn, C., Feichtinger, H., 2004. Outcome of transplantation of autologous retinal pigment epithelium in age-related macular degeneration: a prospective trial. Invest Ophthalmol Vis Sci 45, 4151–4160. https://doi.org/10.1167/iovs.04-0118

Binder, S., Stolba, U., Krebs, I., Kellner, L., Jahn, C., Feichtinger, H., Povelka, M., Frohner, U., Kruger, A., Hilgers, R.-D., Krugluger, W., 2002. Transplantation of autologous retinal pigment epithelium in eyes with foveal neovascularization resulting from age-related macular degeneration: a pilot study. Am J Ophthalmol 133, 215–225. https://doi.org/10.1016/s0002-9394(01)01373-3

Bindewald, A., Roth, F., Van Meurs, J., Holz, F.G., 2004. [Transplantation of retinal pigment pithelium (RPE) following CNV removal in patients with AMD. Techniques, results, outlook]. Ophthalmologe 101, 886–894. https://doi.org/10.1007/s00347-004-1077-2

Bissell, M.J., Barcellos-Hoff, M.H., 1987. The influence of extracellular matrix on gene expression: is structure the message? J Cell Sci Suppl 8, 327–343. https://doi.org/10.1242/jcs.1987.supplement_8.18

Blaauwgeers, H.G., Holtkamp, G.M., Rutten, H., Witmer, A.N., Koolwijk, P., Partanen, T.A., Alitalo, K., Kroon, M.E., Kijlstra, A., van Hinsbergh, V.W., Schlingemann, R.O., 1999. Polarized vascular endothelial growth factor secretion by human retinal pigment epithelium and localization of vascular endothelial growth factor receptors on the inner choriocapillaris. Evidence for a trophic paracrine relation. Am J Pathol 155, 421–428. https://doi.org/10.1016/S0002-9440(10)65138-3

Blenkinsop, T.A., Saini, J.S., Maminishkis, A., Bharti, K., Wan, Q., Banzon, T., Lotfi, M., Davis, J., Singh, D., Rizzolo, L.J., Miller, S., Temple, S., Stern, J.H., 2015. Human

Adult Retinal Pigment Epithelial Stem Cell–Derived RPE Monolayers Exhibit Key Physiological Characteristics of Native Tissue. Invest. Ophthalmol. Vis. Sci. 56, 7085. https://doi.org/10.1167/iovs.14-16246

Blume, L.-F., Denker, M., Gieseler, F., Kunze, T., 2010. Temperature corrected transepithelial electrical resistance (TEER) measurement to quantify rapid changes in paracellular permeability. Pharmazie 65, 19–24.

Bok, D., 1993. The retinal pigment epithelium: a versatile partner in vision. J Cell Sci Suppl 17, 189–195. https://doi.org/10.1242/jcs.1993.supplement_17.27

Bok, D., Hall, M.O., 1971. The role of the pigment epithelium in the etiology of inherited retinal dystrophy in the rat. J Cell Biol 49, 664–682. https://doi.org/10.1083/jcb.49.3.664

Booij, J.C., Baas, D.C., Beisekeeva, J., Gorgels, T.G.M.F., Bergen, A. a. B., 2010. The dynamic nature of Bruch's membrane. Prog Retin Eye Res 29, 1–18. https://doi.org/10.1016/j.preteyeres.2009.08.003

Bost, L.M., Aotaki-Keen, A.E., Hjelmeland, L.M., 1992. Coexpression of FGF-5 and bFGF by the retinal pigment epithelium in vitro. Exp Eye Res 55, 727–734. https://doi.org/10.1016/0014-4835(92)90177-t

Boulton, M., Dayhaw-Barker, P., 2001. The role of the retinal pigment epithelium: topographical variation and ageing changes. Eye (Lond) 15, 384–389. https://doi.org/10.1038/eye.2001.141

Buchholz, D.E., Hikita, S.T., Rowland, T.J., Friedrich, A.M., Hinman, C.R., Johnson, L.V., Clegg, D.O., 2009. Derivation of functional retinal pigmented epithelium from induced pluripotent stem cells. Stem Cells 27, 2427–2434. https://doi.org/10.1002/stem.189

C, M., J, A., R, J., 1984. Prenatal and postnatal growth of the human Descemet's membrane. Investigative ophthalmology & visual science 25.

Campbell, A., Brieva, T., Raviv, L., Rowley, J., Niss, K., Brandwein, H., Oh, S., Karnieli, O., 2015. Concise Review: Process Development Considerations for Cell Therapy. Stem Cells Transl Med 4, 1155–1163. https://doi.org/10.5966/sctm.2014-0294

Campochiaro, P.A., Hackett, S.F., Vinores, S.A., Freund, J., Csaky, C., LaRochelle, W., Henderer, J., Johnson, M., Rodriguez, I.R., Friedman, Z., 1994. Platelet-derived growth factor is an autocrine growth stimulator in retinal pigmented epithelial cells. J Cell Sci 107 (Pt 9), 2459–2469. https://doi.org/10.1242/jcs.107.9.2459

Campochiaro, P.A., Jerdon, J.A., Glaser, B.M., 1986. The extracellular matrix of human retinal pigment epithelial cells in vivo and its synthesis in vitro. Invest Ophthalmol Vis Sci 27, 1615–1621.

Campochiaro, P.A., Sugg, R., Grotendorst, G., Hjelmeland, L.M., 1989. Retinal pigment epithelial cells produce PDGF-like proteins and secrete them into their media. Exp Eye Res 49, 217–227. https://doi.org/10.1016/0014-4835(89)90092-4

Cao, W., Wen, R., Li, F., Lavail, M.M., Steinberg, R.H., 1997. Mechanical injury increases bFGF and CNTF mRNA expression in the mouse retina. Exp Eye Res 65, 241–248. https://doi.org/10.1006/exer.1997.0328

Capeáns, C., Piñeiro, A., Pardo, M., Sueiro-López, C., Blanco, M.J., Domínguez, F., Sánchez-Salorio, M., 2003. Amniotic membrane as support for human retinal pigment epithelium (RPE) cell growth. Acta Ophthalmol Scand 81, 271–277. https://doi.org/10.1034/j.1600-0420.2003.00076.x

Carlsson, E., Supharattanasitthi, W., Jackson, M., Paraoan, L., 2020. Increased Rate of Retinal Pigment Epithelial Cell Migration and Pro-Angiogenic Potential Ensuing From Reduced Cystatin C Expression. Invest Ophthalmol Vis Sci 61, 9. https://doi.org/10.1167/iovs.61.2.9

Carr, A.-J., Vugler, A.A., Hikita, S.T., Lawrence, J.M., Gias, C., Chen, L.L., Buchholz, D.E., Ahmado, A., Semo, M., Smart, M.J.K., Hasan, S., da Cruz, L., Johnson, L.V., Clegg, D.O., Coffey, P.J., 2009. Protective effects of human iPS-derived retinal pigment epithelium cell transplantation in the retinal dystrophic rat. PLoS One 4, e8152. https://doi.org/10.1371/journal.pone.0008152

Carr, A.-J.F., Smart, M.J.K., Ramsden, C.M., Powner, M.B., da Cruz, L., Coffey, P.J., 2013. Development of human embryonic stem cell therapies for age-related macular degeneration. Trends Neurosci 36, 385–395. https://doi.org/10.1016/j.tins.2013.03.006

Caruelle, D., Groux-Muscatelli, B., Gaudric, A., Sestier, C., Coscas, G., Caruelle, J.P., Barritault, D., 1989. Immunological study of acidic fibroblast growth factor (aFGF) distribution in the eye. J Cell Biochem 39, 117–128. https://doi.org/10.1002/jcb.240390204

Chakravarthy, U., Peto, T., 2020. Current Perspective on Age-Related Macular Degeneration. JAMA 324, 794. https://doi.org/10.1001/jama.2020.5576

Chambers, S.M., Fasano, C.A., Papapetrou, E.P., Tomishima, M., Sadelain, M., Studer, L., 2009. Highly efficient neural conversion of human ES and iPS cells by dual inhibition of SMAD signaling. Nat Biotechnol 27, 275–280. https://doi.org/10.1038/nbt.1529

Chen, L., Perera, N.D., Karoukis, A.J., Feathers, K.L., Ali, R.R., Thompson, D.A., Fahim, A.T., 2022. Oxidative stress differentially impacts apical and basolateral secretion of angiogenic factors from human iPSC-derived retinal pigment epithelium cells. Sci Rep 12, 12694. https://doi.org/10.1038/s41598-022-16701-6

Cho, M.S., Kim, S.J., Ku, S.-Y., Park, J.H., Lee, H., Yoo, D.H., Park, U.C., Song, S.A., Choi, Y.M., Yu, H.G., 2012. Generation of retinal pigment epithelial cells from human embryonic stem cell-derived spherical neural masses. Stem Cell Research 9, 101–109. https://doi.org/10.1016/j.scr.2012.05.002

Choi, K.-E., Anh, V.T.Q., Oh, J.-H., Yun, C., Kim, S.-W., 2021. Normative Data of Axial Length, Retinal Thickness Measurements, Visual Evoked Potentials, and Full-Field Electroretinography in Female, Wild-Type Minipigs. Trans. Vis. Sci. Tech. 10, 3. https://doi.org/10.1167/tvst.10.12.3

Chong, N.H.V., Keonin, J., Luthert, P.J., Frennesson, C.I., Weingeist, D.M., Wolf, R.L., Mullins, R.F., Hageman, G.S., 2005. Decreased thickness and integrity of the macular elastic layer of Bruch's membrane correspond to the distribution of lesions associated with age-related macular degeneration. Am J Pathol 166, 241–251. https://doi.org/10.1016/S0002-9440(10)62248-1

Coffey, P.J., Girman, S., Wang, S.M., Hetherington, L., Keegan, D.J., Adamson, P., Greenwood, J., Lund, R.D., 2002. Long-term preservation of cortically dependent visual function in RCS rats by transplantation. Nature Neuroscience 5, 53–56. https://doi.org/10.1038/nn782

Coffey, P.J., Whiteley, S.J., Lund, R.D., 2000. Preservation and restoration of vision following transplantation. Prog Brain Res 127, 489–499. https://doi.org/10.1016/s0079-6123(00)27024-6

Connolly, S.E., Hjelmeland, L.M., LaVail, M.M., 1992. Immunohistochemical localization of basic fibroblast growth factor in mature and developing retinas of normal and RCS rats. Curr Eye Res 11, 1005–1017. https://doi.org/10.3109/02713689209033499

Connon, C.J., Doutch, J., Chen, B., Hopkinson, A., Mehta, J.S., Nakamura, T., Kinoshita, S., Meek, K.M., 2010. The variation in transparency of amniotic membrane used in ocular surface regeneration. Br J Ophthalmol 94, 1057–1061. https://doi.org/10.1136/bjo.2008.153064

da Cruz, L., Chen, F.K., Ahmado, A., Greenwood, J., Coffey, P., 2007. RPE transplantation and its role in retinal disease. Prog Retin Eye Res 26, 598–635. https://doi.org/10.1016/j.preteyeres.2007.07.001

da Cruz, L., Fynes, K., Georgiadis, O., Kerby, J., Luo, Y.H., Ahmado, A., Vernon, A., Daniels, J.T., Nommiste, B., Hasan, S.M., Gooljar, S.B., Carr, A.-J.F., Vugler, A., Ramsden, C.M., Bictash, M., Fenster, M., Steer, J., Harbinson, T., Wilbrey, A., Tufail, A., Feng, G., Whitlock, M., Robson, A.G., Holder, G.E., Sagoo, M.S., Loudon, P.T., Whiting, P., Coffey, P.J., 2018. Phase 1 clinical study of an embryonic stem cell-derived retinal pigment epithelium patch in age-related macular degeneration. Nat Biotechnol 36, 328–337. https://doi.org/10.1038/nbt.4114

Dawson, D.W., Volpert, O.V., Gillis, P., Crawford, S.E., Xu, H., Benedict, W., Bouck, N.P., 1999. Pigment epithelium-derived factor: a potent inhibitor of angiogenesis. Science 285, 245–248. https://doi.org/10.1126/science.285.5425.245

D'Cruz, P.M., Yasumura, D., Weir, J., Matthes, M.T., Abderrahim, H., LaVail, M.M., Vollrath, D., 2000. Mutation of the receptor tyrosine kinase gene Mertk in the retinal dystrophic RCS rat. Hum Mol Genet 9, 645–651. https://doi.org/10.1093/hmg/9.4.645

de Melo, G.B., Gomes, J.A.P., da Glória, M.A., Martins, M.C., Haapalainen, E.F., 2007. [Morphological assessment of different amniotic membrane epithelial denuding techniques]. Arq Bras Oftalmol 70, 407–411. https://doi.org/10.1590/s0004-27492007000300005

de Oliveira, R.C., Wilson, S.E., 2020. Descemet's membrane development, structure, function and regeneration. Experimental Eye Research 197, 108090. https://doi.org/10.1016/j.exer.2020.108090

De Rotth, A., 1940. PLASTIC REPAIR OF CONJUNCTIVAL DEFECTS WITH FETAL MEMBRANES. Archives of Ophthalmology 23, 522–525. https://doi.org/10.1001/archopht.1940.00860130586006

Deigner, P.S., Law, W.C., Cañada, F.J., Rando, R.R., 1989. Membranes as the energy source in the endergonic transformation of vitamin A to 11-cis-retinol. Science 244, 968–971. https://doi.org/10.1126/science.2727688

Del Priore, L.V., Kaplan, H.J., Tezel, T.H., Hayashi, N., Berger, A.S., Green, W.R., 2001. Retinal pigment epithelial cell transplantation after subfoveal membranectomy in age-related macular degeneration: clinicopathologic correlation. Am J Ophthalmol 131, 472–480. https://doi.org/10.1016/s0002-9394(00)00850-3

Diniz, B., Thomas, P., Thomas, B., Ribeiro, R., Hu, Y., Brant, R., Ahuja, A., Zhu, D., Liu, L., Koss, M., Maia, M., Chader, G., Hinton, D.R., Humayun, M.S., 2013. Subretinal Implantation of Retinal Pigment Epithelial Cells Derived From Human Embryonic Stem Cells: Improved Survival When Implanted as a Monolayer. Invest. Ophthalmol. Vis. Sci. 54, 5087. https://doi.org/10.1167/iovs.12-11239

Dornonville de la Cour, M., 1993. Ion transport in the retinal pigment epithelium. A study with double barrelled ion-selective microelectrodes. Acta Ophthalmol Suppl (1985) 1–32.

Driessen, C.A., Janssen, B.P., Winkens, H.J., van Vugt, A.H., de Leeuw, T.L., Janssen, J.J., 1995. Cloning and expression of a cDNA encoding bovine retinal pigment epithelial 11-cis retinol dehydrogenase. Investigative Ophthalmology & Visual Science 36, 1988–1996.

Drukker, M., Katz, G., Urbach, A., Schuldiner, M., Markel, G., Itskovitz-Eldor, J., Reubinoff, B., Mandelboim, O., Benvenisty, N., 2002. Characterization of the

expression of MHC proteins in human embryonic stem cells. Proc Natl Acad Sci U S A 99, 9864–9869. https://doi.org/10.1073/pnas.142298299

Eamegdool, S.S., Sitiwin, E.I., Cioanca, A.V., Madigan, M.C., 2020. Extracellular matrix and oxidative stress regulate human retinal pigment epithelium growth. Free Radic Biol Med 146, 357–371. https://doi.org/10.1016/j.freeradbiomed.2019.11.018

Ed, H., 1980. Development of the vertebrate cornea. International review of cytology 63. https://doi.org/10.1016/s0074-7696(08)61760-x

Edelman, J.L., Lin, H., Miller, S.S., 1994. Acidification stimulates chloride and fluid absorption across frog retinal pigment epithelium. Am J Physiol 266, C946-956. https://doi.org/10.1152/ajpcell.1994.266.4.C946

Eghrari, A.O., Rasooly, M.M., Fliotsos, M.J., Kinard, J., Odozor, O., Cunningham, D., Bishop, R.J., Guerrerio, A.L., Frischmeyer-Guerrerio, P.A., 2020. Corneal thinning and cornea guttata in patients with mutations in TGFB2. Can J Ophthalmol 55, 336–341. https://doi.org/10.1016/j.jcjo.2020.03.007

Feng, Q., Lu, S.-J., Klimanskaya, I., Gomes, I., Kim, D., Chung, Y., Honig, G.R., Kim, K.-S., Lanza, R., 2010. Hemangioblastic derivatives from human induced pluripotent stem cells exhibit limited expansion and early senescence. Stem Cells 28, 704–712. https://doi.org/10.1002/stem.321

Fernandes, M., McArdle, B., Schiff, L., Blenkinsop, T.A., 2018. Stem Cell–Derived Retinal Pigment Epithelial Layer Model from Adult Human Globes Donated for Corneal Transplants. Current Protocols in Stem Cell Biology 45, e53. https://doi.org/10.1002/cpsc.53

Fernandes, R.A.B., Stefanini, F.R., Falabella, P., Koss, M.J., Wells, T., Diniz, B., Ribeiro, R., Schor, P., Maia, M., Penha, F.M., Hinton, D.R., Tai, Y.-C., Humayun, M., 2017. Development of a new tissue injector for subretinal transplantation of human embryonic stem cell derived retinal pigmented epithelium. Int J Retina Vitreous 3, 41. https://doi.org/10.1186/s40942-017-0095-6

Fiejdasz, S., Horak, W., Lewandowska-Łańcucka, J., Szuwarzyński, M., Salwiński, J., Nowakowska, M., 2018. Tuning of elasticity and surface properties of hydrogel cell culture substrates by simple chemical approach. Journal of Colloid and Interface Science 524, 102–113. https://doi.org/10.1016/j.jcis.2018.04.004

Fisher, S.K., Steinberg, R.H., 1982. Origin and organization of pigment epithelial apical projections to cones in cat retina. J Comp Neurol 206, 131–145. https://doi.org/10.1002/cne.902060204

Flaxel, C.J., Adelman, R.A., Bailey, S.T., Fawzi, A., Lim, J.I., Vemulakonda, G.A., Ying, G., 2020. Age-Related Macular Degeneration Preferred Practice Pattern®. Ophthalmology 127, P1–P65. https://doi.org/10.1016/j.ophtha.2019.09.024

Flores, R., Carneiro, Â., Vieira, M., Tenreiro, S., Seabra, M.C., 2021. Age-Related Macular Degeneration: Pathophysiology, Management, and Future Perspectives. Ophthalmologica 244, 495–511. https://doi.org/10.1159/000517520

Frambach, D.A., Roy, C.E., Valentine, J.L., Weiter, J.J., 1989. Precocious retinal adhesion is affected by furosemide and ouabain. Curr Eye Res 8, 553–556. https://doi.org/10.3109/02713688908995753

Fuhrmann, S., 2010. Eye morphogenesis and patterning of the optic vesicle. Curr Top Dev Biol 93, 61–84. https://doi.org/10.1016/B978-0-12-385044-7.00003-5

Fujii, S., Yoshida, S., Inagaki, E., Hatou, S., Tsubota, K., Takahashi, M., Shimmura, S., Sugita, S., 2019. Immunological Properties of Neural Crest Cells Derived from Human Induced Pluripotent Stem Cells. Stem Cells Dev 28, 28–43. https://doi.org/10.1089/scd.2018.0058

Gehrs, K.M., Anderson, D.H., Johnson, L.V., Hageman, G.S., 2016. Age-related macular degeneration—emerging pathogenetic and therapeutic concepts 36.

Gess, A.J., Fung, A.E., Rodriguez, J.G., 2011. Imaging in Neovascular Age-Related Macular Degeneration. Seminars in Ophthalmology 26, 225–233. https://doi.org/10.3109/08820538.2011.582533

Ghezzi, C.E., Rnjak-Kovacina, J., Kaplan, D.L., 2015. Corneal tissue engineering: recent advances and future perspectives. Tissue Eng Part B Rev 21, 278–287. https://doi.org/10.1089/ten.TEB.2014.0397

Giordano, G.G., Thomson, R.C., Ishaug, S.L., Mikos, A.G., Cumber, S., Garcia, C.A., Lahiri-Munir, D., 1997. Retinal pigment epithelium cells cultured on synthetic biodegradable polymers. J Biomed Mater Res 34, 87–93. https://doi.org/10.1002/(sici)1097-4636(199701)34:1<87::aid-jbm12>3.0.co;2-m

Gordon, S.R., 2014. Fibronectin antibody labels corneal stromal collagen fibrils in situ along their length and circumference and demonstrates distinct staining along the cell and stromal interfaces of Descemet's membrane. Curr Eye Res 39, 312–316. https://doi.org/10.3109/02713683.2013.841260

Gottsch, J.D., Zhang, C., Sundin, O.H., Bell, W.R., Stark, W.J., Green, W.R., 2005. Fuchs corneal dystrophy: aberrant collagen distribution in an L450W mutant of the COL8A2 gene. Invest Ophthalmol Vis Sci 46, 4504–4511. https://doi.org/10.1167/iovs.05-0497

Griff, E.R., 1990. Response properties of the toad retinal pigment epithelium. Invest Ophthalmol Vis Sci 31, 2353–2360.

Gullapalli, V.K., Sugino, I.K., Van Patten, Y., Shah, S., Zarbin, M.A., 2005. Impaired RPE survival on aged submacular human Bruch's membrane. Exp Eye Res 80, 235–248. https://doi.org/10.1016/j.exer.2004.09.006

Gunatillake, P., Mayadunne, R., Adhikari, R., 2006. Recent developments in biodegradable synthetic polymers. Biotechnol Annu Rev 12, 301–347. https://doi.org/10.1016/S1387-2656(06)12009-8

Guymer, R., Luthert, P., Bird, A., 1999. Changes in Bruch's membrane and related structures with age. Prog Retin Eye Res 18, 59–90. https://doi.org/10.1016/s1350-9462(98)00012-3

Ha, T., Aj, T., P, W., Mc, G., Aj, L., 2011. Optimisation of polymer scaffolds for retinal pigment epithelium (RPE) cell transplantation. The British journal of ophthalmology 95. https://doi.org/10.1136/bjo.2009.166728

Haeseleer, F., Huang, J., Lebioda, L., Saari, J.C., Palczewski, K., 1998. Molecular Characterization of a Novel Short-chain Dehydrogenase/Reductase That Reduces All-trans-retinal. Journal of Biological Chemistry 273, 21790–21799. https://doi.org/10.1074/jbc.273.34.21790

Hamann, S., la Cour, M., Lui, G.M., Bundgaard, M., Zeuthen, T., 2000. Transport of protons and lactate in cultured human fetal retinal pigment epithelial cells. Pflugers Arch 440, 84–92. https://doi.org/10.1007/s004249900236

Hao, Y., Ma, D.H., Hwang, D.G., Kim, W.S., Zhang, F., 2000. Identification of antiangiogenic and antiinflammatory proteins in human amniotic membrane. Cornea 19, 348–352. https://doi.org/10.1097/00003226-200005000-00018

Hargrave, P.A., 2001. Rhodopsin structure, function, and topography the Friedenwald lecture. Invest Ophthalmol Vis Sci 42, 3–9.

Harkin, D.G., Dunphy, S.E., Shadforth, A.M.A., Dawson, R.A., Walshe, J., Zakaria, N., 2017. Mounting of Biomaterials for Use in Ophthalmic Cell Therapies. Cell Transplant 26, 1717–1732. https://doi.org/10.1177/0963689717723638

Hartmann-Fritsch, F., Marino, D., Reichmann, E., 2016. About ATMPs, SOPs and GMP: The Hurdles to Produce Novel Skin Grafts for Clinical Use. Transfusion Medicine and Hemotherapy 43, 344–352. https://doi.org/10.1159/000447645

Hazim, R.A., Karumbayaram, S., Jiang, M., Dimashkie, A., Lopes, V.S., Li, D., Burgess, B.L., Vijayaraj, P., Alva-Ornelas, J.A., Zack, J.A., Kohn, D.B., Gomperts, B.N., Pyle, A.D., Lowry, W.E., Williams, D.S., 2017a. Differentiation of RPE cells from integration-free iPS cells and their cell biological characterization. Stem Cell Res Ther 8, 217. https://doi.org/10.1186/s13287-017-0652-9

Hazim, R.A., Karumbayaram, S., Jiang, M., Dimashkie, A., Lopes, V.S., Li, D., Burgess, B.L., Vijayaraj, P., Alva-Ornelas, J.A., Zack, J.A., Kohn, D.B., Gomperts, B.N., Pyle, A.D., Lowry, W.E., Williams, D.S., 2017b. Differentiation of RPE cells from integration-free iPS cells and their cell biological characterization. Stem Cell Res Ther 8, 217. https://doi.org/10.1186/s13287-017-0652-9

Ho, T.C., Del Priore, L.V., 1997. Reattachment of cultured human retinal pigment epithelium to extracellular matrix and human Bruch's membrane. Invest Ophthalmol Vis Sci 38, 1110–1118.

Hodgkinson, C.A., Moore, K.J., Nakayama, A., Steingrímsson, E., Copeland, N.G., Jenkins, N.A., Arnheiter, H., 1993. Mutations at the mouse microphthalmia locus are associated with defects in a gene encoding a novel basic-helix-loop-helix-zipper protein. Cell 74, 395–404. https://doi.org/10.1016/0092-8674(93)90429-t

Hofmann, K.P., n.d. Signalling States of Photoactivated Rhodopsin, in: Novartis Foundation Symposium 224 - Rhodopsins and Phototransduction. John Wiley & Sons, Ltd, pp. 158–190. https://doi.org/10.1002/9780470515693.ch10

Hongisto, H., Ilmarinen, T., Vattulainen, M., Mikhailova, A., Skottman, H., 2017. Xeno- and feeder-free differentiation of human pluripotent stem cells to two distinct ocular epithelial cell types using simple modifications of one method. Stem Cell Res Ther 8, 291. https://doi.org/10.1186/s13287-017-0738-4

Hoon, M., Okawa, H., Della Santina, L., Wong, R.O.L., 2014. Functional architecture of the retina: Development and disease. Progress in Retinal and Eye Research 42, 44–84. https://doi.org/10.1016/j.preteyeres.2014.06.003

Hopkinson, A., McIntosh, R.S., Tighe, P.J., James, D.K., Dua, H.S., 2006. Amniotic membrane for ocular surface reconstruction: donor variations and the effect of handling on TGF-beta content. Invest Ophthalmol Vis Sci 47, 4316–4322. https://doi.org/10.1167/iovs.05-1415

Hopkinson, A., Shanmuganathan, V.A., Gray, T., Yeung, A.M., Lowe, J., James, D.K., Dua, H.S., 2008. Optimization of amniotic membrane (AM) denuding for tissue engineering. Tissue Eng Part C Methods 14, 371–381. https://doi.org/10.1089/ten.tec.2008.0315

Hori, J., Wang, M., Kamiya, K., Takahashi, H., Sakuragawa, N., 2006. Immunological characteristics of amniotic epithelium. Cornea 25, S53-58. https://doi.org/10.1097/01.ico.0000247214.31757.5c

Hornof, M., Toropainen, E., Urtti, A., 2005. Cell culture models of the ocular barriers. Eur J Pharm Biopharm 60, 207–225. https://doi.org/10.1016/j.ejpb.2005.01.009

Hotaling, N.A., Khristov, V., Wan, Q., Sharma, R., Jha, B.S., Lotfi, M., Maminishkis, A., Simon, C.G., Bharti, K., 2016. Nanofiber Scaffold-Based Tissue-Engineered Retinal Pigment Epithelium to Treat Degenerative Eye Diseases. J Ocul Pharmacol Ther 32, 272–285. https://doi.org/10.1089/jop.2015.0157

Hou, P., Li, Y., Zhang, X., Liu, C., Guan, J., Li, H., Zhao, T., Ye, J., Yang, W., Liu, K., Ge, J., Xu, J., Zhang, Q., Zhao, Y., Deng, H., 2013. Pluripotent stem cells induced from mouse somatic cells by small-molecule compounds. Science 341, 651–654. https://doi.org/10.1126/science.1239278

Houlihan, J.M., Biro, P.A., Harper, H.M., Jenkinson, H.J., Holmes, C.H., 1995. The human amnion is a site of MHC class Ib expression: evidence for the expression of HLA-E and HLA-G. J Immunol 154, 5665–5674.

Hsu, S.C., Molday, R.S., 1994. Glucose metabolism in photoreceptor outer segments. Its role in phototransduction and in NADPH-requiring reactions. J Biol Chem 269, 17954–17959.

Hughes, B.A., Takahira, M., 1996. Inwardly rectifying K+ currents in isolated human retinal pigment epithelial cells. Invest Ophthalmol Vis Sci 37, 1125–1139.

Hyer, J., Mima, T., Mikawa, T., 1998. FGF1 patterns the optic vesicle by directing the placement of the neural retina domain. Development 125, 869–877. https://doi.org/10.1242/dev.125.5.869

Hynes, S.R., Lavik, E.B., 2010. A tissue-engineered approach towards retinal repair: scaffolds for cell transplantation to the subretinal space. Graefes Arch Clin Exp Ophthalmol 248, 763–778. https://doi.org/10.1007/s00417-009-1263-7

Idelson, M., Alper, R., Obolensky, A., Ben-Shushan, E., Hemo, I., Yachimovich-Cohen, N., Khaner, H., Smith, Y., Wiser, O., Gropp, M., Cohen, M.A., Even-Ram, S., Berman-Zaken, Y., Matzrafi, L., Rechavi, G., Banin, E., Reubinoff, B., 2009. Directed differentiation of human embryonic stem cells into functional retinal pigment epithelium cells. Cell Stem Cell 5, 396–408. https://doi.org/10.1016/j.stem.2009.07.002

Ishida, K., Panjwani, N., Cao, Z., Streilein, J.W., 2003. Participation of pigment epithelium in ocular immune privilege. 3. Epithelia cultured from iris, ciliary body, and retina suppress T-cell activation by partially non-overlapping mechanisms. Ocul Immunol Inflamm 11, 91–105. https://doi.org/10.1076/ocii.11.2.91.15914

J, H., C, A., S, W., 2015. RPE necroptosis in response to oxidative stress and in AMD. Ageing research reviews 24. https://doi.org/10.1016/j.arr.2015.09.002

Jafari, A., Rezaei-Tavirani, M., Niknejad, H., Zali, H., 2021. Tumor Targeting by Conditioned Medium Derived From Human Amniotic Membrane: New Insight in Breast Cancer Therapy. Technol Cancer Res Treat 20, 15330338211036318. https://doi.org/10.1177/15330338211036318

Jha, B.S., Bharti, K., 2015. Regenerating Retinal Pigment Epithelial Cells to Cure Blindness: A Road Towards Personalized Artificial Tissue. Curr Stem Cell Rep 1, 79–91. https://doi.org/10.1007/s40778-015-0014-4

Jirsova, K., Jones, G.L.A., 2017. Amniotic membrane in ophthalmology: properties, preparation, storage and indications for grafting-a review. Cell Tissue Bank 18, 193–204. https://doi.org/10.1007/s10561-017-9618-5

Johnson, M., Dabholkar, A., Huang, J.-D., Presley, J.B., Chimento, M.F., Curcio, C.A., 2007. Comparison of morphology of human macular and peripheral Bruch's

membrane in older eyes. Curr Eye Res 32, 791–799. https://doi.org/10.1080/02713680701550660

Joussen, A.M., Heussen, F.M.A., Joeres, S., Llacer, H., Prinz, B., Rohrschneider, K., Maaijwee, K.J.M., van Meurs, J., Kirchhof, B., 2006. Autologous translocation of the choroid and retinal pigment epithelium in age-related macular degeneration. Am J Ophthalmol 142, 17–30. https://doi.org/10.1016/j.ajo.2006.01.090

Joussen, A.M., Joeres, S., Fawzy, N., Heussen, F.M.A., Llacer, H., van Meurs, J.C., Kirchhof, B., 2007. Autologous translocation of the choroid and retinal pigment epithelium in patients with geographic atrophy. Ophthalmology 114, 551–560. https://doi.org/10.1016/j.ophtha.2006.08.016

Kador, K.E., Alsehli, H.S., Zindell, A.N., Lau, L.W., Andreopoulos, F.M., Watson, B.D., Goldberg, J.L., 2014. Retinal ganglion cell polarization using immobilized guidance cues on a tissue-engineered scaffold. Acta Biomater 10, 4939–4946. https://doi.org/10.1016/j.actbio.2014.08.032

Kamao, H., Mandai, M., Ohashi, W., Hirami, Y., Kurimoto, Y., Kiryu, J., Takahashi, M., 2017. Evaluation of the Surgical Device and Procedure for Extracellular Matrix-Scaffold-Supported Human iPSC-Derived Retinal Pigment Epithelium Cell Sheet Transplantation. Invest Ophthalmol Vis Sci 58, 211–220. https://doi.org/10.1167/iovs.16-19778

Kashani, A.H., Lebkowski, J.S., Rahhal, F.M., Avery, R.L., Salehi-Had, H., Dang, W., Lin, C.-M., Mitra, D., Zhu, D., Thomas, B.B., Hikita, S.T., Pennington, B.O., Johnson, L.V., Clegg, D.O., Hinton, D.R., Humayun, M.S., 2018. A bioengineered retinal pigment epithelial monolayer for advanced, dry age-related macular degeneration. Sci Transl Med 10, eaao4097. https://doi.org/10.1126/scitranslmed.aao4097

Kawasaki, H., Suemori, H., Mizuseki, K., Watanabe, K., Urano, F., Ichinose, H., Haruta, M., Takahashi, M., Yoshikawa, K., Nishikawa, S.-I., Nakatsuji, N., Sasai, Y., 2002. Generation of dopaminergic neurons and pigmented epithelia from primate ES cells by stromal cell-derived inducing activity. Proc Natl Acad Sci U S A 99, 1580–1585. https://doi.org/10.1073/pnas.032662199

Keane, T.J., Londono, R., Turner, N.J., Badylak, S.F., 2012. Consequences of ineffective decellularization of biologic scaffolds on the host response. Biomaterials 33, 1771–1781. https://doi.org/10.1016/j.biomaterials.2011.10.054

Keane, T.J., Swinehart, I.T., Badylak, S.F., 2015. Methods of tissue decellularization used for preparation of biologic scaffolds and in vivo relevance. Methods 84, 25–34. https://doi.org/10.1016/j.ymeth.2015.03.005

Keller, G., 2005. Embryonic stem cell differentiation: emergence of a new era in biology and medicine. Genes Dev 19, 1129–1155. https://doi.org/10.1101/gad.1303605

Kenyon, E., Yu, K., La Cour, M., Miller, S.S., 1994. Lactate transport mechanisms at apical and basolateral membranes of bovine retinal pigment epithelium. Am J Physiol 267, C1561-1573. https://doi.org/10.1152/ajpcell.1994.267.6.C1561

Khaliq, A., Patel, B., Jarvis-Evans, J., Moriarty, P., McLeod, D., Boulton, M., 1995. Oxygen modulates production of bFGF and TGF-beta by retinal cells in vitro. Exp Eye Res 60, 415–423. https://doi.org/10.1016/s0014-4835(05)80098-3

Khristov, V., Maminishkis, A., Amaral, J., Rising, A., Bharti, K., Miller, S., 2018. Validation of iPS Cell-Derived RPE Tissue in Animal Models, in: Ash, J.D., Anderson, R.E., LaVail, M.M., Bowes Rickman, C., Hollyfield, J.G., Grimm, C. (Eds.), Retinal Degenerative Diseases, Advances in Experimental Medicine and Biology. Springer International Publishing, Cham, pp. 633–640. https://doi.org/10.1007/978-3-319-75402-4_77

Kiilgaard, J.F., Scherfig, E., Prause, J.U., la Cour, M., 2012. Transplantation of amniotic membrane to the subretinal space in pigs. Stem Cells Int 2012, 716968. https://doi.org/10.1155/2012/716968

Kim, K., Doi, A., Wen, B., Ng, K., Zhao, R., Cahan, P., Kim, J., Aryee, M.J., Ji, H., Ehrlich, L.I.R., Yabuuchi, A., Takeuchi, A., Cunniff, K.C., Hongguang, H., McKinney-Freeman, S., Naveiras, O., Yoon, T.J., Irizarry, R.A., Jung, N., Seita, J., Hanna, J., Murakami, P., Jaenisch, R., Weissleder, R., Orkin, S.H., Weissman, I.L., Feinberg, A.P., Daley, G.Q., 2010. Epigenetic memory in induced pluripotent stem cells. Nature 467, 285–290. https://doi.org/10.1038/nature09342

King, G.L., Suzuma, K., 2000. Pigment-epithelium-derived factor--a key coordinator of retinal neuronal and vascular functions. N Engl J Med 342, 349–351. https://doi.org/10.1056/NEJM200002033420511

Kiser, P.D., 2022. Retinal pigment epithelium 65 kDa protein (RPE65): An update. Prog Retin Eye Res 88, 101013. https://doi.org/10.1016/j.preteyeres.2021.101013

Klimanskaya, I., Hipp, J., Rezai, K.A., West, M., Atala, A., Lanza, R., 2004. Derivation and comparative assessment of retinal pigment epithelium from human embryonic stem cells using transcriptomics. Cloning Stem Cells 6, 217–245. https://doi.org/10.1089/clo.2004.6.217

Kniesel, U., Wolburg, H., 1993. Tight junction complexity in the retinal pigment epithelium of the chicken during development. Neurosci Lett 149, 71–74. https://doi.org/10.1016/0304-3940(93)90350-t

Kokkinaki, M., Sahibzada, N., Golestaneh, N., 2011. Human induced pluripotent stem-derived retinal pigment epithelium (RPE) cells exhibit ion transport, membrane potential, polarized vascular endothelial growth factor secretion, and gene expression pattern similar to native RPE. Stem Cells 29, 825–835. https://doi.org/10.1002/stem.635

Krishna, Y., Sheridan, C., Kent, D., Kearns, V., Grierson, I., Williams, R., 2011. Expanded polytetrafluoroethylene as a substrate for retinal pigment epithelial cell growth and transplantation in age-related macular degeneration. Br J Ophthalmol 95, 569–573. https://doi.org/10.1136/bjo.2009.169953

Kuroki, M., Voest, E.E., Amano, S., Beerepoot, L.V., Takashima, S., Tolentino, M., Kim, R.Y., Rohan, R.M., Colby, K.A., Yeo, K.T., Adamis, A.P., 1996. Reactive oxygen intermediates increase vascular endothelial growth factor expression in vitro and in vivo. J Clin Invest 98, 1667–1675. https://doi.org/10.1172/JCI118962

Kvanta, A., 1994. Expression and secretion of transforming growth factor-beta in transformed and nontransformed retinal pigment epithelial cells. Ophthalmic Res 26, 361–367. https://doi.org/10.1159/000267502

la Cour, M., 1985. The retinal pigment epithelium controls the potassium activity in the subretinal space. Acta Ophthalmol Suppl (1985) 173, 9–10. https://doi.org/10.1111/j.1755-3768.1985.tb06827.x

Lamba, D.A., Karl, M.O., Ware, C.B., Reh, T.A., 2006. Efficient generation of retinal progenitor cells from human embryonic stem cells. Proc Natl Acad Sci U S A 103, 12769–12774. https://doi.org/10.1073/pnas.0601990103

Lamme, E.N., de Vries, H.J., van Veen, H., Gabbiani, G., Westerhof, W., Middelkoop, E., 1996. Extracellular matrix characterization during healing of full-thickness wounds treated with a collagen/elastin dermal substitute shows improved skin regeneration in pigs. J Histochem Cytochem 44, 1311–1322. https://doi.org/10.1177/44.11.8918906

Lane, A., Philip, L.R., Ruban, L., Fynes, K., Smart, M., Carr, A., Mason, C., Coffey, P., 2014. Engineering efficient retinal pigment epithelium differentiation from human pluripotent stem cells. Stem Cells Transl Med 3, 1295–1304. https://doi.org/10.5966/sctm.2014-0094

Last, J.A., Liliensiek, S.J., Nealey, P.F., Murphya, C.J., 2009. Determining the mechanical properties of human corneal basement membranes with Atomic Force Microscopy. J Struct Biol 167, 19–24. https://doi.org/10.1016/j.jsb.2009.03.012

Last, J.A., Thomasy, S.M., Croasdale, C.R., Russell, P., Murphy, C.J., 2012. Compliance profile of the human cornea as measured by atomic force microscopy. Micron 43, 1293–1298. https://doi.org/10.1016/j.micron.2012.02.014

Lavail, M.M., Li, L., Turner, J.E., Yasumura, D., 1992. Retinal pigment epithelial cell transplantation in RCS rats: Normal metabolism in rescued photoreceptors. Experimental Eye Research 55, 555–562. https://doi.org/10.1016/S0014-4835(05)80168-X

Leach, L.L., Buchholz, D.E., Nadar, V.P., Lowenstein, S.E., Clegg, D.O., 2015. Canonical/β-catenin Wnt pathway activation improves retinal pigmented epithelium

derivation from human embryonic stem cells. Invest Ophthalmol Vis Sci 56, 1002–1013. https://doi.org/10.1167/iovs.14-15835

LeCun, Y., Bengio, Y., Hinton, G., 2015. Deep learning. Nature 521, 436–444. https://doi.org/10.1038/nature14539

Lee, C.J., Fishman, H.A., Bent, S.F., 2007. Spatial cues for the enhancement of retinal pigment epithelial cell function in potential transplants. Biomaterials 28, 2192–2201. https://doi.org/10.1016/j.biomaterials.2007.01.018

Lee, C.J., Huie, P., Leng, T., Peterman, M.C., Marmor, M.F., Blumenkranz, M.S., Bent, S.F., Fishman, H.A., 2002. Microcontact printing on human tissue for retinal cell transplantation. Arch Ophthalmol 120, 1714–1718. https://doi.org/10.1001/archopht.120.12.1714

Lesueur, L., Arne, J.L., Mignon-Conte, M., Malecaze, F., 1994. Structural and ultrastructural changes in the developmental process of premature infants' and children's corneas. Cornea 13, 331–338. https://doi.org/10.1097/00003226-199407000-00008

Lim, J.-M., Byun, S., Chung, S., Park, T.H., Seo, J.-M., Joo, C.-K., Chung, H., Cho, D.-I., 2004. Retinal pigment epithelial cell behavior is modulated by alterations in focal cell-substrate contacts. Invest Ophthalmol Vis Sci 45, 4210–4216. https://doi.org/10.1167/iovs.03-1036

Lim, L.S., Mitchell, P., Seddon, J.M., Holz, F.G., Wong, T.Y., 2012. Age-related macular degeneration. The Lancet 379, 1728–1738. https://doi.org/10.1016/S0140-6736(12)60282-7

Lim, L.S., Riau, A., Poh, R., Tan, D.T., Beuerman, R.W., Mehta, J.S., 2009. Effect of dispase denudation on amniotic membrane. Mol Vis 15, 1962–1970.

Liu, Z., Yu, N., Holz, F.G., Yang, F., Stanzel, B.V., 2014. Enhancement of retinal pigment epithelial culture characteristics and subretinal space tolerance of scaffolds with 200 nm fiber topography. Biomaterials 35, 2837–2850. https://doi.org/10.1016/j.biomaterials.2013.12.069

Lopez, P.F., Sippy, B.D., Lambert, H.M., Thach, A.B., Hinton, D.R., 1996. Transdifferentiated retinal pigment epithelial cells are immunoreactive for vascular endothelial growth factor in surgically excised age-related macular degeneration-related choroidal neovascular membranes. Invest Ophthalmol Vis Sci 37, 855–868.

López-Valladares, M.J., Teresa Rodríguez-Ares, M., Touriño, R., Gude, F., Teresa Silva, M., Couceiro, J., 2010. Donor age and gestational age influence on growth factor levels in human amniotic membrane. Acta Ophthalmol 88, e211-216. https://doi.org/10.1111/j.1755-3768.2010.01908.x

Lu, B., Zhu, D., Hinton, D., Humayun, M.S., Tai, Y.-C., 2012. Mesh-supported submicron parylene-C membranes for culturing retinal pigment epithelial cells. Biomed Microdevices 14, 659–667. https://doi.org/10.1007/s10544-012-9645-8

Lu, L., Garcia, C.A., Mikos, A.G., 1998. Retinal pigment epithelium cell culture on thin biodegradable poly(DL-lactic-co-glycolic acid) films. J Biomater Sci Polym Ed 9, 1187–1205. https://doi.org/10.1163/156856298x00721

Lu, L., Nyalakonda, K., Kam, L., Bizios, R., Göpferich, A., Mikos, A.G., 2001. Retinal pigment epithelial cell adhesion on novel micropatterned surfaces fabricated from synthetic biodegradable polymers. Biomaterials 22, 291–297. https://doi.org/10.1016/s0142-9612(00)00179-4

Ma, Z., Han, L., Wang, C., Dou, H., Hu, Y., Feng, X., Xu, Y., Wang, Z., Yin, Z., Liu, Y., 2009. Autologous transplantation of retinal pigment epithelium-Bruch's membrane complex for hemorrhagic age-related macular degeneration. Invest Ophthalmol Vis Sci 50, 2975–2981. https://doi.org/10.1167/iovs.08-2573

MacLaren, R.E., Uppal, G.S., Balaggan, K.S., Tufail, A., Munro, P.M.G., Milliken, A.B., Ali, R.R., Rubin, G.S., Aylward, G.W., da Cruz, L., 2007. Autologous Transplantation of the Retinal Pigment Epithelium and Choroid in the Treatment of Neovascular Age-Related Macular Degeneration. Ophthalmology 114, 561-570.e2. https://doi.org/10.1016/j.ophtha.2006.06.049

Magalhães, P.O., Lopes, A.M., Mazzola, P.G., Rangel-Yagui, C., Penna, T.C.V., Pessoa, A., 2007. Methods of endotoxin removal from biological preparations: a review. J Pharm Pharm Sci 10, 388–404.

Makadia, H.K., Siegel, S.J., 2011. Poly Lactic-co-Glycolic Acid (PLGA) as Biodegradable Controlled Drug Delivery Carrier. Polymers (Basel) 3, 1377–1397. https://doi.org/10.3390/polym3031377

Mallon, B.S., Park, K.-Y., Chen, K.G., Hamilton, R.S., McKay, R.D.G., 2006. Toward xeno-free culture of human embryonic stem cells. Int J Biochem Cell Biol 38, 1063–1075. https://doi.org/10.1016/j.biocel.2005.12.014

Mandai, M., Kurimoto, Y., Takahashi, M., 2017. Autologous Induced Stem-Cell-Derived Retinal Cells for Macular Degeneration. N Engl J Med 377, 792–793. https://doi.org/10.1056/NEJMc1706274

Mannermaa, E., Reinisalo, M., Ranta, V.-P., Vellonen, K.-S., Kokki, H., Saarikko, A., Kaarniranta, K., Urtti, A., 2010. Filter-cultured ARPE-19 cells as outer blood-retinal barrier model. Eur J Pharm Sci 40, 289–296. https://doi.org/10.1016/j.ejps.2010.04.001

Marmor, M.F., 1979. Retinal detachment from hyperosmotic intravitreal injection. Invest Ophthalmol Vis Sci 18, 1237–1244.

Martin, D.M., Yee, D., Feldman, E.L., 1992. Gene expression of the insulin-like growth factors and their receptors in cultured human retinal pigment epithelial cells. Brain Res Mol Brain Res 12, 181–186. https://doi.org/10.1016/0169-328x(92)90082-m

Matter, K., Balda, M.S., 2003. Functional analysis of tight junctions. Methods 30, 228–234. https://doi.org/10.1016/s1046-2023(03)00029-x

May-Simera, H.L., Wan, Q., Jha, B.S., Hartford, J., Khristov, V., Dejene, R., Chang, J., Patnaik, S., Lu, Q., Banerjee, P., Silver, J., Insinna-Kettenhofen, C., Patel, D., Lotfi, M., Malicdan, M., Hotaling, N., Maminishkis, A., Sridharan, R., Brooks, B., Miyagishima, K., Gunay-Aygun, M., Pal, R., Westlake, C., Miller, S., Sharma, R., Bharti, K., 2018. Primary Cilium-Mediated Retinal Pigment Epithelium Maturation Is Disrupted in Ciliopathy Patient Cells. Cell Rep 22, 189–205. https://doi.org/10.1016/j.celrep.2017.12.038

McGill, T.J., Bohana-Kashtan, O., Stoddard, J.W., Andrews, M.D., Pandit, N., Rosenberg-Belmaker, L.R., Wiser, O., Matzrafi, L., Banin, E., Reubinoff, B., Netzer, N., Irving, C., 2017. Long-Term Efficacy of GMP Grade Xeno-Free hESC-Derived RPE Cells Following Transplantation. Transl Vis Sci Technol 6, 17. https://doi.org/10.1167/tvst.6.3.17

McGill, T.J., Cottam, B., Lu, B., Wang, S., Girman, S., Tian, C., Huhn, S.L., Lund, R.D., Capela, A., 2012. Transplantation of human central nervous system stem cells - neuroprotection in retinal degeneration. Eur J Neurosci 35, 468–477. https://doi.org/10.1111/j.1460-9568.2011.07970.x

McLenachan, S., Hao, E., Zhang, D., Zhang, L., Edel, M., Chen, F., 2017. Bioengineered Bruch's-like extracellular matrix promotes retinal pigment epithelial differentiation. Biochem Biophys Rep 10, 178–185. https://doi.org/10.1016/j.bbrep.2017.03.008

Merkle, F.T., Ghosh, S., Kamitaki, N., Mitchell, J., Avior, Y., Mello, C., Kashin, S., Mekhoubad, S., Ilic, D., Charlton, M., Saphier, G., Handsaker, R.E., Genovese, G., Bar, S., Benvenisty, N., McCarroll, S.A., Eggan, K., 2017. Human pluripotent stem cells recurrently acquire and expand dominant negative P53 mutations. Nature 545, 229–233. https://doi.org/10.1038/nature22312

Meyer, J.S., Shearer, R.L., Capowski, E.E., Wright, L.S., Wallace, K.A., McMillan, E.L., Zhang, S.-C., Gamm, D.M., 2009. Modeling early retinal development with human embryonic and induced pluripotent stem cells. Proc Natl Acad Sci U S A 106, 16698–16703. https://doi.org/10.1073/pnas.0905245106

Mi, S., Chen, B., Wright, B., Connon, C.J., 2010. Ex vivo construction of an artificial ocular surface by combination of corneal limbal epithelial cells and a compressed collagen scaffold containing keratocytes. Tissue Eng Part A 16, 2091–2100. https://doi.org/10.1089/ten.TEA.2009.0748

Mi, S., David, A.L., Chowdhury, B., Jones, R.R., Hamley, I.W., Squires, A.M., Connon, C.J., 2012. Tissue engineering a fetal membrane. Tissue Eng Part A 18, 373–381. https://doi.org/10.1089/ten.TEA.2011.0194

Miettinen, T.P., Björklund, M., 2017. Mitochondrial Function and Cell Size: An Allometric Relationship. Trends Cell Biol 27, 393–402. https://doi.org/10.1016/j.tcb.2017.02.006

Miyagishima, K.J., Wan, Q., Corneo, B., Sharma, R., Lotfi, M.R., Boles, N.C., Hua, F., Maminishkis, A., Zhang, C., Blenkinsop, T., Khristov, V., Jha, B.S., Memon, O.S., D'Souza, S., Temple, S., Miller, S.S., Bharti, K., 2016. In Pursuit of Authenticity: Induced Pluripotent Stem Cell-Derived Retinal Pigment Epithelium for Clinical Applications. Stem Cells Translational Medicine 5, 1562–1574. https://doi.org/10.5966/sctm.2016-0037

Miyoshi, S., Nakazawa, H., Kawata, K., Tomochika, K., Tobe, K., Shinoda, S., 1998. Characterization of the hemorrhagic reaction caused by Vibrio vulnificus metalloprotease, a member of the thermolysin family. Infect Immun 66, 4851–4855. https://doi.org/10.1128/IAI.66.10.4851-4855.1998

Moore, D.J., Clover, G.M., 2001. The effect of age on the macromolecular permeability of human Bruch's membrane. Invest Ophthalmol Vis Sci 42, 2970–2975.

Nazari, H., Zhang, L., Zhu, D., Chader, G.J., Falabella, P., Stefanini, F., Rowland, T., Clegg, D.O., Kashani, A.H., Hinton, D.R., Humayun, M.S., 2015. Stem cell based therapies for age-related macular degeneration: The promises and the challenges. Prog Retin Eye Res 48, 1–39. https://doi.org/10.1016/j.preteyeres.2015.06.004

Newman, E., Reichenbach, A., 1996. The Müller cell: a functional element of the retina. Trends Neurosci 19, 307–312. https://doi.org/10.1016/0166-2236(96)10040-0

Nguyen, M., Arnheiter, H., 2000. Signaling and transcriptional regulation in early mammalian eye development: a link between FGF and MITF. Development 127, 3581–3591. https://doi.org/10.1242/dev.127.16.3581

Niknejad, H., Peirovi, H., Jorjani, M., Ahmadiani, A., Ghanavi, J., Seifalian, A.M., 2008. Properties of the amniotic membrane for potential use in tissue engineering. Eur Cell Mater 15, 88–99. https://doi.org/10.22203/ecm.v015a07

Norde, W., Lyklema, J., 1991. Why proteins prefer interfaces. J Biomater Sci Polym Ed 2, 183–202. https://doi.org/10.1080/09205063.1991.9756659

Ohno-Matsui, K., Ichinose, S., Nakahama, K., Yoshida, T., Kojima, A., Mochizuki, M., Morita, I., 2005. The effects of amniotic membrane on retinal pigment epithelial cell differentiation. Mol Vis 11, 1–10.

Ohno-Matsui, K., Ichinose, S., Nakahama, K., Yoshida, T., Kojima, A., Morita, I., n.d. The effects of amniotic membrane on retinal pigment epithelial cell differentiation. Molecular Vision 10.

Ohno-Matsui, K., Morita, I., Tombran-Tink, J., Mrazek, D., Onodera, M., Uetama, T., Hayano, M., Murota, S.I., Mochizuki, M., 2001. Novel mechanism for age-related macular degeneration: an equilibrium shift between the angiogenesis factors VEGF and PEDF. J Cell Physiol 189, 323–333. https://doi.org/10.1002/jcp.10026

Okada, T., Ernst, O.P., Palczewski, K., Hofmann, K.P., 2001. Activation of rhodopsin: new insights from structural and biochemical studies. Trends Biochem Sci 26, 318–324. https://doi.org/10.1016/s0968-0004(01)01799-6

Ortolan, D., Sharma, R., Volkov, A., Maminishkis, A., Hotaling, N.A., Huryn, L.A., Cukras, C., Di Marco, S., Bisti, S., Bharti, K., 2022. Single-cell–resolution map of human retinal pigment epithelium helps discover subpopulations with differential disease sensitivity. Proc. Natl. Acad. Sci. U.S.A. 119, e2117553119. https://doi.org/10.1073/pnas.2117553119

Osakada, F., Jin, Z.-B., Hirami, Y., Ikeda, H., Danjyo, T., Watanabe, K., Sasai, Y., Takahashi, M., 2009. In vitro differentiation of retinal cells from human pluripotent stem cells by small-molecule induction. Journal of Cell Science 122, 3169–3179. https://doi.org/10.1242/jcs.050393

Panda-Jonas, S., Jonas, J.B., Jakobczyk-Zmija, M., 1995. Retinal Photoreceptor Density Decreases with Age. Ophthalmology 102, 1853–1859. https://doi.org/10.1016/S0161-6420(95)30784-1

Parry, S., Strauss, J.F., 1998. Premature rupture of the fetal membranes. N Engl J Med 338, 663–670. https://doi.org/10.1056/NEJM199803053381006

Pearce, K.F., Hildebrandt, M., Greinix, H., Scheding, S., Koehl, U., Worel, N., Apperley, J., Edinger, M., Hauser, A., Mischak-Weissinger, E., Dickinson, A.M., Lowdell, M.W., 2014. Regulation of advanced therapy medicinal products in Europe and the role of academia. Cytotherapy 16, 289–297. https://doi.org/10.1016/j.jcyt.2013.08.003

Peng, S., Adelman, R.A., Rizzolo, L.J., 2010. Minimal effects of VEGF and anti-VEGF drugs on the permeability or selectivity of RPE tight junctions. Invest Ophthalmol Vis Sci 51, 3216–3225. https://doi.org/10.1167/iovs.09-4162

Pera, E.M., Wessely, O., Li, S.Y., De Robertis, E.M., 2001. Neural and head induction by insulin-like growth factor signals. Dev Cell 1, 655–665. https://doi.org/10.1016/s1534-5807(01)00069-7

Pera, M.F., Trounson, A.O., 2004. Human embryonic stem cells: prospects for development. Development 131, 5515–5525. https://doi.org/10.1242/dev.01451

Peterson, S.E., Loring, J.F., 2014. Genomic instability in pluripotent stem cells: implications for clinical applications. J Biol Chem 289, 4578–4584. https://doi.org/10.1074/jbc.R113.516419

Petrus-Reurer, S., Winblad, N., Kumar, P., Gorchs, L., Chrobok, M., Wagner, A.K., Bartuma, H., Lardner, E., Aronsson, M., Plaza Reyes, Á., André, H., Alici, E.,

Kaipe, H., Kvanta, A., Lanner, F., 2020. Generation of Retinal Pigment Epithelial Cells Derived from Human Embryonic Stem Cells Lacking Human Leukocyte Antigen Class I and II. Stem Cell Reports 14, 648–662. https://doi.org/10.1016/j.stemcr.2020.02.006

Peyman, G.A., Blinder, K.J., Paris, C.L., Alturki, W., Nelson, N.C., Desai, U., 1991. A technique for retinal pigment epithelium transplantation for age-related macular degeneration secondary to extensive subfoveal scarring. Ophthalmic Surg 22, 102–108.

Pfeffer, B.A., Clark, V.M., Flannery, J.G., Bok, D., 1986. Membrane receptors for retinol-binding protein in cultured human retinal pigment epithelium. Invest Ophthalmol Vis Sci 27, 1031–1040.

Pittack, C., Grunwald, G.B., Reh, T.A., 1997. Fibroblast growth factors are necessary for neural retina but not pigmented epithelium differentiation in chick embryos. Development 124, 805–816. https://doi.org/10.1242/dev.124.4.805

Rajendran Nair, D.S., Zhu, D., Sharma, R., Martinez Camarillo, J.C., Bharti, K., Hinton, D.R., Humayun, M.S., Thomas, B.B., 2021. Long-Term Transplant Effects of iPSC-RPE Monolayer in Immunodeficient RCS Rats. Cells 10, 2951. https://doi.org/10.3390/cells10112951

Ramrattan, R.S., van der Schaft, T.L., Mooy, C.M., de Bruijn, W.C., Mulder, P.G., de Jong, P.T., 1994. Morphometric analysis of Bruch's membrane, the choriocapillaris, and the choroid in aging. Invest Ophthalmol Vis Sci 35, 2857–2864.

Ramsden, C.M., da Cruz, L., Coffey, P.J., 2016. Stemming the Tide of Age-Related Macular Degeneration: New Therapies for Old Retinas. Invest Ophthalmol Vis Sci 57, ORSFb1-3. https://doi.org/10.1167/iovs.15-18643

Ramsden, C.M., Powner, M.B., Carr, A.-J.F., Smart, M.J.K., Cruz, L. da, Coffey, P.J., 2013. Stem cells in retinal regeneration: past, present and future. Development (Cambridge, England) 140, 2576. https://doi.org/10.1242/dev.092270

Rattner, A., Smallwood, P.M., Nathans, J., 2000. Identification and Characterization of All-trans-retinol Dehydrogenase from Photoreceptor Outer Segments, the Visual Cycle Enzyme That Reduces All-trans-retinal to All-trans-retinol. Journal of Biological Chemistry 275, 11034–11043. https://doi.org/10.1074/jbc.275.15.11034

Reh, T.A., Lamba, D., Gust, J., 2010. Directing human embryonic stem cells to a retinal fate. Methods Mol Biol 636, 139–153. https://doi.org/10.1007/978-1-60761-691-7_9

Riau, A.K., Beuerman, R.W., Lim, L.S., Mehta, J.S., 2010. Preservation, sterilization and de-epithelialization of human amniotic membrane for use in ocular surface

reconstruction. Biomaterials 31, 216–225. https://doi.org/10.1016/j.biomaterials.2009.09.034

Roberts, J.M., Forrester, J.V., 1990. Factors affecting the migration and growth of endothelial cells from microvessels of bovine retina. Exp Eye Res 50, 165–172. https://doi.org/10.1016/0014-4835(90)90227-I

Rowland, T.J., Buchholz, D.E., Clegg, D.O., 2012. Pluripotent human stem cells for the treatment of retinal disease. J Cell Physiol 227, 457–466. https://doi.org/10.1002/jcp.22814

Roy, R., Haase, T., Ma, N., Bader, A., Becker, M., Seifert, M., Choi, Y.-H., Falk, V., Stamm, C., 2016. Decellularized amniotic membrane attenuates postinfarct left ventricular remodeling. J Surg Res 200, 409–419. https://doi.org/10.1016/j.jss.2015.08.022

Rózanowski, B., Burke, J.M., Boulton, M.E., Sarna, T., Rózanowska, M., 2008. Human RPE melanosomes protect from photosensitized and iron-mediated oxidation but become pro-oxidant in the presence of iron upon photodegradation. Invest Ophthalmol Vis Sci 49, 2838–2847. https://doi.org/10.1167/iovs.08-1700

Rutledge, S.D., Douglas, T.A., Nicholson, J.M., Vila-Casadesús, M., Kantzler, C.L., Wangsa, D., Barroso-Vilares, M., Kale, S.D., Logarinho, E., Cimini, D., 2016. Selective advantage of trisomic human cells cultured in non-standard conditions. Sci Rep 6, 22828. https://doi.org/10.1038/srep22828

Saikia, P., Medeiros, C.S., Thangavadivel, S., Wilson, S.E., 2018. Basement membranes in the cornea and other organs that commonly develop fibrosis. Cell Tissue Res 374, 439–453. https://doi.org/10.1007/s00441-018-2934-7

Savage, V.M., Allen, A.P., Brown, J.H., Gillooly, J.F., Herman, A.B., Woodruff, W.H., West, G.B., 2007. Scaling of number, size, and metabolic rate of cells with body size in mammals. Proc Natl Acad Sci U S A 104, 4718–4723. https://doi.org/10.1073/pnas.0611235104

Schulze, U., Hampel, U., Sel, S., Goecke, T.W., Thäle, V., Garreis, F., Paulsen, F., 2012. Fresh and cryopreserved amniotic membrane secrete the trefoil factor family peptide 3 that is well known to promote wound healing. Histochem Cell Biol 138, 243–250. https://doi.org/10.1007/s00418-012-0943-2

Schwartz, S.D., Hubschman, J.-P., Heilwell, G., Franco-Cardenas, V., Pan, C.K., Ostrick, R.M., Mickunas, E., Gay, R., Klimanskaya, I., Lanza, R., 2012. Embryonic stem cell trials for macular degeneration: a preliminary report. Lancet 379, 713–720. https://doi.org/10.1016/S0140-6736(12)60028-2

Schwartz, S.D., Regillo, C.D., Lam, B.L., Eliott, D., Rosenfeld, P.J., Gregori, N.Z., Hubschman, J.-P., Davis, J.L., Heilwell, G., Spirn, M., Maguire, J., Gay, R., Bateman, J., Ostrick, R.M., Morris, D., Vincent, M., Anglade, E., Del Priore, L.V.,

Lanza, R., 2015. Human embryonic stem cell-derived retinal pigment epithelium in patients with age-related macular degeneration and Stargardt's macular dystrophy: follow-up of two open-label phase 1/2 studies. The Lancet 385, 509–516. https://doi.org/10.1016/S0140-6736(14)61376-3

Shah, A.R., Williams, G.A., 2016. Regulatory and Economic Considerations of Retinal Drugs. Dev Ophthalmol 55, 376–380. https://doi.org/10.1159/000438965

Shao, L., Wu, W.-S., 2010. Gene-delivery systems for iPS cell generation. Expert Opin Biol Ther 10, 231–242. https://doi.org/10.1517/14712590903455989

Sharma, R., Bose, D., Maminishkis, A., Bharti, K., 2020. Retinal Pigment Epithelium Replacement Therapy for Age-Related Macular Degeneration: Are We There Yet? Annu. Rev. Pharmacol. Toxicol. 60, 553–572. https://doi.org/10.1146/annurev-pharmtox-010919-023245

Sharma, R., Bose, D., Montford, J., Ortolan, D., Bharti, K., 2022. Triphasic developmentally guided protocol to generate retinal pigment epithelium from induced pluripotent stem cells. STAR Protocols 3, 101582. https://doi.org/10.1016/j.xpro.2022.101582

Sharma, R., Khristov, V., Rising, A., Jha, B.S., Dejene, R., Hotaling, N., Li, Y., Stoddard, J., Stankewicz, C., Wan, Q., Zhang, C., Campos, M.M., Miyagishima, K.J., McGaughey, D., Villasmil, R., Mattapallil, M., Stanzel, B., Qian, H., Wong, W., Chase, L., Charles, S., McGill, T., Miller, S., Maminishkis, A., Amaral, J., Bharti, K., 2019. Clinical-grade stem cell–derived retinal pigment epithelium patch rescues retinal degeneration in rodents and pigs. Science Translational Medicine 11. https://doi.org/10.1126/scitranslmed.aat5580

Sheridan, C., Williams, R., Grierson, I., 2004. Basement membranes and artificial substrates in cell transplantation. Graefe's Arch Clin Exp Ophthalmol 242, 68–75. https://doi.org/10.1007/s00417-003-0800-z

Sheridan, C.M., Mason, S., Pattwell, D.M., Kent, D., Grierson, I., Williams, R., 2009. Replacement of the RPE monolayer. Eye (Lond) 23, 1910–1915. https://doi.org/10.1038/eye.2008.420

Sheth-Shah, R., Vernon, A.J., Seetharaman, S., Neale, M.H., Daniels, J.T., 2016. Regulatory requirements in the good manufacturing practice production of an epithelial cell graft for ocular surface reconstruction. Regenerative Medicine 11, 307–320. https://doi.org/10.2217/rme-2015-0020

Shortt, A.J., Secker, G.A., Rajan, M.S., Meligonis, G., Dart, J.K., Tuft, S.J., Daniels, J.T., 2008. Ex vivo expansion and transplantation of limbal epithelial stem cells. Ophthalmology 115, 1989–1997. https://doi.org/10.1016/j.ophtha.2008.04.039

Shuttleworth, C.A., 1997. Type VIII collagen. Int J Biochem Cell Biol 29, 1145–1148. https://doi.org/10.1016/s1357-2725(97)00033-2

Sidney, L.E., Branch, M.J., Dunphy, S.E., Dua, H.S., Hopkinson, A., 2014. Concise review: evidence for CD34 as a common marker for diverse progenitors. Stem Cells 32, 1380–1389. https://doi.org/10.1002/stem.1661

Silverman, M.S., Hughes, S.E., 1990. Photoreceptor rescue in the RCS rat without pigment epithelium transplantation. Curr Eye Res 9, 183–191. https://doi.org/10.3109/02713689008995205

Singh, M.S., Park, S.S., Albini, T.A., Canto-Soler, M.V., Klassen, H., MacLaren, R.E., Takahashi, M., Nagiel, A., Schwartz, S.D., Bharti, K., 2020. Retinal stem cell transplantation: Balancing safety and potential. Progress in Retinal and Eye Research 75, 100779. https://doi.org/10.1016/j.preteyeres.2019.100779

Singh, S., Woerly, S., McLaughlin, B.J., 2001. Natural and artificial substrates for retinal pigment epithelial monolayer transplantation. Biomaterials 22, 3337–3343. https://doi.org/10.1016/s0142-9612(01)00171-5

Singhal, S., Vemuganti, G.K., 2005. Primary adult human retinal pigment epithelial cell cultures on human amniotic membranes. Indian J Ophthalmol 53, 109–113. https://doi.org/10.4103/0301-4738.16174

Slomiany, M.G., Rosenzweig, S.A., 2004. Autocrine effects of IGF-I-induced VEGF and IGFBP-3 secretion in retinal pigment epithelial cell line ARPE-19. Am J Physiol Cell Physiol 287, C746-753. https://doi.org/10.1152/ajpcell.00568.2003

Song, W.K., Park, K.-M., Kim, H.-J., Lee, J.H., Choi, J., Chong, S.Y., Shim, S.H., Del Priore, L.V., Lanza, R., 2015. Treatment of macular degeneration using embryonic stem cell-derived retinal pigment epithelium: preliminary results in Asian patients. Stem Cell Reports 4, 860–872. https://doi.org/10.1016/j.stemcr.2015.04.005

Sorkio, A., Hongisto, H., Kaarniranta, K., Uusitalo, H., Juuti-Uusitalo, K., Skottman, H., 2014. Structure and barrier properties of human embryonic stem cell-derived retinal pigment epithelial cells are affected by extracellular matrix protein coating. Tissue Eng Part A 20, 622–634. https://doi.org/10.1089/ten.TEA.2013.0049

Sorkio, A.E., Vuorimaa-Laukkanen, E.P., Hakola, H.M., Liang, H., Ujula, T.A., Valle-Delgado, J.J., Österberg, M., Yliperttula, M.L., Skottman, H., 2015. Biomimetic collagen I and IV double layer Langmuir-Schaefer films as microenvironment for human pluripotent stem cell derived retinal pigment epithelial cells. Biomaterials 51, 257–269. https://doi.org/10.1016/j.biomaterials.2015.02.005

Soto-Gutierrez, A., Yagi, H., Uygun, B.E., Navarro-Alvarez, N., Uygun, K., Kobayashi, N., Yang, Y.-G., Yarmush, M.L., 2010. Cell Delivery: From Cell Transplantation to Organ Engineering. Cell Transplant 19, 655–665. https://doi.org/10.3727/096368910X508753

Souied, E., Pulido, J., Staurenghi, G., 2017. Autologous Induced Stem-Cell-Derived Retinal Cells for Macular Degeneration. N Engl J Med 377, 792. https://doi.org/10.1056/NEJMc1706274

Sparrow, J.R., Hicks, D., Hamel, C.P., 2010. The Retinal Pigment Epithelium in Health and Disease. Curr Mol Med 10, 802–823. https://doi.org/10.2174/156652410793937813

Sridhar, A., Steward, M.M., Meyer, J.S., 2013. Nonxenogeneic growth and retinal differentiation of human induced pluripotent stem cells. Stem Cells Transl Med 2, 255–264. https://doi.org/10.5966/sctm.2012-0101

Srinivasan, B., Kolli, A.R., Esch, M.B., Abaci, H.E., Shuler, M.L., Hickman, J.J., 2015. TEER measurement techniques for in vitro barrier model systems. J Lab Autom 20, 107–126. https://doi.org/10.1177/2211068214561025

Stahl, A., 2020. The Diagnosis and Treatment of Age-Related Macular Degeneration. Deutsches Ärzteblatt international. https://doi.org/10.3238/arztebl.2020.0513

Stanga, P.E., Kychenthal, A., Fitzke, F.W., Halfyard, A.S., Chan, R., Bird, A.C., Aylward, G.W., 2001. Retinal pigment epithelium translocation and central visual function in age related macular degeneration: preliminary results. Int Ophthalmol 23, 297–307. https://doi.org/10.1023/a:1014482025960

Stanzel, B.V., Espana, E.M., Grueterich, M., Kawakita, T., Parel, J.-M., Tseng, S.C.G., Binder, S., 2005. Amniotic membrane maintains the phenotype of rabbit retinal pigment epithelial cells in culture. Exp Eye Res 80, 103–112. https://doi.org/10.1016/j.exer.2004.06.032

Stanzel, B.V., Liu, Z., Brinken, R., Braun, N., Holz, F.G., Eter, N., 2012. Subretinal delivery of ultrathin rigid-elastic cell carriers using a metallic shooter instrument and biodegradable hydrogel encapsulation. Invest Ophthalmol Vis Sci 53, 490–500. https://doi.org/10.1167/iovs.11-8260

Steinberg, R.H., Linsenmeier, R.A., Griff, E.R., 1983. Three light-evoked responses of the retinal pigment epithelium. Vision Res 23, 1315–1323. https://doi.org/10.1016/0042-6989(83)90107-4

Steinberg, R.H., Wood, I., 1974. Pigment epithelial cell ensheathment of cone outer segments in the retina of the domestic cat. Proc R Soc Lond B Biol Sci 187, 461–478. https://doi.org/10.1098/rspb.1974.0088

Strauss, O., 2005. The Retinal Pigment Epithelium in Visual Function. Physiological Reviews 85, 845–881. https://doi.org/10.1152/physrev.00021.2004

Streilein, J.W., Ma, N., Wenkel, H., Ng, T.F., Zamiri, P., 2002. Immunobiology and privilege of neuronal retina and pigment epithelium transplants. Vision Res 42, 487–495. https://doi.org/10.1016/s0042-6989(01)00185-7

Sugasawa, K., Deguchi, J., Okami, T., Yamamoto, A., Omori, K., Uyama, M., Tashiro, Y., 1994. Immunocytochemical analyses of distributions of Na, K-ATPase and GLUT1, insulin and transferrin receptors in the developing retinal pigment epithelial cells. Cell Struct Funct 19, 21–28. https://doi.org/10.1247/csf.19.21

Sugino, I.K., Gullapalli, V.K., Sun, Q., Wang, J., Nunes, C.F., Cheewatrakoolpong, N., Johnson, A.C., Degner, B.C., Hua, J., Liu, T., Chen, W., Li, H., Zarbin, M.A., 2011a. Cell-Deposited Matrix Improves Retinal Pigment Epithelium Survival on Aged Submacular Human Bruch's Membrane. Invest. Ophthalmol. Vis. Sci. 52, 1345. https://doi.org/10.1167/iovs.10-6112

Sugino, I.K., Sun, Q., Wang, J., Nunes, C.F., Cheewatrakoolpong, N., Rapista, A., Johnson, A.C., Malcuit, C., Klimanskaya, I., Lanza, R., Zarbin, M.A., 2011b. Comparison of FRPE and Human Embryonic Stem Cell–Derived RPE Behavior on Aged Human Bruch's Membrane. Invest. Ophthalmol. Vis. Sci. 52, 4979. https://doi.org/10.1167/iovs.10-5386

Swaroop, A., Kim, D., Forrest, D., 2010. Transcriptional regulation of photoreceptor development and homeostasis in the mammalian retina. Nat Rev Neurosci 11, 563–576. https://doi.org/10.1038/nrn2880

Takahashi, K., Yamanaka, S., 2006. Induction of pluripotent stem cells from mouse embryonic and adult fibroblast cultures by defined factors. Cell 126, 663–676. https://doi.org/10.1016/j.cell.2006.07.024

Tanihara, H., Inatani, M., Honda, Y., 1997. Growth factors and their receptors in the retina and pigment epithelium. Progress in Retinal and Eye Research 16, 271–301. https://doi.org/10.1016/S1350-9462(96)00028-6

Taylor, C.J., Bolton, E.M., Pocock, S., Sharples, L.D., Pedersen, R.A., Bradley, J.A., 2005. Banking on human embryonic stem cells: estimating the number of donor cell lines needed for HLA matching. Lancet 366, 2019–2025. https://doi.org/10.1016/S0140-6736(05)67813-0

Tezel, T.H., Del Priore, L.V., 1997. Reattachment to a substrate prevents apoptosis of human retinal pigment epithelium. Graefes Arch Clin Exp Ophthalmol 235, 41–47. https://doi.org/10.1007/BF01007836

Tezel, T.H., Del Priore, L.V., Berger, A.S., Kaplan, H.J., 2007. Adult retinal pigment epithelial transplantation in exudative age-related macular degeneration. Am J Ophthalmol 143, 584–595. https://doi.org/10.1016/j.ajo.2006.12.007

Tezel, T.H., Del Priore, L.V., Kaplan, H.J., 2004. Reengineering of Aged Bruch's Membrane to Enhance Retinal Pigment Epithelium Repopulation. Investigative Ophthalmology & Visual Science 45, 3337–3348. https://doi.org/10.1167/iovs.04-0193

Tezel, T.H., Kaplan, H.J., Priore, L.V.D., 1999. Fate of Human Retinal Pigment Epithelial Cells Seeded onto Layers of Human Bruch's Membrane 40.

Tezel, T.H., Priore, L.V.D., 1999. Repopulation of Different Layers of Host Human Bruch's Membrane by Retinal Pigment Epithelial Cell Grafts 40.

Thomas, B.B., Zhu, D., Zhang, L., Thomas, P.B., Hu, Y., Nazari, H., Stefanini, F., Falabella, P., Clegg, D.O., Hinton, D.R., Humayun, M.S., 2016. Survival and Functionality of hESC-Derived Retinal Pigment Epithelium Cells Cultured as a Monolayer on Polymer Substrates Transplanted in RCS Rats. Invest Ophthalmol Vis Sci 57, 2877–2887. https://doi.org/10.1167/iovs.16-19238

Thomas, C.J., Mirza, R.G., Gill, M.K., 2021. Age-Related Macular Degeneration. Medical Clinics of North America 105, 473–491. https://doi.org/10.1016/j.mcna.2021.01.003

Thomson, H.A.J., Treharne, A.J., Walker, P., Grossel, M.C., Lotery, A.J., 2011. Optimisation of polymer scaffolds for retinal pigment epithelium (RPE) cell transplantation. Br J Ophthalmol 95, 563–568. https://doi.org/10.1136/bjo.2009.166728

Thumann, G., Schraermeyer, U., Bartz-Schmidt, K.U., Heimann, K., 1997. Descemet's membrane as membranous support in RPE/IPE transplantation. Curr Eye Res 16, 1236–1238. https://doi.org/10.1076/ceyr.16.12.1236.5031

Toomey, C.B., Johnson, L.V., Bowes Rickman, C., 2018. Complement factor H in AMD: Bridging genetic associations and pathobiology. Prog Retin Eye Res 62, 38–57. https://doi.org/10.1016/j.preteyeres.2017.09.001

Treharne, A.J., Thomson, H.A.J., Grossel, M.C., Lotery, A.J., 2012. Developing methacrylate-based copolymers as an artificial Bruch's membrane substitute. J Biomed Mater Res A 100, 2358–2364. https://doi.org/10.1002/jbm.a.34178

Treumer, F., Bunse, A., Klatt, C., Roider, J., 2007. Autologous retinal pigment epithelium–choroid sheet transplantation in age related macular degeneration: morphological and functional results. Br J Ophthalmol 91, 349–353. https://doi.org/10.1136/bjo.2006.102152

Turinetto, V., Orlando, L., Giachino, C., 2017. Induced Pluripotent Stem Cells: Advances in the Quest for Genetic Stability during Reprogramming Process. Int J Mol Sci 18, 1952. https://doi.org/10.3390/ijms18091952

Vaajasaari, H., Ilmarinen, T., Juuti-Uusitalo, K., Rajala, K., Onnela, N., Narkilahti, S., Suuronen, R., Hyttinen, J., Uusitalo, H., Skottman, H., 2011. Toward the defined and xeno-free differentiation of functional human pluripotent stem cell-derived retinal pigment epithelial cells. Mol Vis 17, 558–575.

Vahle, A.-K., Domikowsky, B., Schwöppe, C., Krähling, H., Mally, S., Schäfers, M., Hermann, S., Shahin, V., Haier, J., Schwab, A., Stock, C., 2014. Extracellular

matrix composition and interstitial pH modulate NHE1-mediated melanoma cell motility. International Journal of Oncology 44, 78–90. https://doi.org/10.3892/ijo.2013.2158

Van Cruchten, S., Vrolyk, V., Perron Lepage, M.-F., Baudon, M., Voute, H., Schoofs, S., Haruna, J., Benoit-Biancamano, M.-O., Ruot, B., Allegaert, K., 2017. Pre- and Postnatal Development of the Eye: A Species Comparison. Birth Defects Res 109, 1540–1567. https://doi.org/10.1002/bdr2.1100

Vugler, A., Carr, A.-J., Lawrence, J., Chen, L.L., Burrell, K., Wright, A., Lundh, P., Semo, M., Ahmado, A., Gias, C., da Cruz, L., Moore, H., Andrews, P., Walsh, J., Coffey, P., 2008. Elucidating the phenomenon of HESC-derived RPE: anatomy of cell genesis, expansion and retinal transplantation. Exp Neurol 214, 347–361. https://doi.org/10.1016/j.expneurol.2008.09.007

Vyawahare, H., Shinde, P., n.d. Age-Related Macular Degeneration: Epidemiology, Pathophysiology, Diagnosis, and Treatment. Cureus 14, e29583. https://doi.org/10.7759/cureus.29583

Walsh, N., Valter, K., Stone, J., 2001. Cellular and subcellular patterns of expression of bFGF and CNTF in the normal and light stressed adult rat retina. Exp Eye Res 72, 495–501. https://doi.org/10.1006/exer.2000.0984

Warnke, P.H., Alamein, M., Skabo, S., Stephens, S., Bourke, R., Heiner, P., Liu, Q., 2013. Primordium of an artificial Bruch's membrane made of nanofibers for engineering of retinal pigment epithelium cell monolayers. Acta Biomater 9, 9414–9422. https://doi.org/10.1016/j.actbio.2013.07.029

Weisz, J.M., Humayun, M.S., De Juan, E., Del Cerro, M., Sunness, J.S., Dagnelie, G., Soylu, M., Rizzo, L., Nussenblatt, R.B., 1999. Allogenic fetal retinal pigment epithelial cell transplant in a patient with geographic atrophy. Retina 19, 540–545. https://doi.org/10.1097/00006982-199911000-00011

Wenkel, H., Streilein, J.W., 2000. Evidence that retinal pigment epithelium functions as an immune-privileged tissue. Invest Ophthalmol Vis Sci 41, 3467–3473.

White, C., DiStefano, T., Olabisi, R., 2017. The influence of substrate modulus on retinal pigment epithelial cells. J Biomed Mater Res A 105, 1260–1266. https://doi.org/10.1002/jbm.a.35992

Whiting, P., Kerby, J., Coffey, P., da Cruz, L., McKernan, R., 2015. Progressing a human embryonic stem-cell-based regenerative medicine therapy towards the clinic. Philos Trans R Soc Lond B Biol Sci 370, 20140375. https://doi.org/10.1098/rstb.2014.0375

Wickham, H., 2011. The Split-Apply-Combine Strategy for Data Analysis. Journal of Statistical Software 40, 1–29. https://doi.org/10.18637/jss.v040.i01

Wickham, H., François, R., Henry, L., Müller, K., 2020. A Grammar of Data Manipulation [R package dplyr version 1.0.2].

Wilmut, I., Leslie, S., Martin, N.G., Peschanski, M., Rao, M., Trounson, A., Turner, D., Turner, M.L., Yamanaka, S., Taylor, C.J., 2015. Development of a global network of induced pluripotent stem cell haplobanks. Regen Med 10, 235–238. https://doi.org/10.2217/rme.15.1

Wilshaw, S.-P., Kearney, J.N., Fisher, J., Ingham, E., 2006. Production of an acellular amniotic membrane matrix for use in tissue engineering. Tissue Eng 12, 2117–2129. https://doi.org/10.1089/ten.2006.12.2117

Wong, W.L., Su, X., Li, X., Cheung, C.M.G., Klein, R., Cheng, C.-Y., Wong, T.Y., 2014. Global prevalence of age-related macular degeneration and disease burden projection for 2020 and 2040: a systematic review and meta-analysis. The Lancet Global Health 2, e106–e116. https://doi.org/10.1016/S2214-109X(13)70145-1

Wood, E.H., Tang, P.H., De la Huerta, I., Korot, E., Muscat, S., Palanker, D.A., Williams, G.A., 2019. STEM CELL THERAPIES, GENE-BASED THERAPIES, OPTOGENETICS, AND RETINAL PROSTHETICS: Current State and Implications for the Future. Retina 39, 820–835. https://doi.org/10.1097/IAE.0000000000002449

Yahalomi, T., Pikkel, Y., Arnon, R., Porat, D., Pikkel, J., 2023. The HIT Study—The Hydroxychloroquine Effect in the Treatment of Patients with Age-Related Macular Degeneration: A Randomized Controlled Trial. Medicina 59, 551. https://doi.org/10.3390/medicina59030551

Yamanaka, S., 2020. Pluripotent Stem Cell-Based Cell Therapy-Promise and Challenges. Cell Stem Cell 27, 523–531. https://doi.org/10.1016/j.stem.2020.09.014

Young, R.W., 1971. Shedding of discs from rod outer segments in the rhesus monkey. J Ultrastruct Res 34, 190–203. https://doi.org/10.1016/s0022-5320(71)90014-1

Zareidoost, A., Yousefpour, M., Ghaseme, B., Amanzadeh, A., 2012. The relationship of surface roughness and cell response of chemical surface modification of titanium. J Mater Sci Mater Med 23, 1479–1488. https://doi.org/10.1007/s10856-012-4611-9

Zeiss, C.J., 2010. Animals as models of age-related macular degeneration: an imperfect measure of the truth. Vet Pathol 47, 396–413. https://doi.org/10.1177/0300985809359598

Zhang, T., Yam, G.H.-F., Riau, A.K., Poh, R., Allen, J.C., Peh, G.S., Beuerman, R.W., Tan, D.T., Mehta, J.S., 2013. The effect of amniotic membrane de-epithelialization method on its biological properties and ability to promote limbal epithelial cell culture. Invest Ophthalmol Vis Sci 54, 3072–3081. https://doi.org/10.1167/iovs.12-10805